DAMPING RING
FOR
THE SLAC LINEAR COLLIDER

Thesis by
Leonid Zinovy Rivkin

In Partial Fulfillment of the Requirements
for the Degree of
Doctor of Philosophy

California Institute of Technology
Pasadena, California
1986

(Submitted September 24, 1985)

Acknowledgements

My thesis work, including initial work on PEP mini–beta projects, has touched on many different aspects of accelerator physics and has, therefore, brought me in contact with more people I can possibly thank. I would like to express my appreciation to all the unnamed SLAC staff members for their help.

I was fortunate to have two advisors, who complemented each other. Barry Barish, my Caltech advisor, gave me the opportunity and freedom to move into the field of accelerator physics. He allowed me great independence, while at the same time staying close enough to be supportive. John Rees, my SLAC advisor, took more of the brunt of attention to cumbersome details. The many challenging discussions I had with him were intellectual fun and taught me many things.

Helmut Wiedemann, who designed the damping ring and was so generous with ideas and suggestions, also guided my first steps into the wide world of accelerator physics during many night–shifts at PEP.

I spent many happy hours with Bill Davies–White, Ted Fieguth and Gerry Fischer during initial commissioning of the damping ring, a circle of people that grew later to include Matt Allen, Karl Bane, Jean–Pierre Delahaye, Albert Hofmann, Andrew Hutton, Martin Lee, Wayne Linebarger, Roger Miller, Phil Morton, Marc Ross, Klaus Wille, Perry Wilson and Mark Woodley.

I am especially indebted to Phil Morton and Albert Hofmann for all I learned from them.

Fellow SLAC accelerator physicists which were so generous with their time and help include Alex Chao, Martin Donald, Dick Helm, Sam Kheifets, Ewan Paterson, Ron Ruth, John Seeman, Roger Servranckx, John Sheppard, Jim Spencer, Rae Stiening and Bill Weng.

I would like also to thank Bill Atwood and Rainer Pitthan of the DELCO experiment who inspired and encouraged me to take part in the development of an asymmetric mini/micro beta insert for PEP, thus launching me on my career as an accelerator physicist.

And last, but not least, I want to thank my family and my friends who made it all possible.

Abstract

The results of a comprehensive set of measurements on the first purposeful 1.21 GeV high tune, high field damping ring for the SLAC Linear Collider are reported.

Current dependent effects such as parasitic mode losses, head tail instabilities, synchrotron and betatron frequency shifts were measured to estimate the impedance. All results agree reasonably well with expectations and indicate no limitations to the design performance. A current of 55 mA ($4 \cdot 10^{10}$ particles), which represents 80% of the design intensity, has been successfully stored in the ring with no sign of instabilities.

Some changes to the optics design that are being incorporated into the positron and electron damping rings now under construction are described. They are based on the operating experience with the present electron damping ring and include an improvement of the bending magnets and strengthening of the chromaticity correction scheme. As a consequence, the normalized equilibrium transverse emittance of the beam is expected to be 16 μ m rad.

Some properties of possible lattices for a future very high energy linear collider damping ring are discussed in the appendices.

Table of Contents

List of Tables

Chapter 1. Introduction

The electron–positron colliders have proven to be an extremely powerful tool for high energy particle physics. They have grown in size from table top machines to the 2.2 km circumference Positron Electron Project at SLAC and a similar size ring PETRA at DESY with the available center–of–mass energy up to 40 Gev. The Large Electron Positron storage ring[1] is under construction at CERN and will have the circumference of 27 km and the center–of–mass energy of 110 Gev in its first stage of operation and up to 210 Gev with major additions.

It is unlikely that further advances in the available center–of–mass energy will be achieved by building a bigger circular collider. The reason is that the particles lose energy in a circular machine into the synchrotron radiation, and the lost power is proportional to the fourth power of the energy. This causes the costs and the size of a circular collider to grow as the square of the energy[2]. The experimental data on this law are shown in Fig. 1 where the size and energy of many storage rings, either already built or under construction, is given.

The linear collider[3] is a new technology that can provide a way to achieve much higher energies since the synchrotron radiation losses are absent. The idea is to use two linear accelerators to accelerate bunches of electrons and positrons to the design energy and bring them into collisions.

SLAC Linear Collider[4], project that is under construction at the Stanford Linear Accelerator Center, is the first step in testing and developing this new technology. Besides the high energy physics motivation for building the SLC, the experience gained from this project will help in designing and building a very high

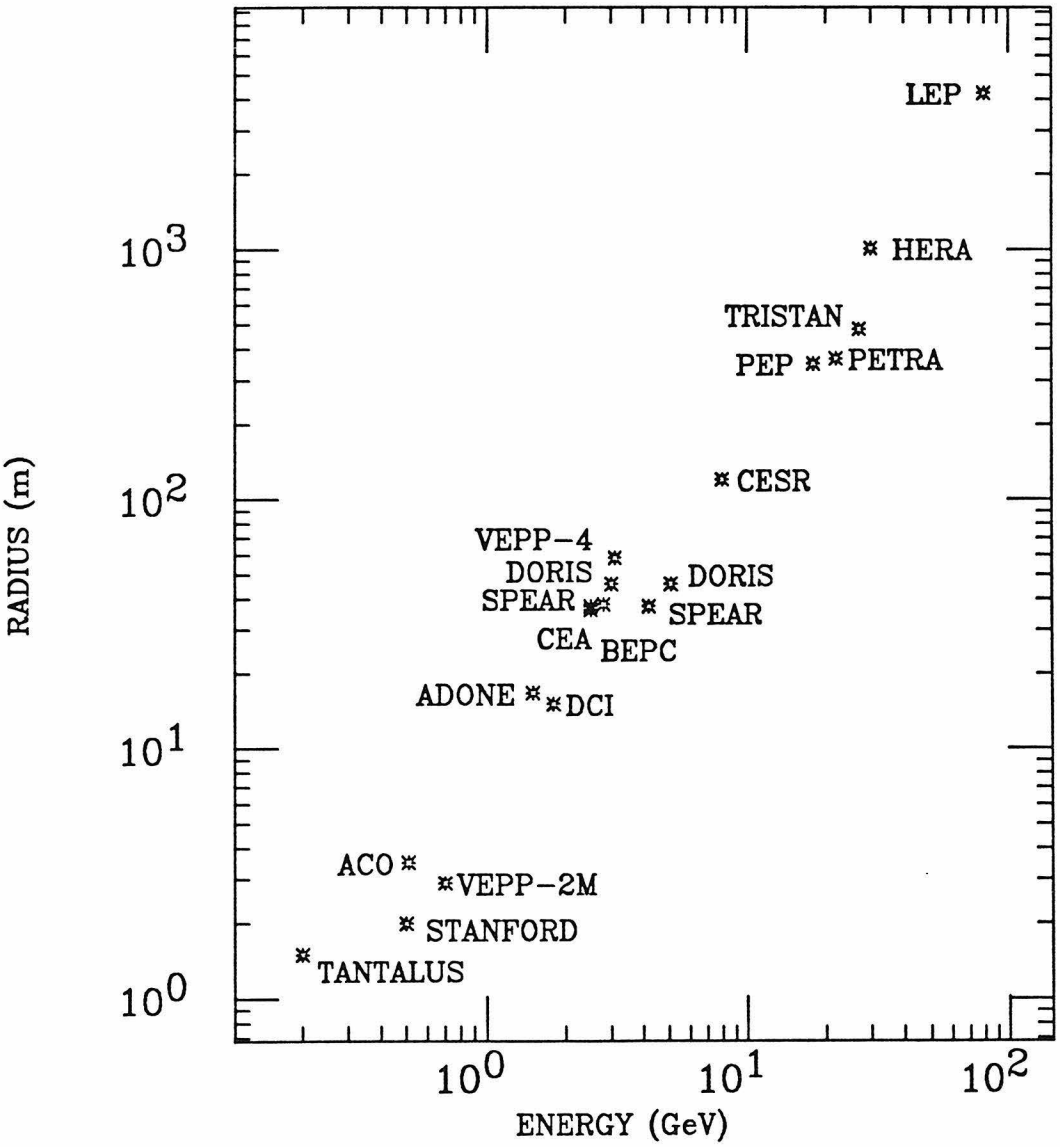

Figure 1. Average radius *vs* energy for the majority of the storage rings

energy linear collider.

In order to be useful for the high energy physics a linear collider has to have high luminosity which is defined as the event rate for a process of unit crossection. If the repetition rate of the linac is f and the bunches are equally populated, N particles each, the luminosity can be written as

$$\mathcal{L} = \frac{fN^2}{A}$$

where A is the effective transverse area over which the collisions take place. In the case of the circular colliders f stands for the revolution frequency and is on the order of a few hundred KHz. Present linac technology limits the repetition rates to below a few hundred Hz. Circular machines also typically have higher number of particles in the bunches since they can accumulate. In order to obtain comparable or higher luminosities, the effective interaction area A has to be drastically reduced in the linear colliders. It is directly proportional to the transverse phase space volume occupied by the bunch or to its emittance ε. If the transverse distribution of particles in a bunch is gaussian with the standard deviation σ_r in both horizontal and vertical planes, the effective collision area is

$$A = 4\pi\sigma_r^2 = 4\pi\beta^*\varepsilon$$

where we have expressed σ_r in terms of the emittance of the beam and the envelope function β^* at the collision point (see **Appendix A**).

The lower limit on the β^* is set at present by the higher order aberrations in the final optical elements before the collision point. The SLC design calls for $\beta^* = 5\,\mathrm{mm}$. In order to achieve useful luminosity, the invariant transverse emittance of the beam at the final energy of 50 GeV has to be

$$\gamma\varepsilon_{design} = 3 \times 10^{-5}\, m\,rad$$

while the typical invariant emittance of positron beam, which is obtained from a

converter target that is struck by an electron beam, is

$$\gamma\varepsilon_{in}^{+} = 1 \times 10^{-2}\, m\, rad$$

Damping rings are used to reduce the transverse emittance of the positron beam and also of the electron beam. The electron beam, obtained as it is from a hot cathode, has a smaller emittance, but it requires some damping nonetheless. The subject of this thesis is the first such damping ring that was built for the SLC project.

§1.1 Scope of the Thesis

In this dissertation we are going to describe the experiments and the development work done during the tests of the first purposeful damping ring. Some aspects and optimization of a possible lattice for a damping ring for a future linear collider are discussed in the appendices.

Chapter 2. Design Parameters

In this chapter we will describe the basic design parameters of the damping ring as well as introduce the necessary notation.

§2.1 Equilibrium Transverse Emittance

The equilibrium transverse emittance of the beam in a storage ring is the result of two competing processes. The quantum fluctuations due to the emission of synchrotron radiation blow up the beam. The process of radiation damping tends to reduce the transverse beam size. The balance struck between these two processes determines the value for the equilibrium emittance.

§§2.1.1 *Betatron Motion*

We will consider only rings with the design orbit lying in the horizontal plane. The magnetic field in the midplane is purely vertical and can be specified by giving the value for the field in the midplane $B_y(x, s)$ and the values for the field derivatives there. In particular, in linear approximation, the gradient of the field

$$k \equiv -\frac{1}{B\rho}\frac{\partial B_y}{\partial x}$$

is specified. Here $B\rho$ is the so called particle rigidity

$$B[\text{Tesla}]\rho[\text{m}] = 3.33564\, E[\text{GeV}]$$

The field on the design orbit will be characterized by the curvature function[5]

$$G(s) \equiv \frac{1}{\rho}$$

and we will usually consider the case of the so–called separate function lattice where the bending is done by pure dipole magnets and $G(s)$ is non–zero only inside them.

Let us disregard (or turn off) radiation effects for a moment. An electron executes betatron oscillations around the design orbit. The equation of motion is that of a harmonic oscillator with periodically modulated frequency[5], so called Hill's equation:

$$x''_\beta + k(s)x_\beta = 0$$

where $k(s)$ is a periodic function, with a period of at most the circumference of the ring. The solution to the above equation can be parametrized as follows:

$$x_\beta(s) = a\sqrt{\beta(s)}\cos\left(\phi(s) + \phi_0\right)$$

where a is a constant, the betatron phase $\phi(s)$ is defined as

$$\phi(s) = \int_0^s \frac{ds}{\beta(s)}$$

and $\beta(s)$ is a periodic function with a period of at most the circumference of the ring and is sometimes called an *envelope function* (see **Appendix A**). The betatron phase advance in one revolution, divided by 2π, is called the tune ν.

Introducing the rest of the Courant–Snyder parameters

$$\alpha \equiv -\frac{1}{2}\beta' \qquad \gamma \equiv \frac{1+\alpha^2}{\beta}$$

we can write down the Courant–Snyder invariant of the betatron motion[6] or the square of the invariant amplitude

$$a^2 = \gamma x_\beta^2 + 2\alpha x_\beta x'_\beta + \beta {x'_\beta}^2$$

The above expression relates the displacement x_β and the slope x'_β at any azimuth in the ring. It also describes an ellipse in the (x_β, x'_β) phase space and the square of the invariant amplitude is just the area of this ellipse divided by π or the *emittance*.

The presence of dispersion in the ring causes a particle with an energy different from the design energy to execute betatron oscillations around a new closed orbit, different from the design orbit. The total horizontal displacement of this orbit from the design orbit can be written as

$$x(s) = x_\beta(s) + \eta(s)\delta$$

where δ is the fractional energy deviation and $\eta(s)$ is the *dispersion function* that describes the displaced orbit and satisfies the following equation[5]

$$\eta'' + k(s)\eta = G(s)$$

§§2.1.2 *Quantum Fluctuations*

If we now turn on the radiation, the invariant amplitude of the electron's betatron oscillations will no longer remain constant. Let us consider an electron that emits a photon of energy u along the tangent to its trajectory. This is a good approximation since most of the synchrotron radiation is emitted into a cone with an opening angle of $1/\gamma$, which is much less than the typical slope of the trajectory. The particle's energy is reduced, but its displacement and the slope of the trajectory do not change, so we can write

$$\Delta x = 0 = \Delta x_\beta - \eta \frac{u}{E} \qquad \Delta x' = 0 = \Delta x'_\beta - \eta' \frac{u}{E}$$

where E is the design energy and we have assumed that prior to the photon emission the particle had the design energy. If our particle was following the design trajectory before radiating, *i.e.* its invariant betatron amplitude was zero, it now starts performing betatron oscillations with its square of the invariant amplitude given by

$$a^2 = \gamma \Delta x_\beta^2 + 2\alpha \Delta x_\beta x'_\beta + \beta \Delta x'^2_\beta = (\frac{u}{E})^2 \mathcal{H}$$

Here we have introduced

$$\mathcal{H} \equiv \gamma \eta^2 + 2\alpha \eta \eta' + \beta \eta'^2$$

a function that will play a very important role in what follows. It describes the growth of the invariant betatron amplitudes due to the radiation–induced quantum fluctuations.

Taking into account the spectrum of the synchrotron radiation[5] we can write the full expression for the growth of the square of the invariant betatron amplitude

due to the quantum excitation as

$$\frac{d\,a^2}{dt} = Q_x = \frac{2C_q E U_0}{T_0 \oint G^2\,ds} \cdot \oint |G^3| \mathcal{H}\,ds$$

where the quantum constant

$$C_q = \frac{55}{32\sqrt{3}} \frac{\hbar c}{(mc^2)^3} = 1.468 \cdot 10^{-6} \frac{m}{GeV^2},$$

E is the design energy, U_0 is the radiation loss per turn

$$U_0 = \frac{2r_e E^4}{3(mc^2)^3} \oint G^2\,ds$$

and T_0 is the revolution time along the design orbit.

In an ideal storage ring with the design orbit lying in a horizontal plane the vertical dispersion is zero everywhere and there are no quantum fluctuations that drive the betatron oscillations in the vertical plane.

§§2.1.3 *Radiation Damping*

Turning on the radiation also introduces damping of the betatron oscillations. While radiating, an electron loses both transverse and longitudinal momentum. The momentum is replenished each turn in the RF accelerating cavities only in the longitudinal direction. The transverse momentum error and the oscillations amplitude gradually shrink. As is shown in Ref. 5, the vertical betatron oscillations decay exponentially with the damping time

$$\tau_y = \frac{2ET_0}{U_0}, \qquad J_y = 1$$

the horizontal betatron oscillations with damping time

$$\tau_x = \frac{1}{J_x}\frac{2ET_0}{U_0}, \qquad J_x = 1 - \mathcal{D}$$

and the energy oscillations with damping time

$$\tau_\epsilon = \frac{1}{J_\epsilon}\frac{2ET_0}{U_0}, \qquad J_\epsilon = 2 + \mathcal{D}$$

Here we have introduced the so–called damping partition numbers J_i such that

$$\tau_i = \frac{\tau_0}{J_i} \qquad \tau_0 = \frac{2ET_0}{U_0}$$

and a new function of the lattice parameters

$$\mathcal{D} \equiv \frac{\oint G(2k + G^2)\eta \, ds}{\oint G^2 \, ds}$$

which is independent of the energy of the beam.

§§2.1.4 *Equilibrium Emittance*

The total rate of change of the square of the invariant betatron amplitudes can be summarized then as

$$\frac{d\langle a^2\rangle}{dt} = Q_x - \frac{2\langle a^2\rangle}{\tau_x}$$

A stationary distribution of the horizontal betatron oscillations of many particles is then characterized by the mean square horizontal spread of the beam

$$\sigma_{x\beta}^2 = \frac{1}{2}\langle a^2\rangle\beta_x(s) = \frac{1}{4}\tau_x Q_x \beta_x(s)$$

The ratio

$$\varepsilon_x \equiv \frac{\sigma_{x\beta}^2(s)}{\beta_x(s)} = \frac{1}{4}\tau_x Q_x$$

is called the horizontal equilibrium beam emittance. It is independent of the azimuth s.

Writing out τ_x and Q_x we can write the emittance as

$$\varepsilon_x = \frac{C_q E^2}{J_x} \frac{\oint |G^3| \mathcal{H}\, ds}{\oint G^2\, ds}$$

or in case of a separate function lattice, where G is non–zero only in the dipole magnets and is equal there to $1/\rho$,

$$\varepsilon_x = \frac{C_q E^2 \langle \mathcal{H} \rangle_{\text{mag}}}{J_x \rho}$$

where $\langle \mathcal{H} \rangle_{\text{mag}}$ is the average value of $\mathcal{H}$ in the dipoles, defined as

$$\langle \mathcal{H} \rangle_{\text{mag}} = \frac{1}{2\pi\rho} \int_{\text{mag}} \mathcal{H}\, ds$$

§§*2.1.5 Synchrotron Radiation Integrals*

We have seen in a few equations above various integrals of the lattice functions and betatron functions around the ring. It is convenient to introduce special notation for these integrals and express the main parameters of the ring as functions of them.[7] The integrals are calculated by most of the computer optics programs that are used in the design of the accelerators like COMFORT[8], MAD[9] and PATRICIA.[10,11]

$$I_1 \equiv \oint \eta G\, ds \qquad I_2 \equiv \oint G^2\, ds \qquad I_3 \equiv \oint |G^3|\, ds$$

$$I_4 \equiv \oint \eta G(2k + G^2)\, ds \qquad I_5 \equiv \oint |G^3| \mathcal{H}\, ds$$

where

$$\mathcal{H} = \gamma\eta^2 + 2\alpha\eta\eta' + \beta\eta'^2$$

Some of the parameters of the ring that we have encountered so far are expressed in terms of these integrals as follows:

- The radiation loss per turn

$$U_0 = \frac{2r_e}{(mc^2)^3} E^4 I_2 = \frac{C_\gamma}{2\pi} E^4 I_2; \qquad C_\gamma = 8.846 \cdot 10^{-5} \frac{\text{m}}{\text{GeV}^3}$$

- The $\mathcal{D}$ function and the damping partition numbers

$$\mathcal{D} = \frac{I_4}{I_2} \quad \Longrightarrow \quad J_x = 1 - \frac{I_4}{I_2}, \qquad J_\epsilon = 2 + \frac{I_4}{I_2}$$

  and the damping times are

$$\tau_x = \frac{4\pi T_0}{C_\gamma E^3} \frac{1}{I_2 - I_4}; \quad \tau_y = \frac{4\pi T_0}{C_\gamma E^3} \frac{1}{I_2}; \quad \tau_\epsilon = \frac{4\pi T_0}{C_\gamma E^3} \frac{1}{2I_2 + I_4}$$

- The equilibrium horizontal emittance

$$\varepsilon_x = \frac{C_q E^2}{J_x} \frac{I_5}{I_2} = C_q E^2 \frac{I_5}{I_4 - I_2}, \qquad C_q = 1.468 \cdot 10^{-6} \frac{\text{m}}{\text{GeV}^2}$$

Two additional parameters that we shall have need of are[5]

- The equilibrium energy spread of the beam

$$\left(\frac{\sigma_\epsilon}{E}\right)^2 = \frac{C_q E^2}{J_\epsilon} \frac{I_3}{I_2} = C_q E^2 \frac{I_3}{2I_2 + I_4}$$

- The orbit dilation or "momentum compaction" factor

$$\alpha = \frac{I_1}{L}$$

where L is the circumference of the design orbit.

It connects the change in orbit length with the relative particle energy change:

$$\frac{\Delta L}{L} = \alpha \frac{\Delta E}{E}$$

§2.2 Choice of Parameters

The main parameters of the SLC project that determined the properties of the damping ring optics[12,13] were

- required damped beam invariant emittance of both electrons and positrons

$$\gamma\varepsilon_{out}^{\pm} = 3 \times 10^{-5}\, m\, rad$$

- the design repetition frequency of the collider

$$f = 180\,\mathrm{Hz}$$

- the design initial emittances of the electron and positron beams to be damped down

$$\gamma\varepsilon_{in}^{+} = 1 \times 10^{-2}\, m\, rad$$
$$\gamma\varepsilon_{in}^{-} = 3 \times 10^{-4}\, m\, rad$$

The requirements on the positron damping ring, being more stringent since the input positron emittance is much higher that the input electron emittance, determined the optics parameters of both rings, because we wished to build and operate identical machines.

The output emittance of the damping ring can be written as

$$\gamma\varepsilon_{out} = \gamma\varepsilon_0(1 - e^{-2t/\tau}) + \gamma\varepsilon_{in}e^{-2t/\tau}$$

where $\gamma\varepsilon_0$ is the invariant equilibrium emittance, $\gamma\varepsilon_{in}$ is the invariant input emittance, t is the time spent in the ring by the beam, and τ is the damping time. The factor of two in the exponent is there because the emittance damps down with half of the horizontal damping time since it is proportional to the area occupied by the beam in the (x, x') phase space, and both x and x' damp down with the damping time τ.

In the next two subsections we will give some qualitative reasons for some of the design parameters choices.

§§*2.2.1 Damping Time*

The damping time has to be very short, since the time allowed for damping the emittance down, as determined by the repetition rate, is $t = 5.5\,\text{msec}$. During this time the emittance has to be reduced by a factor

$$\frac{\varepsilon_{in}}{\varepsilon_{out}} \approx 330,$$

thus the damping time has to be shorter than

$$\tau \leq \frac{2t}{\ln 330} = 1.9\,\text{msec}$$

assuming $\varepsilon_0 \ll \varepsilon_{in}$ In fact, it was decided to operate with two bunches of positrons in the damping ring, in order to double the time spent in the ring by each positron bunch and thus to permit doubling the minimum damping time to

$$\tau \leq 3.8\,\text{msec}$$

The damping time can be written as (see previous section)

$$\tau = \frac{2ET_0}{U_0} = \frac{4\pi T_0}{C_\gamma E^3}\frac{1}{I_2}, \qquad C_\gamma = 8.846 \cdot 10^{-5}\,\frac{\mathrm{m}}{\mathrm{GeV}^3}$$

where T_0 is the revolution time, U_0 is the radiation energy loss per turn, E is the energy of the beam, and I_2 is the second synchrotron radiation integral

$$I_2 = \oint \frac{ds}{\rho^2} \propto \frac{1}{E^2}\oint B^2\,ds, \qquad B[\mathrm{Tesla}]\rho[\mathrm{m}] = 3.33564\,E[\mathrm{GeV}]$$

and we have assumed that the horizontal partition number $J_x = 1$ which was the case for the separated function lattice the designers had in mind.

We see from the above formulae that we have to make T_0, the revolution time, as short as possible, and the magnetic field B as high as possible. The revolution time was limited from below by the properties of the kicker magnet, since we have to inject a positron bunch into the ring while another bunch is circulating. The sum of the rise and fall times of the kicker pulse has to be less than one half of the revolution time. The choice was

$$T_0 = 117.6\,\mathrm{nsec}$$

which corresponds to the circumference of the ring of $C = 35.27\,\mathrm{m}$. The magnetic field was chosen to be

$$B = 19.8\,\mathrm{KG}$$

the highest we could obtain without using superconducting magnets.

§§2.2.2 *The Equilibrium Emittance*

The lattice that was chosen for the damping ring is the FODO cell lattice that

has been used extensively in the present storage rings. Its name derives from the sequence of the focusing elements and the bending magnets. It consists of repetitive cells, each containing one focusing and one defocusing quadrupole, separated by uniform field dipole magnets. The main properties of the lattice are described in more detail in **Appendix B.**

The equilibrium transverse emittance in such a lattice is proportional to the cube of the bending angle per dipole magnet

$$\theta = \frac{L_b}{\rho}$$

where L_b is the length of the bending magnet and ρ is the bending radius. It is also a strong function of the horizontal betatron phase advance per cell and reaches its minimum around 130° per cell[14]. With such a phase advance we can write the approximate expression for the emittance in the FODO cell lattice as follows

$$\gamma\varepsilon_0 = C_\psi \frac{1}{F_m}(BL_m)^3, \qquad C_\psi = 9.68 \times 10^{-5}\text{Tesla}^{-3}\text{m}^{-2}$$

where F_m is the fraction of the length of the cell that is occupied by the bending magnets, which is usually close to a half. We have assumed that the horizontal partition number $J_x = 1$ in this approximation.

However the choice of the magnetic field strength still allowed reaching the design emittance by making the length of the bending magnet rather short.

$$L_m = 0.32\,\text{m}, \qquad \theta = 9°$$

In addition, in order to reduce the equilibrium and output emittances by a factor of two, the damping rings are designed to operate with fully coupled beams (see more on this in the section on coupling, **Chapter 4**).

§§2.2.3 *The Design Parameters*

After an optimization procedure[12,13] the damping time and equilibrium emittance were chosen to be

$$\tau_x = \tau_y = 3.06\,\text{msec}$$
$$\gamma\varepsilon_x = \gamma\varepsilon_y = 2.16 \times 10^{-5}\, m\,rad$$

such that the output emittance of positrons (after 11.1 msec) and electrons (after 5.56 msec) are

$$\gamma\varepsilon^{+}_{out} = \gamma\varepsilon^{-}_{out} = 2.9 \times 10^{-5}\, m\,rad$$

The operating energy of the damping ring was optimized at 1.21 GeV. Some of the general parameters of the damping ring design are summarized in Table 1.

Table 1. Some general design parameters of the damping ring

Energy	1.210	GeV
Circumference	35.27	m
Revolution Frequency	8.500	MHz
RF	714.000	MHz
Harmonic Number	84	
Transverse Damping Time	3.059	msec
Equilibrium Emittance	$9.1 \cdot 10^{-9}$	rad m
(with full coupling)		
Equilibrium rel. Energy Spread	$7.3 \cdot 10^{-4}$	
Momentum Comp. Factor	.01814	
Energy Loss/Turn	93.1	KeV
Bending Radius	2.0372	m
Bending Field	19.812	KG
CELL - Structure	1/2 FODO 1/2 F	
ν_x	~ 7.20	variable
ν_y	~ 3.20	variable
Acceptance		
in phase space	$\geq 4.13 \cdot 10^{-6}$	rad m
in energy	$\geq \pm 1\%$	
RF System and Related Parameters		
RF - voltage	800	KV
phase	6.7°	
Synchrotron Frequency	107.3	KHz
tune	.0126	
Equilibrium Bunch Length	5.9	mm
Critical photon energy	1.9283	KeV
I (2 bunches)	136.2	ma
P (synchrotron radiation)	12.68	KW

Chapter 3. The Damping Ring

The damping ring complex is located at the west end of the SLAC linear accelerator, one linac sector or 100 meters downstream of the electron injector. In Fig. 2 both damping rings with their transport lines are shown. The positron (north) damping ring is under construction now. The present electron (south) ring has been operational for the past two years and was the subject of the studies reported here.

In Fig. 3 we show the layout of the electron damping ring components.

§3.1 Dipoles

The electron damping ring bending magnet was designed to be a wedge magnet (edges of the magnet are normal to the design orbit) with the specially shaped pole tips to provide the sextupole component of the field for the distributed correction of chromaticity. In Fig. 4 a drawing of the dipole magnet with the pole pieces is given. The bend angle per magnet is 9° and the field is 19.8 kG. The vertical gap is 2 cm.

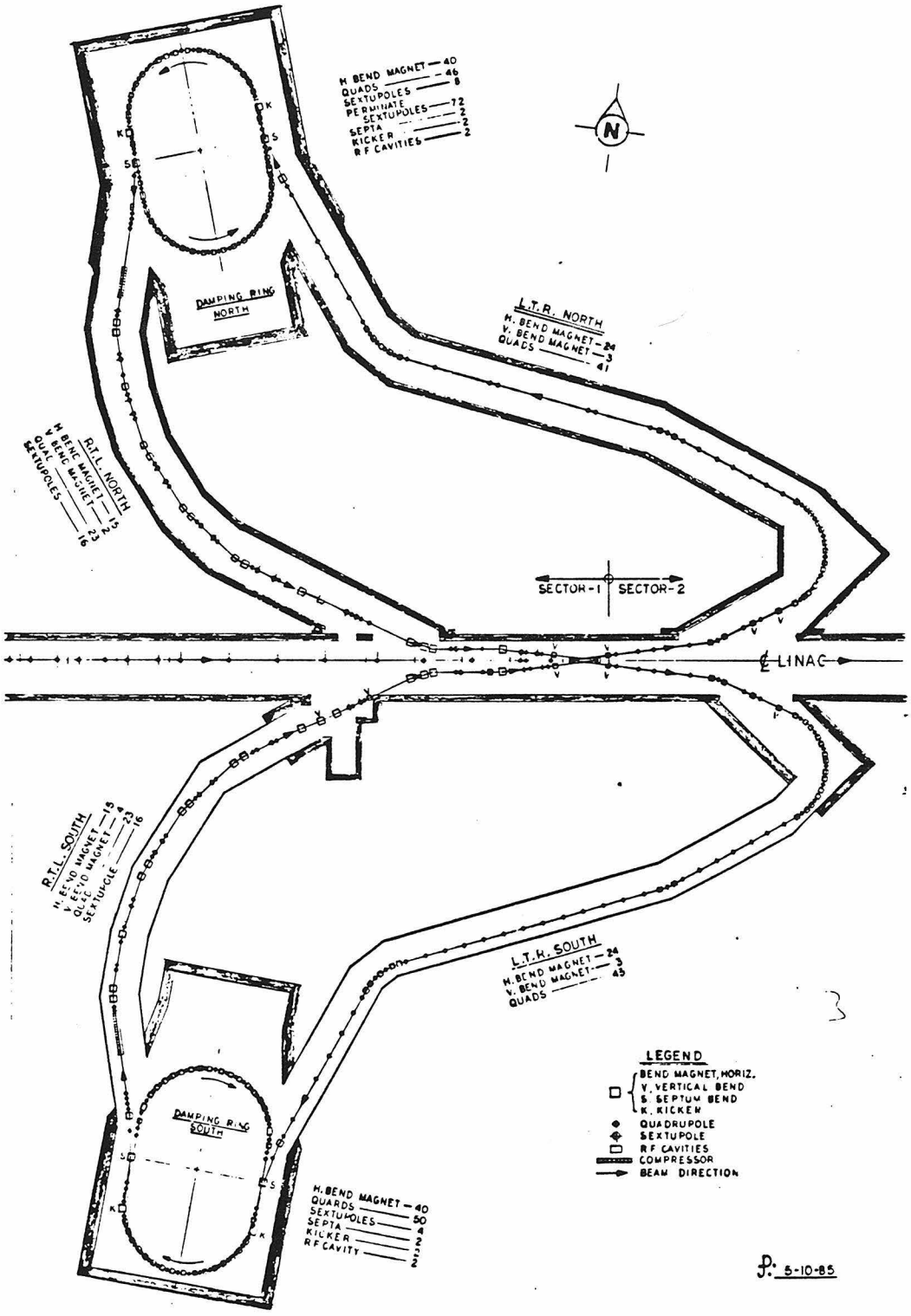

Figure 2. The damping ring complex. The present electron damping ring (south) and the future positron ring are shown with their transport lines.

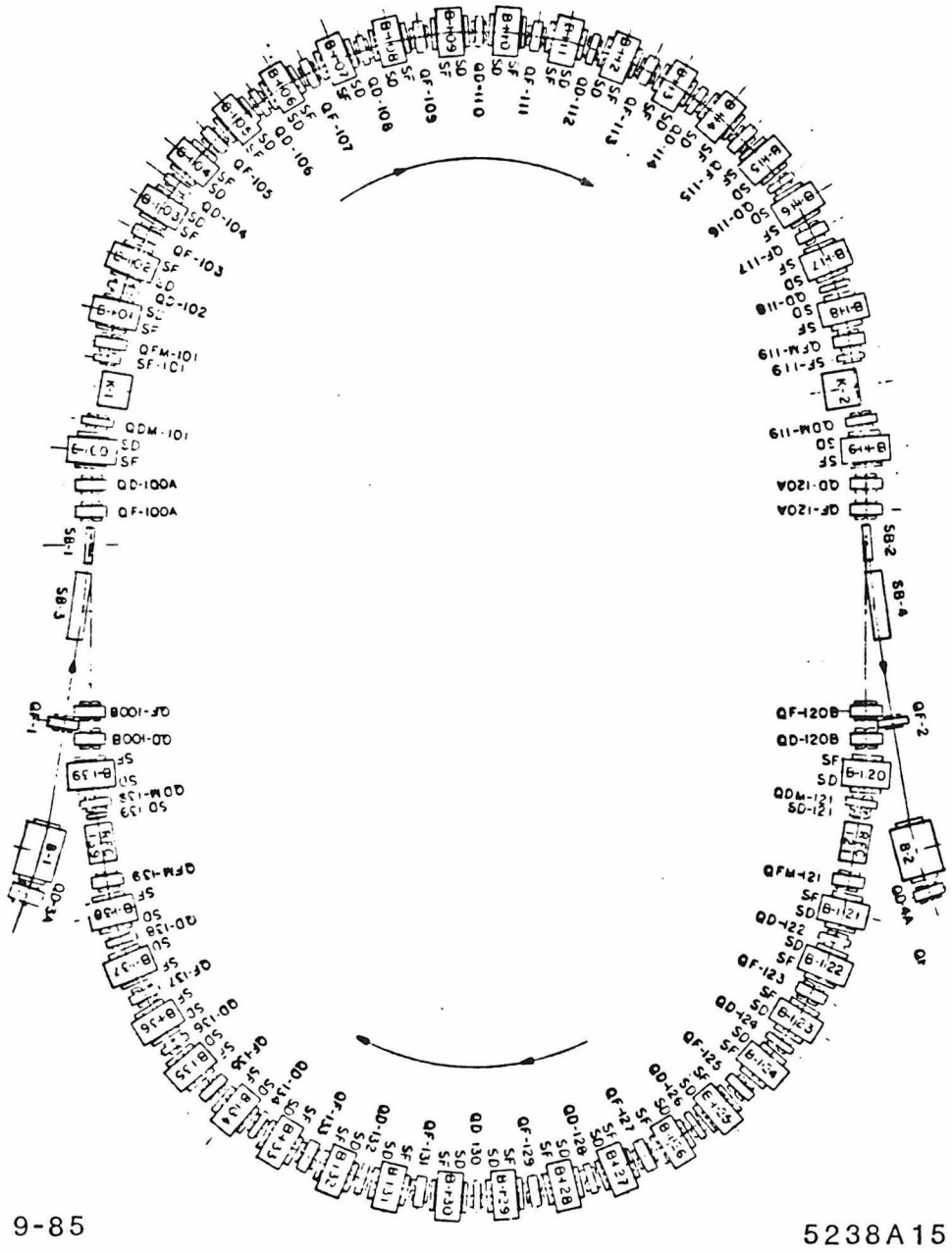

Figure 3. The layout of the electron damping ring components.

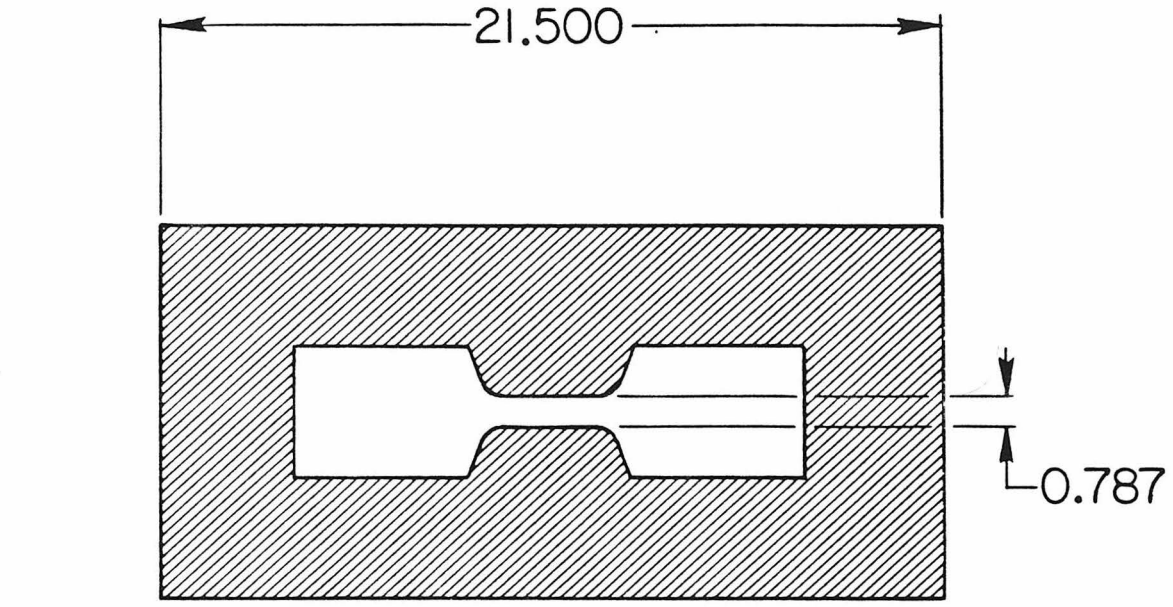

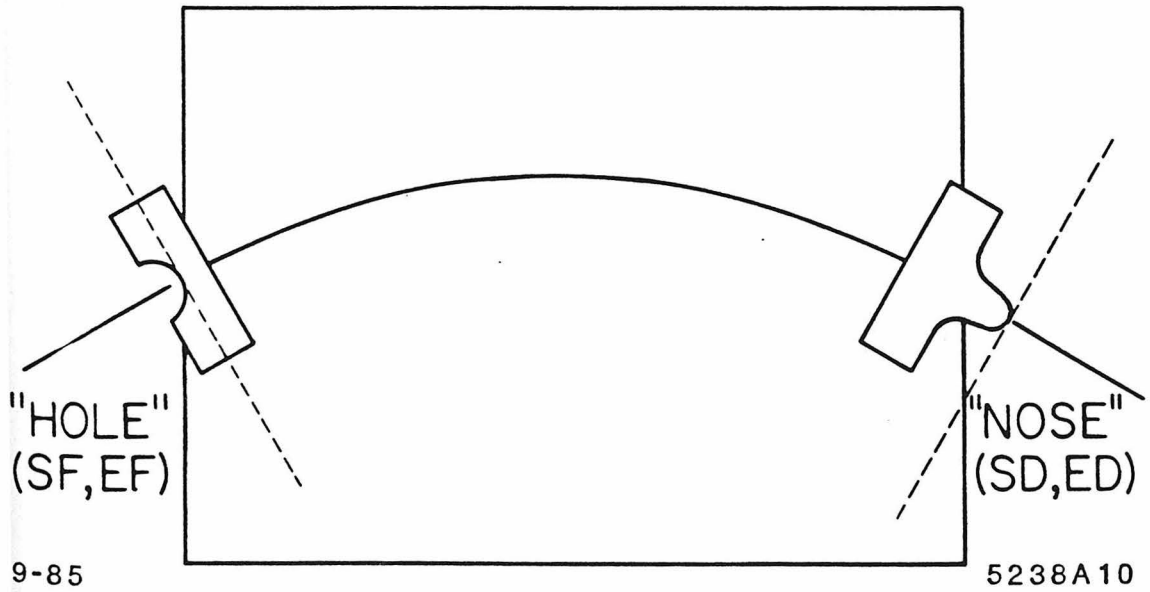

Figure 4. The drawing of the damping ring dipole magnet, showing the specially shaped pole tip pieces that provide the sextupole field component.

§3.2 Quadrupoles

The quadrupole magnets in the electron damping ring are organized into five families. The strong focusing required for the small equilibrium transverse emittance resulted in very large gradients and in the pole–tip fields close to the conventional limit of 10 kG.

The focusing (QF's) and defocusing (QD's) quadrupoles in the arcs have 1–inch bore while the straight section QFI's and QDI's have 2–inch bore. In Fig. 5 we show a drawing of the QD and QF series quadrupole.

§3.3 Sextupoles

The bulk of the chromaticity correction is done with the distributed sextupoles realized as the shaped pole tips of the bending magnets. The sextupole field at the ends of the magnet is obtained from the roughly parabolic shape of the pole tip (see Fig. 4) so that the integrated magnetic field that a particle sees at the end of the magnet is a quadratic function of the distance away from the design trajectory.

A small adjustment of ± 1 unit of chromaticity is provided for by two families of sextupoles, SF and SD, each having two magnets.

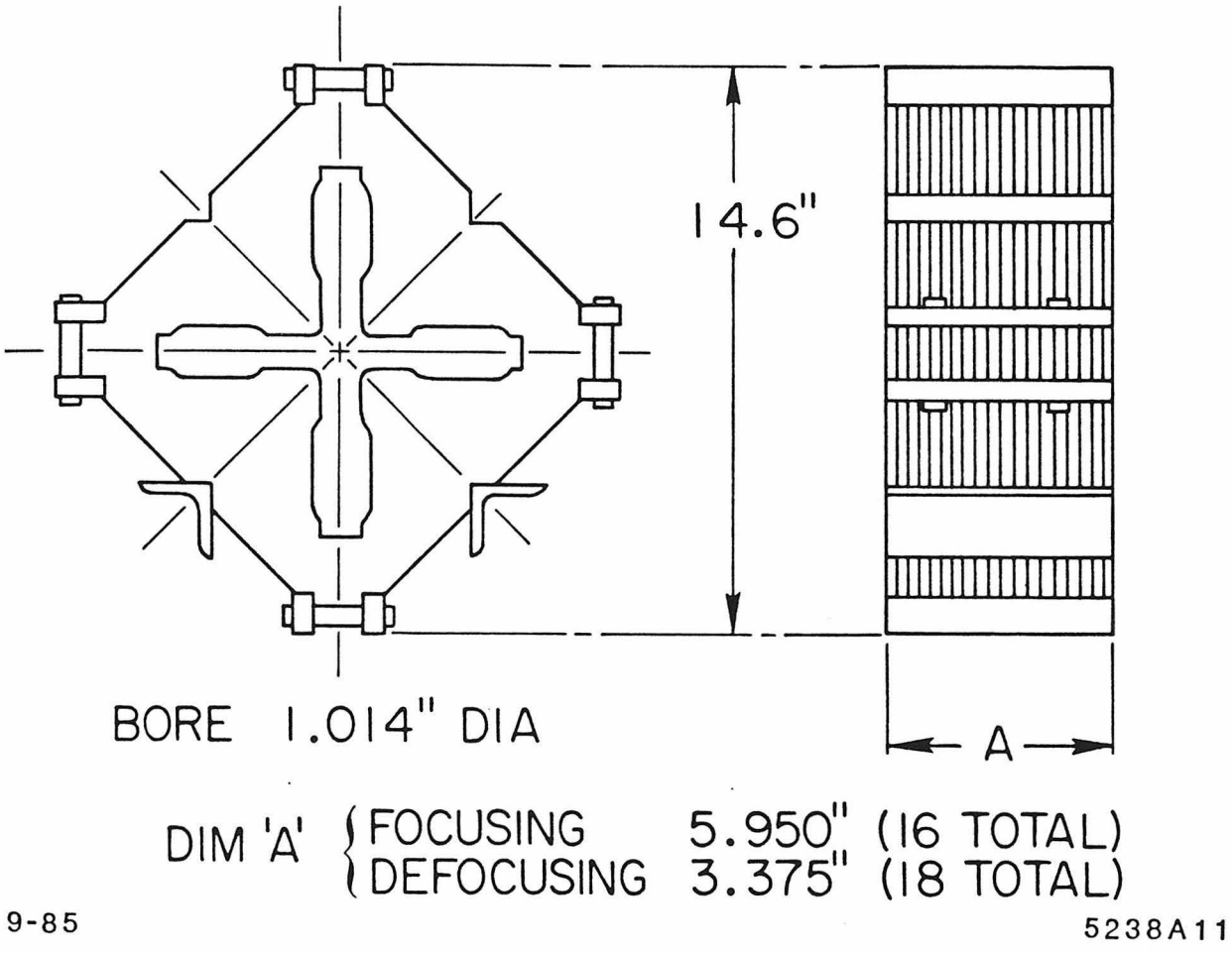

Figure 5. The drawing of the typical damping ring quadrupole.

§3.4 Injection and Extraction Magnets

§§3.4.1 *Septa*

The damping ring contains two DC septa, one in each straight section, for injection and extraction. The current sheet is 1 cm high and 3 mm wide, carrying the operating current of around 2500 A. The two septa provide a total of 7° bend and are powered by a single power supply. Backleg windings are provided to compensate the stray field in the stored–beam region.

§§3.4.2 *Kickers*

The kicker magnets[15] are ferrite loaded transmission lines designed to provide a 7–mrad kick lasting no longer then 58 nsec—half of the revolution period, in order not to disturb the second bunch in the ring.

The vertical gap is 2 cm. The amplitude of the voltage pulse is 40 KV and the vacuum chamber inside the kicker magnet is made out of ceramic that is covered on the inside with a very thin layer of Kovar in order to allow the beam image currents to flow freely and thus to minimize the disruption in the otherwise all metal vacuum pipe to the impedance of the ring (see the section on impedance in **Chapter 4.**)

§3.5 Correctors

Orbit correction is achieved with a set of horizontal and vertical steering correctors distributed around the ring. The majority of the horizontal correctors is implemented as additional windings on the bending magnets. All of the vertical correctors are additional windings on the vertically focusing quadrupoles, powered to provide a dipole field. A few of the horizontal correctors are implemented in the horizontally focusing quads as well. In Fig. 6 we illustrate the implementation of the steering correctors in the damping ring quadrupoles.

§3.6 RF System

The RF system[16] in the damping ring consists of two RF cavities, each made up of two copper cells, driven by single 714 MHz klystron. The maximum energy gain from the system in 800 KeV. Each cavity has a stepping–motor–controlled–tuner that is used to tune it *via* a feedback loop. The tuning range around the central resonant frequency of 714 MHz is ± 200 KHz.

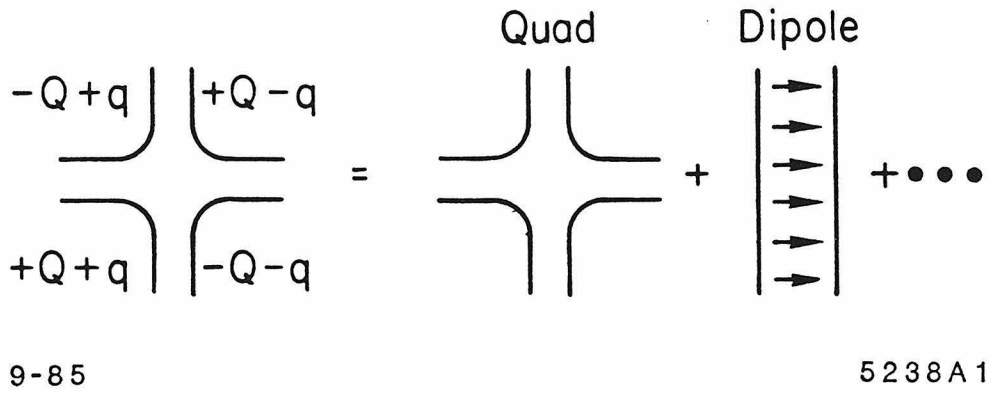

Figure 6. The implementation of the steering correctors in the quadrupole magnets.

§3.7 Vacuum System

The ring vacuum chamber is pumped by two sets of pumps: localized diffusion pumps and distributed ion pumps. The distributed pumps are located in the bending magnet chambers. A few vacuum gauges are provided for monitoring the pressure. Two valves, one at the end of LTR and the other one at the beginning of RTL, can be used to isolate the ring from the transport lines. Pressures on the order of a few nanotorrs have been achieved to date.

Chapter 4. Measurements

§4.1 Optics

From the point of view of linear optics the damping ring is a four–fold symmetric machine. It consists of two arcs with regular FODO cell structure, each arc containing eight cells, and two straight sections that provide space for the injection and extraction of the beam. There are also four matching sections that provide the transition from the arcs to the straight sections. Shown in Fig. 7 are the $\sqrt{\beta_x(s)}$, $\sqrt{\beta_y(s)}$ and $\eta(s)$ in one quarter of the ring.

§§*4.1.1 The Arcs*

The FODO cell lattice of the arcs has been used in many existing storage rings and its properties have been well studied and understood. It determines the major parameters of the damping ring, in particular its emittance, since most of the radiation and focusing occurs in the arcs.

The main characteristics of the FODO lattice can be parametrized in terms of

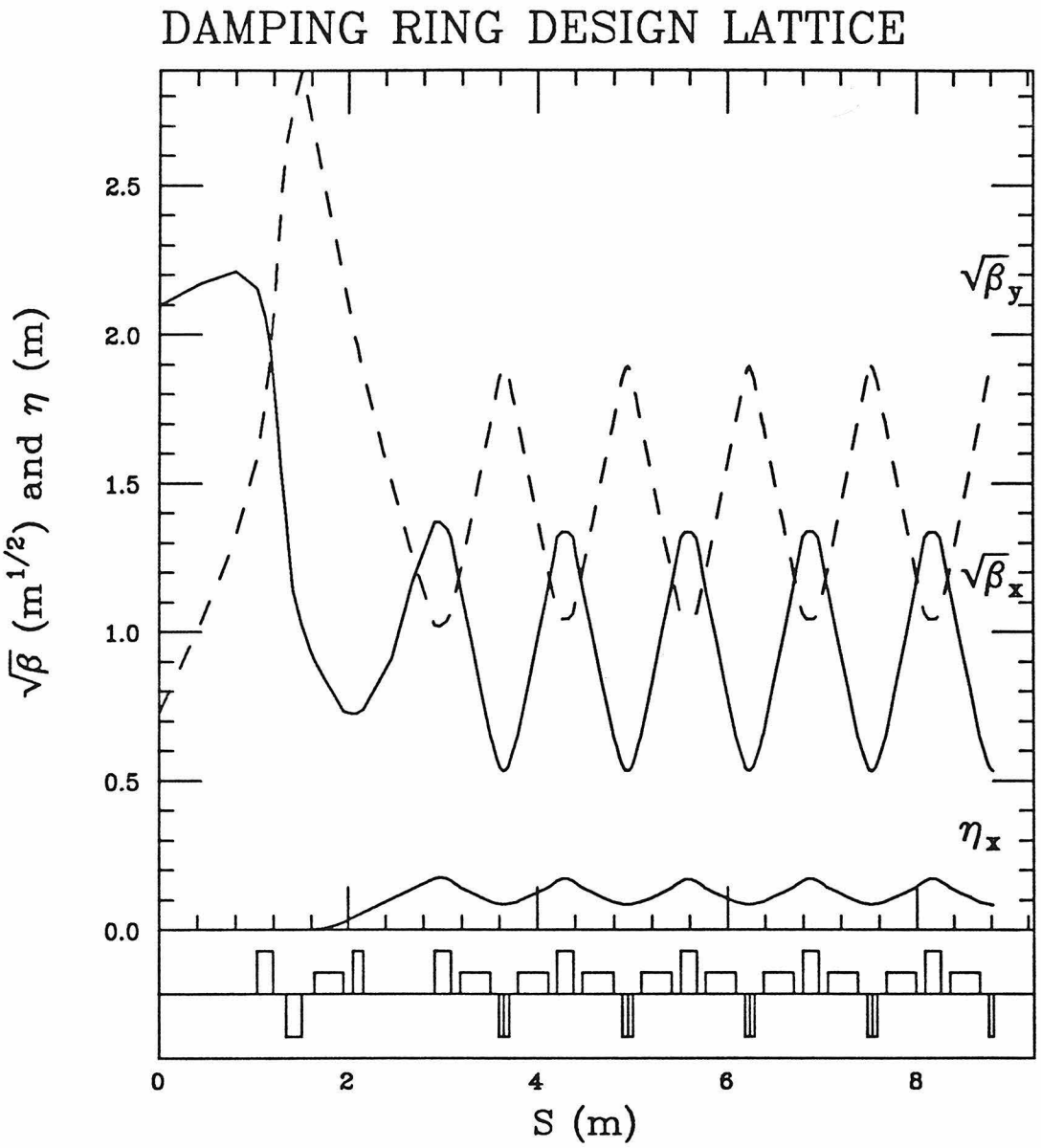

Figure 7. Design envelope functions and dispersion in one quarter of the ring.

the betatron phase advance per cell[17] and the equilibrium emittance that can be achieved with such a lattice is minimum at about 68° horizontal phase advance per half–cell.[14] In the Fig. 8 we show the equilibrium horizontal beam emittance in the Damping Ring as a function of the horizontal betatron phase advance per half–cell. The analytical results in Ref. 14 used various approximations and give a slightly different shape of the curve than calculations done with optics programs. These approximations include thin lens model for the quadrupoles, equal betatron phase advances per cell in both planes and bending magnets filling all the space between the quads; they are discussed in more detail in **Appendix B.**

The design optics configuration in the Damping Ring has the horizontal betatron phase advance per half–cell of 57° which corresponds to the horizontal tune of $\nu_x = 7.2$ and the vertical tune is $\nu_y = 3.2$. The reasons why the operating tune was not chosen at the minimum of the emittance basically have to do with the fact that higher phase advance per cell requires stronger quadrupoles and sextupoles. See more on this in **Appendix B.**

§§*4.1.2 Straight Sections*

In order to facilitate injection and extraction the horizontal beta function in the straight sections is comparatively high, $\beta_x = 4.4m$, and the dispersion is close to zero.

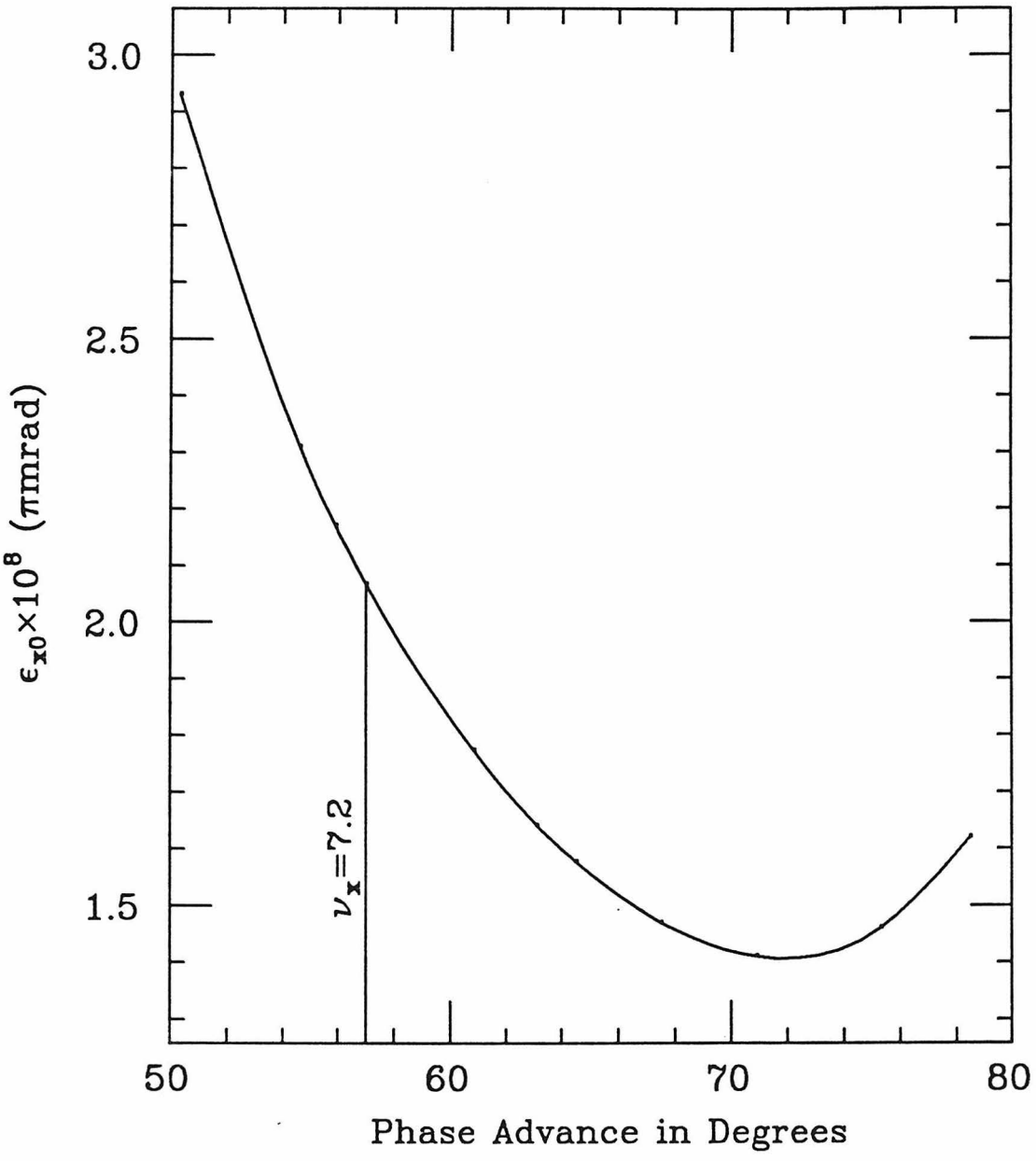

Figure 8. Equilibrium horizontal emittance (ε_{x0}) as a function of the horizontal betatron phase advance per half–cell in the Damping Ring.

§§4.1.3 *Changes in the Design Optics*

The damping ring was optimized and built for operation at a single energy of 1.21 GeV. The bending magnets in the ring are run close to saturation and were carefully measured and shimmed to provide the design optics at that energy. Unfortunately, for the testing which was done during the first year of operation, the linear accelerator was able to provide the electron beam of only 0.95 Gev. The difference in energies was sufficient to cause considerable difficulties, especially due to the fact that the magnets had not been measured at that energy. The lower energy properties of the magnets were determined from the known magnetic measurement data, but yielded results only good to a few percent accuracy.

In addition, an error in the construction of the bending magnets altered their focusing properties. What was supposed to be a sector 9° bending magnet with 4.5° equivalent horizontal focusing at each edge, turned out to have double strength edge focusing, equivalent to 9° at each edge.

As a result, the strengths of the quadrupole families had to be empirically adjusted to obtain the design tunes.

§4.2 Tune Measurement

The tune is the phase advance of the betatron oscillations per one revolution, normalized by 2π

$$\nu = \frac{1}{2\pi} \oint \frac{ds}{\beta(s)}$$

It is equal to the number of the betatron oscillation periods that fit into one turn.

§§4.2.1 *Use of the BPM's on the First Turn*

The problems stated above were diagnosed and a rough set of quadrupole strengths that allowed stored beam were achieved by the following method of measuring the tune.

The ring on the first turn was treated as a transport line and the position of the beam was measured on the BPM's (beam position monitors) as a function of a corrector at the entrance to the ring used as a variable deflector. The changes in position then exhibit a clear betatron oscillation and the number of periods was roughly counted. A very helpful way to view the data is to normalize the position measurements by the reciprocal square root of the β function at the place of the measurement and plot the results *vs* betatron phase advance $\mu(s)$

$$\mu(s) = \frac{1}{2\pi} \int \frac{ds}{\beta(s)}$$

The results then could be fitted to a simple sine wave.

Such measurements on the first turn were also used to check that the phase advances in the two arcs of the ring were roughly the same as well as to check the symmetry of the ring.

§§4.2.2 *Tune Monitor*

The tune is measured with the stored beam. The tune monitor employs two pairs of strip lines positioned at 45° with respect to the horizontal plane. One set serves as a driver and the other as an antenna. A swept frequency spectrum analyzer is used to measure the resonant frequency response of the beam. The spectrum analyzer generates a signal of a given frequency that is applied after amplification to the driver set of striplines and drives the beam. A signal proportional to the center of charge transverse motion of the bunch is picked up by the antenna, passed through a notch filter to remove the revolution frequency and its second harmonic components, is amplified and then spectrum analyzed. Successive passages provide a sampled waveform of the coherent beam oscillations. When the beam is driven at a betatron frequency a resonant response is detected. Since the revolution frequency is sampled, the frequency measured corresponds to the difference between the tune frequency and the nearest harmonic of the revolution frequency.

In fact, the betatron frequencies show up as sidebands around the revolution frequency harmonics. We chose to measure the tune near the zeroth harmonic and for that purpose a swept frequency analyzer that went up to 5 MHz was used (the revolution frequency of the damping ring is 8.5 MHz). We then have to determine the integer part of the tune and whether the fractional part is above or below a half by some other means. The integer part can be determined with the help of the BPM's using stored beam or on the first turn as in the above section.

To determine whether the fractional part is above or below a half we use the fact that a quadrupole lens focuses in one plane and defocuses in the other. The idea is to raise the strength of QF magnets, increase the horizontal focusing, thus pushing up the horizontal tune. If the measured frequency goes up, the fractional part is below half integer, if it goes down, the tune is above a half. In reality,

however, there is a difficulty since we often are confronted with two peaks on the frequency analyzer and do not know *a priori* which one is horizontal and which one is vertical. These can be identified, however, by using the fact that at the focusing quads β_x usually peaks and β_y is usually low. Since the tune shift due to a gradient change is proportional to the β function at the place of change (see section on measuring β), the horizontal tune will therefore move faster then the vertical.

The minimum width of the tune signal on the spectrum analyzer was about 10 KHz, or

$$\Delta\nu_{resolution} \approx 0.001$$

which corresponds to the tune spread for chromaticity of $\xi \approx 1$ and equilibrium relative energy spread being $\delta \approx 10^{-3}$.

§4.3 Orbit Correction

The closed orbit in an actual storage ring does not coincide with the design orbit due to the presence of imperfections in the guide field. The main sources of errors are misalignments of quadrupole magnets and errors in the bending field in the dipole magnets. A set of 26 horizontal and 14 vertical steering magnets in the damping ring is used to correct the closed orbit. All of the vertical correctors and 4 of the horizontal correctors are in the quadrupole magnets. The rest of the horizontal correctors are in the dipole magnets.

There are also 26 beam position monitors[18,19] around the ring. Their resolution was measured[20] to be $100\,\mu m$.

The orbit correction scheme[21,22] used in the damping ring was adopted after the PEP storage ring correction scheme.[23] It provides for approximately uniform

distribution of correctors and beam position monitors in betatron phase. There are four correctors per betatron oscillation period. The drawing of the damping ring in Fig. 9 shows the location of the beam position monitors and correctors.

§4.4 Measuring the Beta Function

Measurements of the β function constitute an important check of the ring optics and are indispensable in building a correct model of a ring with imperfections. The two basic methods used to measure the β function employ the effects caused by changing steering or focusing in the ring.

§§4.4.1 *Quadrupole Trims*

The first method for determining the β function utilizes changes in tune caused by a localized gradient change. The quadrupole magnets in the Damping Ring are arranged into families, each family powered by a single power supply. In order to measure the β function at a particular quadrupole, a passive shunt was used to bypass a variable amount of current around that magnet. Let us briefly describe the basis for the measurement.[6]

At a given azimuth in the ring we can write the transfer matrix for one turn

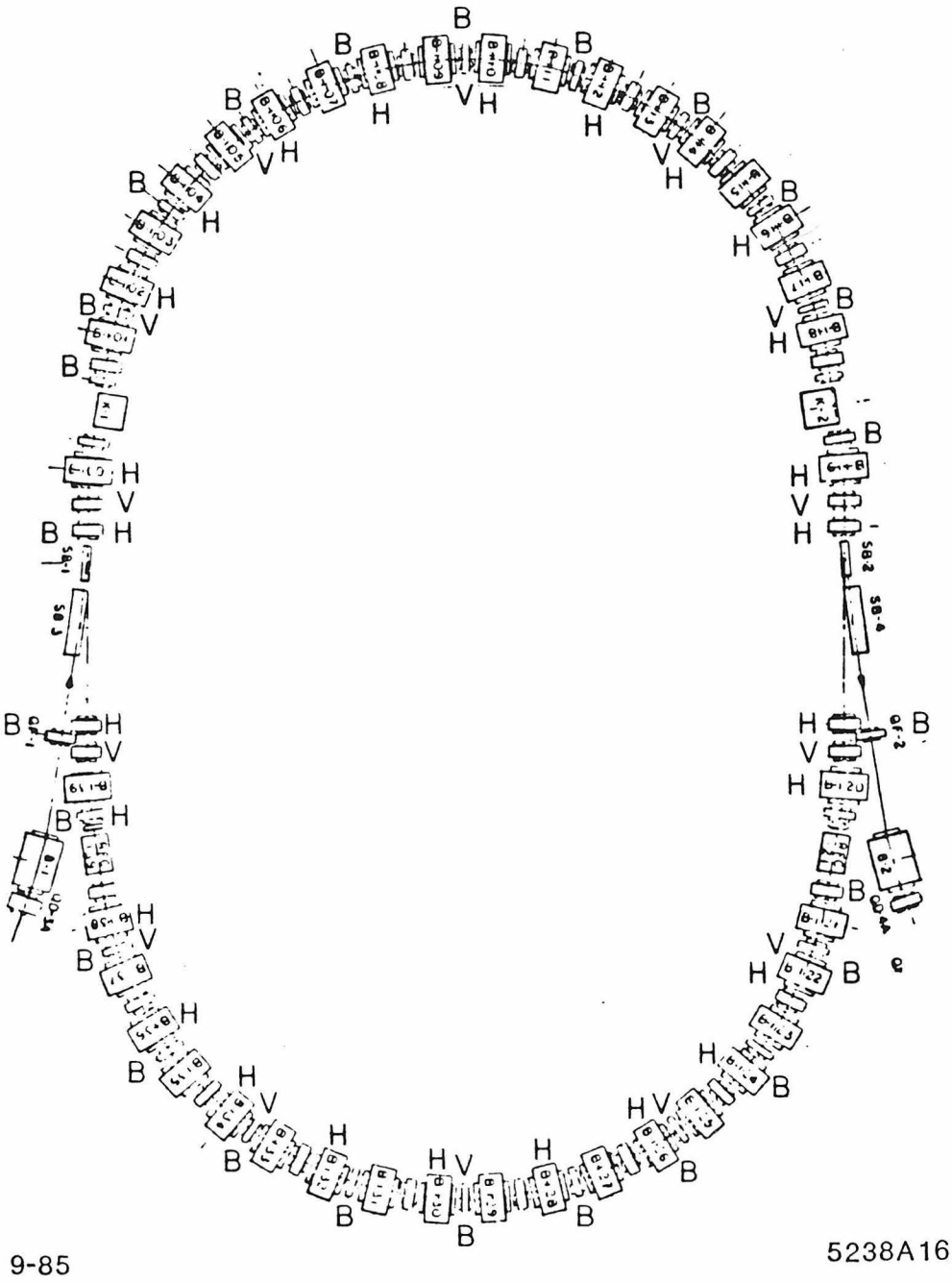

Figure 9. The Damping Ring layout showing the locations of the correctors and beam position monitors.

around the ring in terms of the Courant–Snyder parameters at that location:

$$\mathbf{R} = \begin{pmatrix} \cos 2\pi\nu + \alpha \sin 2\pi\nu & \beta \sin 2\pi\nu \\ -\gamma \sin 2\pi\nu & \cos 2\pi\nu - \alpha \sin 2\pi\nu \end{pmatrix}$$

where ν is the tune. Let us introduce a small localized change of gradient which we will describe as a thin lens of strength k. The new single turn matrix is the product of $\mathbf{R}$ with the matrix representing the thin lens

$$\bar{\mathbf{R}} = \mathbf{R} \cdot \begin{pmatrix} 1 & 0 \\ -k & 1 \end{pmatrix} = \begin{pmatrix} \cos 2\pi\nu + \alpha \sin 2\pi\nu - k\beta \sin 2\pi\nu & \beta \sin 2\pi\nu \\ -\gamma \sin 2\pi\nu - k(\cos 2\pi\nu - \alpha \sin 2\pi\nu) & \cos 2\pi\nu - \alpha \sin 2\pi\nu \end{pmatrix}$$

On the other hand we can write the $\bar{\mathbf{R}}$ matrix in terms of the new values of the Courant–Snyder parameters at that azimuth

$$\bar{\mathbf{R}} = \begin{pmatrix} \cos 2\pi\bar{\nu} + \bar{\alpha} \sin 2\pi\bar{\nu} & \bar{\beta} \sin 2\pi\bar{\nu} \\ -\bar{\gamma} \sin 2\pi\bar{\nu} & \cos 2\pi\bar{\nu} - \bar{\alpha} \sin 2\pi\bar{\nu} \end{pmatrix}$$

Consider now the trace of $\bar{\mathbf{R}}$ in the two representations

$$\frac{1}{2}\mathrm{Tr}\bar{\mathbf{R}} = \cos 2\pi\bar{\nu} = \cos 2\pi\nu - \frac{1}{2}k\beta \sin 2\pi\nu$$

It is customary to make the following approximation to this result. Taking the derivative of both sides with respect to k we obtain

$$\frac{d\nu}{dk} = \frac{1}{4\pi}\beta$$

or for small k

$$\Delta\nu \approx \frac{1}{4\pi}\beta k$$

We can see now from these formulae that a small localized change of gradient introduces a tune shift proportional to the β function at that location. This fact serves as the basis of one of the methods to measure β function.

The tune shift is not the only effect caused by the local gradient change. The β function itself is changed, the very quantity we are trying to measure. Let us examine the magnitude of this change. Notice that the upper right element of the $\bar{\mathbf{R}}$ matrix remains invariant under the gradient change. Taking its derivative with respect to k and evaluating it at $k = 0$, we can write

$$\frac{d\beta}{dk} \sin 2\pi\nu + 2\pi\beta \cos 2\pi\nu \frac{d\nu}{dk} = 0$$

or, for small k, the relative change in β is

$$\frac{\Delta\beta}{\beta} \approx -2\pi\Delta\nu \cot 2\pi\nu$$

Notice the resonant behavior of the β function if the tune is close to an integer or half–integer value. Usually the operating tune is comfortably away from these resonances. However, if one uses the approximations above, one cannot hope to make a measurement of the β function with an accuracy better then 10% if the tune shift during the measurement exceeds $\Delta\nu = 0.01$. Typical resolution of the tune measurement during running–in period was $\Delta\nu = 0.002$.

§§4.4.2 *Averages over the Magnet Strings*

By changing the power supply that controls a given family of quadrupole magnets we can measure an average value of the β function at the locations of those magnets. Since the tune shift due to a small distributed gradient change can be written in the following way

$$\Delta\nu \approx \frac{1}{4\pi} \int \beta(s)k(s)\, ds = \frac{k}{4\pi} \sum_{i=1}^{N} \beta_i$$

the tune shift is proportional to the average β function. Alternatively, some of the linear optics programs like COMFORT[8] print out the values of the derivatives

$$\frac{\partial \nu}{\partial k}$$

which can be compared directly with the results of the measurements.

§§4.4.3 *Cusp Method*

The second method of measuring β uses the localized changes in steering, or "bumps". The change in the closed orbit at an azimuth s_1 due to a single corrector which produces an angular deflection $\Delta\Theta$ at an azimuth s_0 is

$$\Delta x_{co}(s_1) = \frac{\Delta\Theta\sqrt{\beta(s_0)}}{2\sin\pi\nu}\sqrt{\beta(s_1)}\cos\{\phi(s_1) - \phi(s_0) - \pi\nu\}$$

and, in particular, the change in orbit *at the corrector* is simply

$$\Delta x_{co} = \Delta\Theta \cdot \frac{\beta}{2\tan\pi\nu}$$

where $\Delta\Theta$ is the strength of the corrector expressed as an angle in radians of the kick it gives to the beam. Given a combination of a position measuring device and a steering corrector at the same azimuth, one can determine the β function at that place.

We have such combinations in the damping ring in the majority of the defocusing quadrupoles in the arcs as well as in the quadrupoles in the straight sections. The results of such a measurement are shown in Fig. 10, overlaid on the predicted by the model plot of the β functions in the ring.

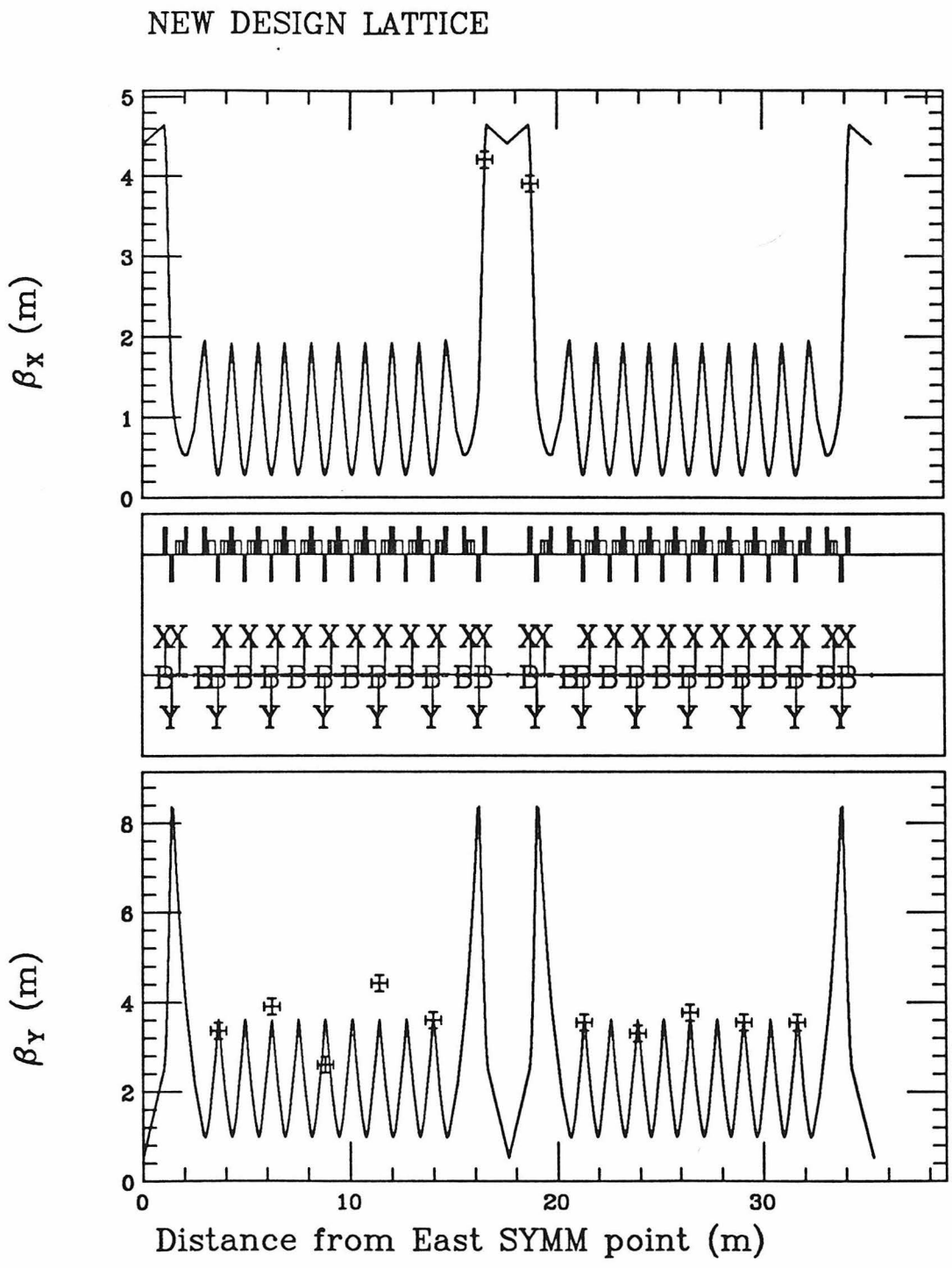

Figure 10. The results of the measurements of the β function using the cusp method. The data is plotted together with the model predictions for the β functions.

Another possibility we had to make a single measurement of this type was to use the synchrotron light monitor to measure the changes in position of the beam at the source point, which is in a dipole that has a horizontal corrector built into it.

§4.5 Dispersion Measurements

The dispersion, $\eta(s)$, is defined here as the first order change in particle position with energy deviation, so that the total deviation from the equilibrium orbit can be written as

$$x = x_\beta + \eta \cdot \frac{\Delta p}{p}$$

i.e. the particle executes betatron oscillations around a new closed orbit described by the η function. In order to measure dispersion in the ring we change the energy of the beam by a small amount and measure the relative change in the beam position.

The length of the orbit that is followed by an electron with an energy different from the design energy will differ from the length of the design orbit by an amount

$$\Delta L = \frac{\Delta p}{p} \oint \frac{\eta(s)}{\rho(s)}\, ds$$

or

$$\frac{\Delta L}{L} = \alpha \frac{\Delta p}{p}$$

where we have used the so called "momentum compaction factor" α (sometimes called "elongation factor")

$$\alpha = \frac{1}{L} \oint \frac{\eta(s)}{\rho(s)}\, ds$$

It is usually calculated by the optics programs like COMFORT[8], MAD[9] and PATRICIA[10,11]

We can change the length of the orbit by changing the frequency of the RF system, since the orbit length always contains an integer number of RF wavelengths:

$$L = h\lambda_{rf}$$

where h is called the harmonic number. In the damping ring $h = 84$. The relative change in orbit length is then

$$\frac{\Delta L}{L} = -\frac{1}{h}\frac{\Delta f_{rf}}{f_{rf}}$$

and the energy change that is introduced this way is

$$\frac{\Delta p}{p} = -\frac{1}{\alpha h}\frac{\Delta f_{rf}}{f_{rf}}$$

The basis for the dispersion measurements described below can thus be summed up in the following formula:

$$\Delta \mathrm{x}(s) = -\frac{\eta(s)}{\alpha h}\frac{\Delta f_{rf}}{f_{rf}}$$

Notice that in order to calculate η from the displacement measurements we have to know the momentum compaction factor. An estimate of its magnitude can be given as[5]

$$\alpha \approx \frac{1}{\nu_x^2}$$

and is usually rather good. For example, in the Damping Ring with the horizontal tune of $\nu_x = 7.2$ the optics programs calculate the value $\alpha = 0.0184$ to be compared with

$$\frac{1}{\nu_x^2} = 0.0193$$

In any case, it enters as an overall factor into the dispersion calculations, so one can still use the results to check the global pattern and matching of the dispersion.

An experimental check of α can be done by measuring the tune of the synchrotron oscillations, ν_s as a function of RF voltage, since the synchrotron tune can be written as

$$\nu_s^2 = \alpha \frac{heV_{RF} \cos \phi_s}{2\pi E}$$

where h is the harmonic number, ϕ_s is the synchronous phase angle and V_{RF} is the amplitude of the RF voltage.

§§4.5.1 *Using BPM's*

We measured the dispersion using the beam position monitors in the ring. An example of the results is given in Fig. 11 where the data points are plotted together with the model predictions for the dispersion.

§§4.5.2 *Using Scrapers*

The scrapers can be used to measure the change in position of the beam as a function of the RF frequency. One of the scrapers is driven towards the beam until it clearly affects the lifetime. The positions of the scraper that result in the same lifetime for different values of the RF frequency are then used to calculate the dispersion at the scrapers.

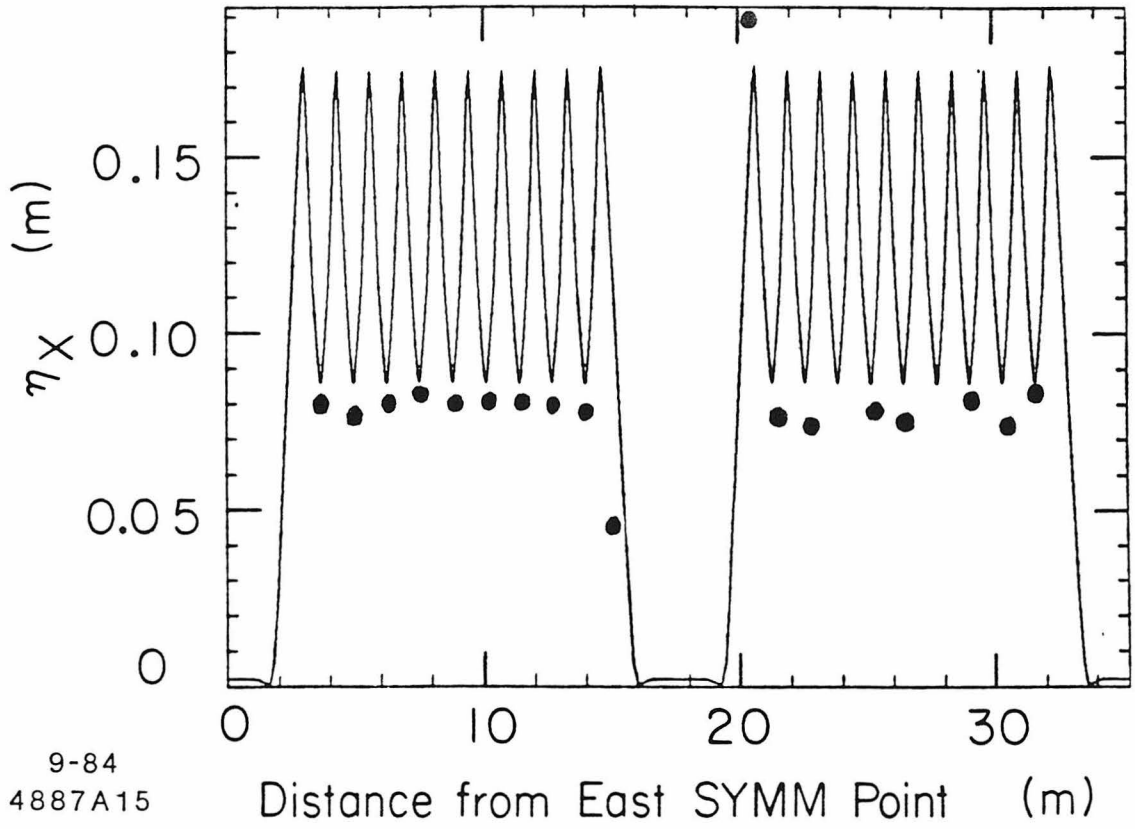

Figure 11. Measured horizontal dispersion plotted together with the model predictions.

§§4.5.3 *Using the Synchrotron Light Monitor*

The synchrotron light monitor affords an opportunity to check the dispersion at the source point of the light. In the damping ring, the dispersion is supposed to be very close to zero at that location and it was important to verify this fact. This measurement is also important for estimating the contribution to the beam size there due to the dispersion during the measurements of emittance.

§4.6 Measuring and Correcting the Chromaticity

Chromaticity is defined as the change in tune as a function of the relative energy deviation:

$$\Delta\nu = \xi \cdot \frac{\Delta p}{p}$$

and characterizes the change in focusing for a change in particle energy. It is the integral around the ring of the focusing strength, weighted by the β function:

$$\xi = -\frac{1}{4\pi} \oint k(s)\beta(s)\, ds$$

The focusing in the damping ring is rather strong in order to achieve a very small emittance. The natural chromaticity of the ring is correspondingly rather high for such a small ring:

$$\xi_x = -7.8, \qquad \xi_y = -8.3$$

The most important effect caused by negative chromaticity is the head–tail instability[5], which limits the stored beam intensity to very low values. The finite

chromaticity makes the betatron oscillation frequency dependent on the relative energy deviation of a particle. Since particles undergo energy or synchrotron oscillations, the betatron frequency is being driven periodically. In addition, the particles in the front of the bunch leave an electromagnetic wake that acts on the particles in the back. Thus the motion of the head and the tail of the bunch become coupled. The mode when the head and the tail oscillate in phase is damped when the chromaticity is positive.

In order to correct the chromaticity, the sextupole magnets are introduced in the ring in places with non–zero dispersion. In these magnets the gradient of the magnetic field is zero on the axis and rises linearly with distance away from the center. Thus particles with different energies see different focusing effect due to these magnets. Arranged properly then, they can bring chromaticity to a positive value.

A given sextupole contributes to the chromaticities in both planes, improving the situation in one plane and worsening it in the other plane. A thin horizontally focusing sextupole of integrated strength m_F (m^{-2}) contributes

$$\Delta\xi_x = \frac{1}{4\pi} m_F \eta \beta_x, \qquad \Delta\xi_y = -\frac{1}{4\pi} m_F \eta \beta_y$$

and it is clear that we have to position at least two sets of sextupoles in places where the β functions in the two planes are very different.

The chromaticity correction scheme in the Damping Ring employs a large number of sextupole elements positioned at the ends of the dipole magnets (see **Chapter 3**). Their strength is fixed and is designed to compensate for the bulk of the chromaticity at $E = 1.21$ GeV. The measured values for $E = 1.21$ GeV were

$$m_F = 27.53\, m^{-2}, \qquad m_D = -23.31\, m^{-2}$$

In addition, four variable sextupoles are provided in the matching sections to allow for the chromaticity variation of

$$\Delta\xi_{x,y} \approx \pm 1$$

They are arranged into two families, SF and SD.

§§4.6.1 *Measuring chromaticity*

The betatron tunes are measured as a function of RF frequency which, in effect, measures the dependence of the tunes on energy deviation (see the section on dispersion measurements). The chromaticity can then be calculated from the following formula

$$\xi_{x,y} = -\alpha f_{RF} \frac{\Delta \nu_{x,y}}{\Delta f_{RF}} = -\alpha h \frac{\Delta f_{x,y}}{\Delta f_{RF}}$$

where h is the harmonic number

$$h = \frac{f_{RF}}{f_{rev}}$$

$f_{x,y}$ are the frequencies of transverse betatron oscillations one measures directly on the spectrum analyzer and f_{rev} is the revolution frequency.

The first measurement of the chromaticity at 0.95 Gev is presented in Fig. 12 and was made with the variable sextupoles turned off in order to find out how much of the negative chromaticity is being compensated by the fixed sextupoles at this energy. The vertical chromaticity was negative. Later on, using both families of variable sextupoles with the same polarity, we were able to bring the vertical chromaticity to a slightly positive value. This was possible after we found a better matched optics in the ring.

The difficulties we experienced in correcting the chromaticity prompted design changes in the sextupoles and their distribution in the new damping ring for positrons and in the rebuilt of the electron ring. The changes in the design are discussed in **Chapter 5** on the results.

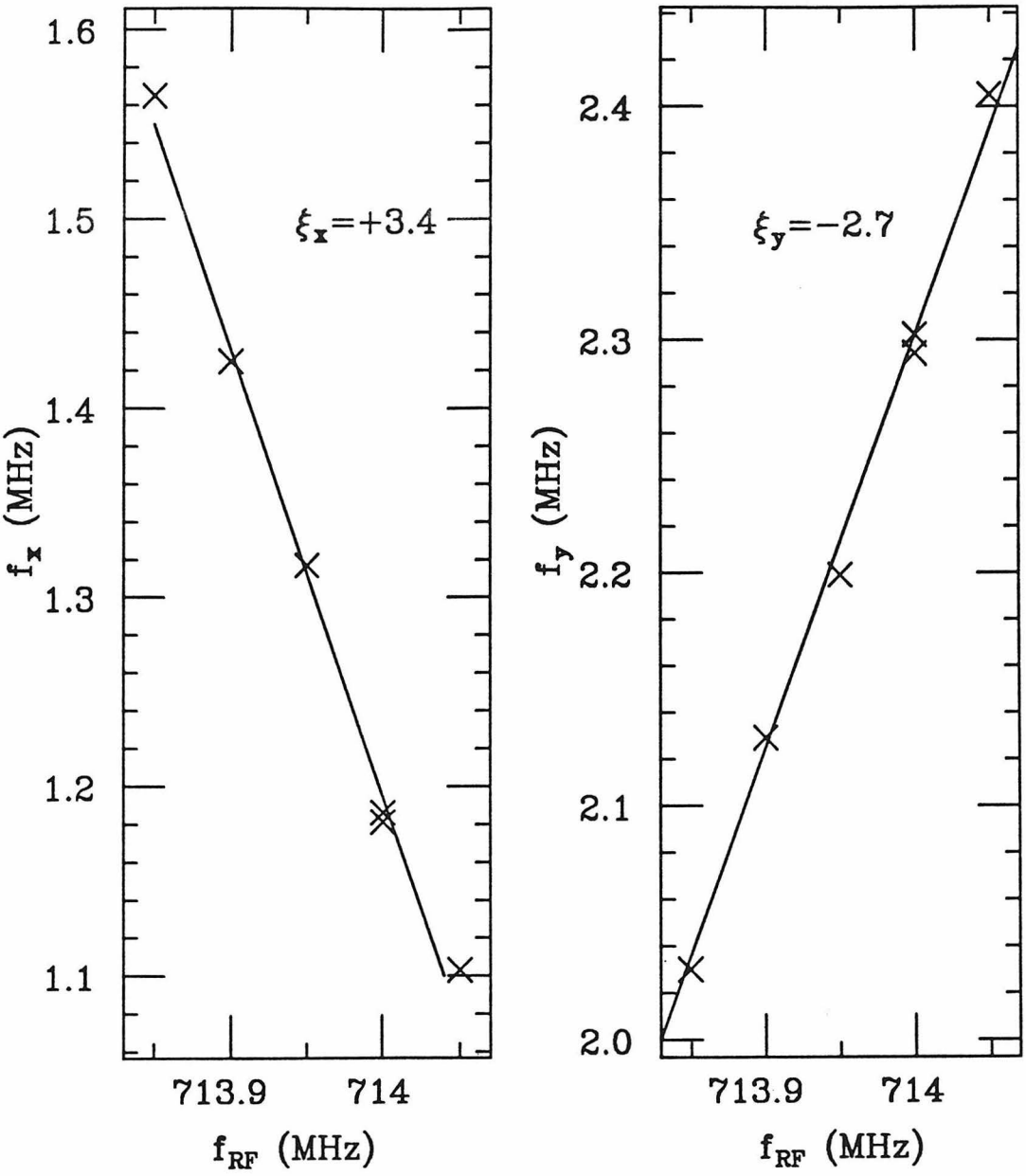

Figure 12. First chromaticity measurement at 0.95 Gev. The variable sextupoles are off.

§4.7 Bunch Length

The SLC design requires very short bunches for reinjection back into the linac from the damping ring in order to minimize the energy spread in the linac. Since the equilibrium rms bunch length in the damping ring is on the order of 1 cm, and the required bunch length for the linac is 0.5 mm, a bunch length compressor is built into the Ring–to–Linac transport line. The compression scheme utilizes the fact that the relative energy spread of the bunch coming out of the damping ring is very small, on the order of 10^{-3}, and can be exchanged for the bunch length. A section of a standard disk–loaded wave guide (a section of S–band linac) is placed in the beginning of the transport line and the S–band RF is timed so that the bunch passes the structure at a zero crossing of the accelerating field. The particles in the front of the bunch are accelerated while the ones in the back are decelerated. The rest of the transport line is non–isochronous *i.e.* the time it takes a particle to pass the line depends on its energy. The front particles, with higher energy, will take longer to reach the linac then the particles in the back, with lower energy. This is because, for example, higher energy particles are not focused enough and their trajectory is longer, in other words, the line is operated above the transition energy[6]. The bunch length will shrink. In Fig. 13 the scheme is illustrated with the phase space plots.

An important parameter in this scheme is the equilibrium bunch length in the ring. The equilibrium between the damping of energy–phase, or synchrotron, oscillations and their excitation by the quantum fluctuations results in the longitudinal phase space distribution with the bunch length related to the energy spread as[5]

$$\sigma_z = c\frac{\alpha}{2\pi f_s}\cdot\frac{\sigma_E}{E} = cT_0\sqrt{\frac{\alpha E}{2\pi h e V_{RF}\cos\phi_s}}\cdot\frac{\sigma_E}{E}$$

where we have written the synchrotron oscillations frequency in terms of the RF

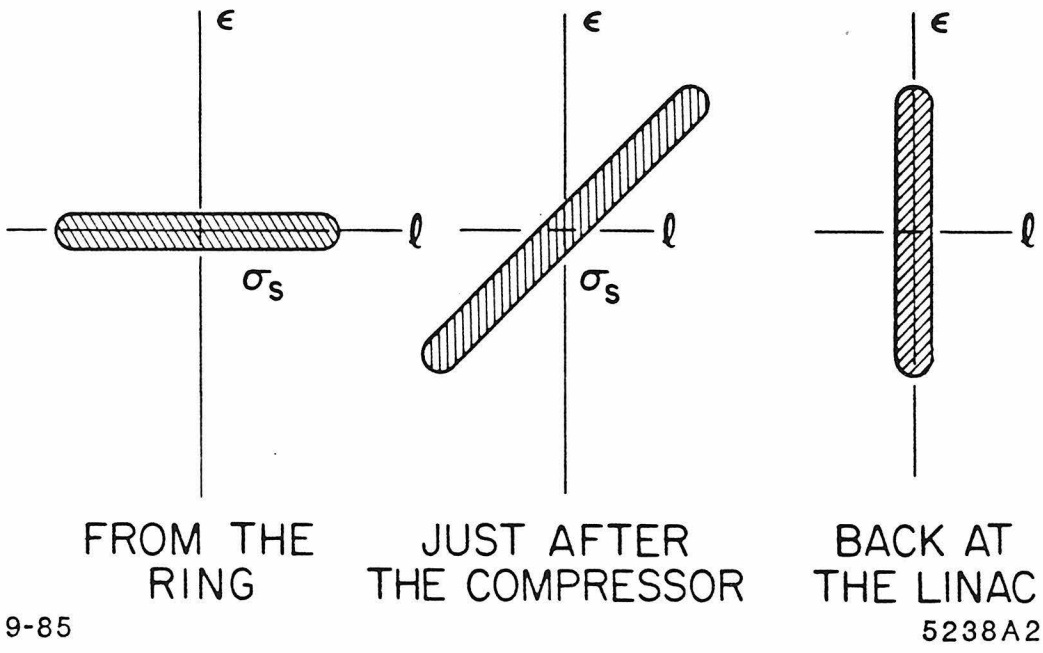

Figure 13. Phase space diagrams illustrating the bunch length compression scheme.

system and ring parameters. The design values for the bunch length and the energy spread in the damping ring at $E = 1.21\,\text{GeV}$ and $V_{RF} = 800\,\text{KeV}$ are

$$\sigma_z = 5.8\,mm \qquad \frac{\sigma_E}{E} = 7.4 \cdot 10^{-4}$$

§§4.7.1 *Streak camera*

The bunch length was measured in the linac after the reinjection using a streak camera.[24,25] A quartz Cherenkov light radiator was inserted into the beam in the linac and the time duration of the light pulse was measured with a streak camera. These measurements were made at different settings of the peak voltage in the compressor accelerating section. In particular the measurement with the compressor off gave us the equilibrium bunch length in the ring. The results are given in Fig. 14 and the measured value of $\sigma_z = 7.4\,mm$ agrees well with the predicted bunch length for the $E = 0.95$ Gev and $V_{RF} = 300\,\text{Kev}$. The energy spread was taken from an optics program predictions for that energy.

§§4.7.2 *Using the Compressor*

Another way to measure the bunch length is to extract it from the horizontal beam size measurements on the profile monitor screen that is positioned shortly after the compressor. The beam size there is dominated by the energy spread introduced by the compressor because the dispersion at this point of the transport

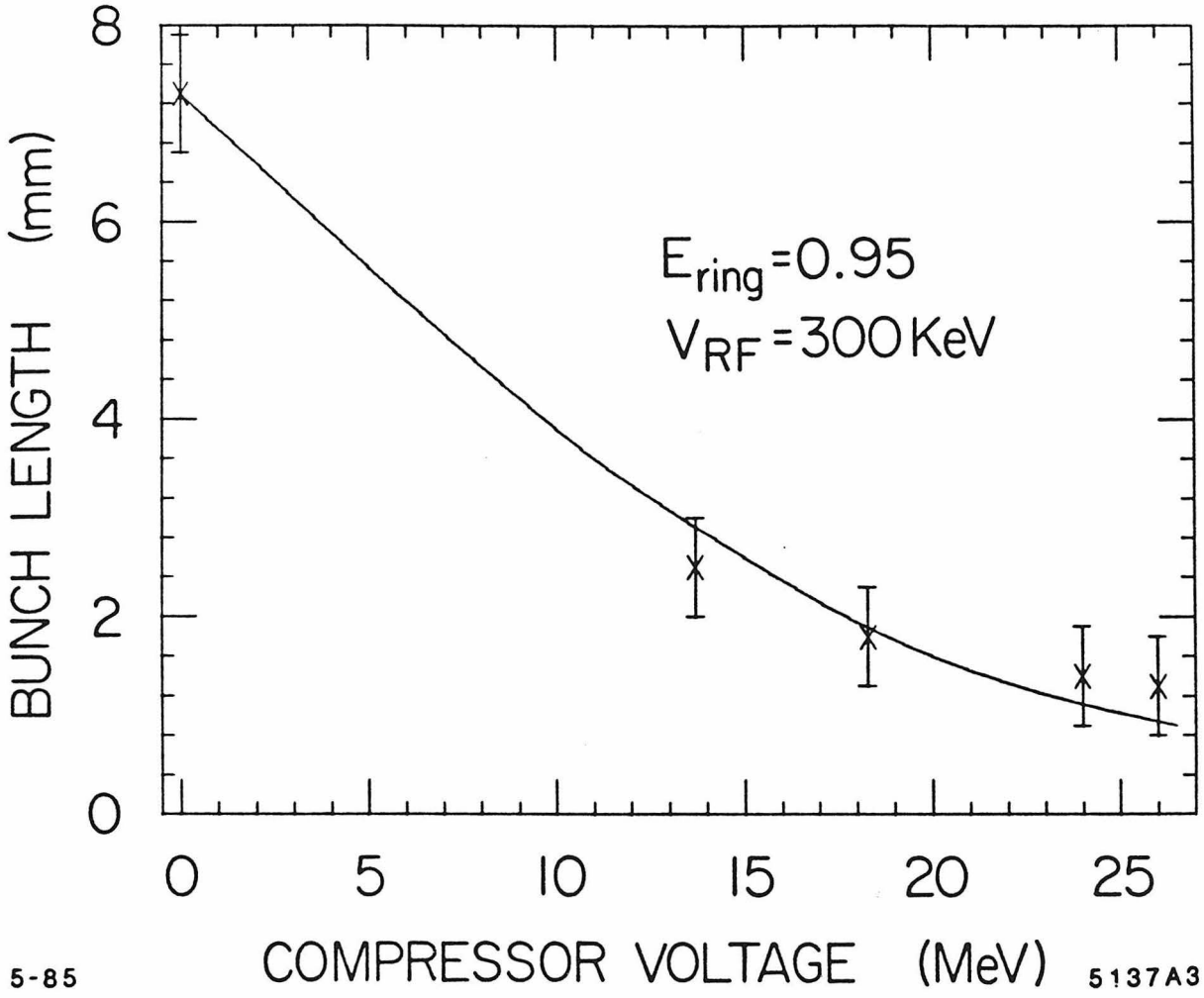

Figure 14. The results of the bunch length measurements using a streak camera.

line is high:

$$\sigma_x = \sqrt{\varepsilon_x \beta_x + \eta_x^2 \delta^2} \approx \eta_x \delta_c$$

where β_x, η_x are the envelope function and dispersion at the screen, ε_x is the output emittance (the measurements can be done with long storage times) and δ and δ_c are the total energy spread and the energy spread due to the compressor. At the design power the compressor introduces up to 2% energy spread, to be compared to a typical storage ring energy spread of 0.1% .

The η_x at the screen can be measured directly by using the compressor at low power, timing the S–band RF so that the bunch rides on the crest of the wave, *i.e.* is being accelerated, and measuring the shift of the beam spot centroid as a function of energy deviation.

The contribution to the energy spread from the compressor is

$$\delta_c = \frac{\hat{V}_C}{E_R} \sin \frac{2\pi\sigma_z}{\lambda_c}$$

where $\hat{V}_C$ is the peak accelerating voltage in MeV, E_R is the energy of the ring, $\lambda_c = 10.5\,\text{cm}$ is the S–band wavelength and σ_z is the length of the bunch coming out of the damping ring. Then the bunch length can be calculated from the measured beam size:

$$\sigma_z = \frac{\lambda_c}{2\pi} \arcsin \frac{E_R \sigma_x}{\eta_x \hat{V}_C}$$

The results of this measurement also agreed well with the calculated predictions. Both methods were used with bunch intensities on the order of $2 - 3 \cdot 10^9$ particles.

§4.8 Damping Times

Damping time is the time it would take an electron to radiate its energy away if it continued to radiate at the same rate.[5] If the energy loss per turn is U_0, we can write

$$\tau_\epsilon = \frac{ET_0}{U_0}$$

where T_0 is the revolution period. In fact, for the three degrees of freedom, the damping times are

$$\tau_x = \frac{\tau_0}{J_x} \qquad \tau_y = \frac{\tau_0}{J_y} \qquad \tau_\epsilon = \frac{\tau_0}{J_\epsilon}$$

where

$$\tau_0 = \frac{2ET_0}{U_0}$$

and $J_{x,y,\epsilon}$ are the so–called damping partition numbers, for which a rather general result is true[26]

$$J_x + J_y + J_\epsilon = 4$$

The damping ring is designed to have very short damping times since the SLC timing scheme allows only very short time for the bunches to damp down to the design emittance. For the 180 pps operation the allowed time is 5.56 msec. The design damping times at $E = 1.21\,\text{GeV}$ are

$$\tau_x = 3.06\,\text{msec} \qquad \tau_y = 3.06\,\text{msec.}$$

§§4.8.1 *Profile Monitor Measurements*

Beam size on the profile monitor in the beginning of the Ring To Linac transport line was measured as a function of time the beam was stored in the

damping ring. Beam size measurements are similar to the ones done to measure emittance and are described in the next section. The damping times were then obtained from a fit of the results to an exponential. We also obtained the damping times from the emittance measurements at different storage times.

The results at 0.95 GeV were

$$\tau_x = 6.7\,\text{msec} \qquad \text{and} \qquad \tau_y = 4.6\,\text{msec}$$

and measurements at the 1.21 GeV gave

$$\tau_x = 3.1\,\text{msec} \qquad \text{and} \qquad \tau_y = 6.8\,\text{msec}$$

We do not understand well the systematic errors in these measurements connected with trying to measure very small beam spots on the profile monitor as well as possible errors that are introduced by an interplay between the coherent and incoherent damping in the ring. The technique is under study.[20]

§§4.8.2 *Radiation Loss per Turn*

Returning to the definitions of the damping times we can write the sum of the damping decrements as

$$\frac{1}{\tau_x} + \frac{1}{\tau_y} + \frac{1}{\tau_\epsilon} = \frac{U_0}{ET_0}(J_x + J_y + J_\epsilon) = \frac{2U_0}{ET_0}$$

By measuring the radiation loss per turn U_0 we were able to determine the sum of the damping decrements.[27] Assuming the predicted values for the partition numbers, we then have a good estimate of the damping times.

Due to phase focusing, the bunch in the ring adjusts itself in time with respect to the RF waveform, so that the energy it gains is equal to the energy lost in one turn. This defines the synchronous phase angle ϕ_s and we can write

$$U_0 = V_{RF} \sin \phi_s$$

where V_{RF} is the peak RF voltage. If we change the RF voltage, the phase angle ϕ_s will change accordingly, to maintain the above relationship, as shown in Fig. 15.

Measuring the phase between the beam and the RF as a function of V_{RF} we can determine U_0. In order to do that, a signal from the RF cavities was compared on a vector voltmeter to a filtered 714 MHz harmonic of the bunch intensity monitor signal. The phase difference between the two, obtained from the device, was plotted on the X–Y recorder as a function of the RF voltage. A typical curve obtained in this manner is shown in Fig. 15. The above relationship between V_{RF} and ϕ_s is true for a single particle. Due to the interaction of the bunch with the surroundings, there is additional energy loss that depends on the intensity of the bunch; it is usually called *parasitic mode loss.* We made the measurements at various intensities and extrapolated the results to zero intensity to eliminate this loss.

The radiation loss per turn at $E = 1.21\,\text{GeV}$ was measured to be

$$U_0 = 84.0\,KeV$$

and the sum of the damping decrements was measured as

$$\Sigma \frac{1}{\tau_i} = \frac{4U_0}{ET_0} = 1180.2\,\text{sec}^{-1}$$

The vertical damping time therefore was measured to be

$$\tau_y = 3.4\,\text{msec}$$

The comparison of the experimental results to the expected damping times is part of the discussion of results in **Chapter 5.**

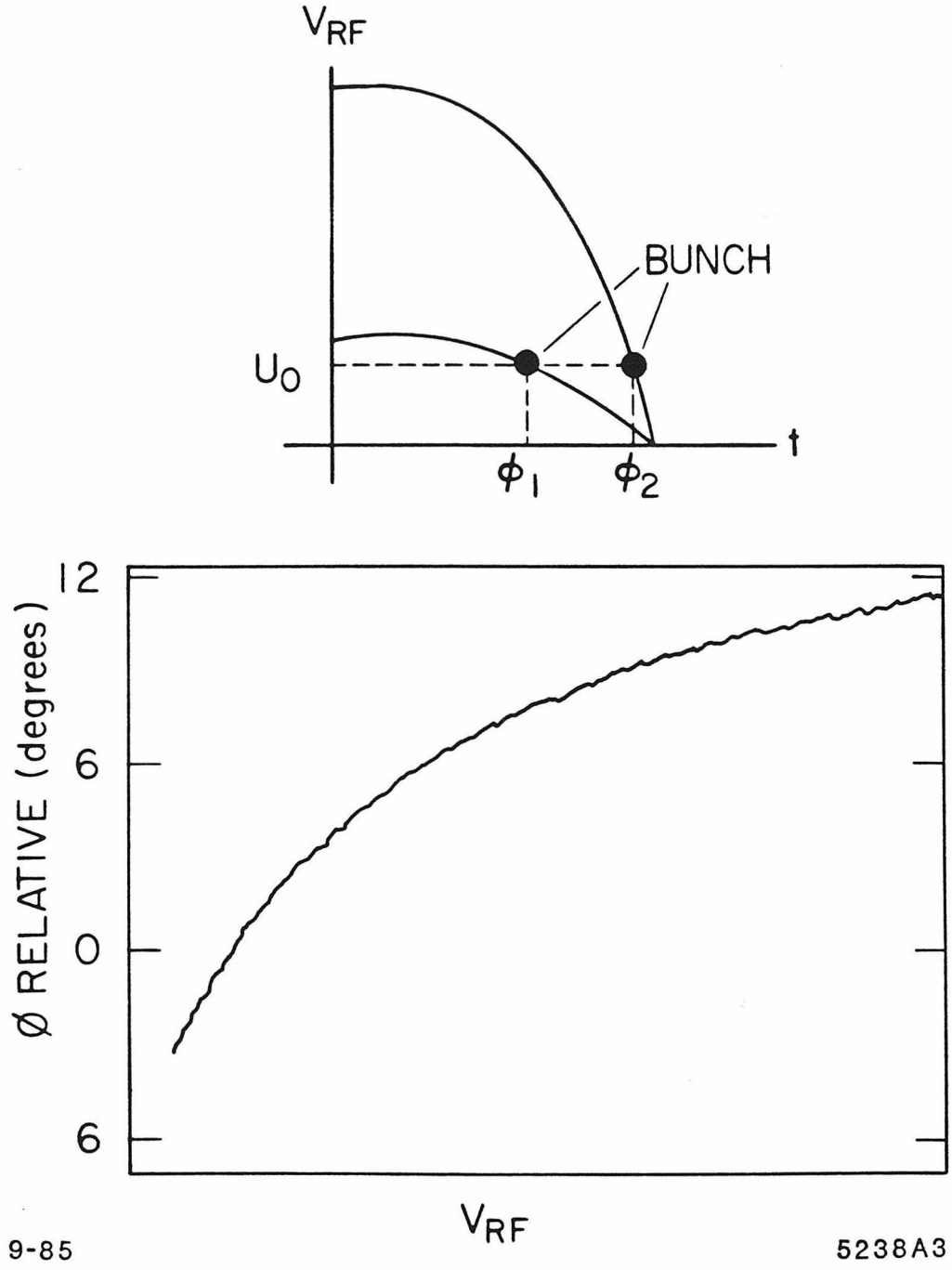

Figure 15. The schematic drawing of the radiation loss per turn measurements

§4.9 Emittance Measurements

Three ways we have used to measure emittance of the Damping Ring beam are described in this section. The quantity measured in all three methods is the beam size, and the emittance is then calculated, using other machine parameters.

§§4.9.1 *Scrapers Method*

Theory

The distribution of particles in a bunch is Gaussian in an ideal linear machine.[5] In a dispersion-free region the standard deviation of the transverse beam distribution can be expressed as

$$\sigma = \sqrt{\beta\varepsilon}$$

where β is the envelope function at the azimuth in question and ε is the equilibrium emittance of the beam. In fact this equation may be regarded as the definition of emittance. Quantum fluctuations in particle amplitudes due to the emission of synchrotron radiation populate the distribution including its tails and if an obstruction is introduced at some distance away from the beam center, some of the particles will be lost. The "quantum" lifetime of the beam due to an aperture at a distance X away from the beam centroid is given by the following simple formula[5]

$$\tau_q = \frac{\tau_\epsilon}{2}\frac{e^\xi}{\xi} \qquad \xi = \frac{n^2}{2} \qquad n = \frac{X}{\sigma}$$

where τ_d is the damping time and n is X in units of σ. These formulae are valid

provided $n \gg 1$. We use the scrapers to introduce such an aperture and measure the lifetime of the beam as a function of scraper position.

The damping time in the Damping Ring is on the order of a few milliseconds, and if the aperture is more than 6 σ away from the beam, the quantum lifetime becomes a few hours. At that point other processes, like multiple Coulomb scattering on the residual gas, become dominant in determining the distribution.

Measurements

The device consists of four copper jaws, each powered by a stepping motor controlled by a computer. The stepping motor calibration is 8 steps per 0.001 inches. The movement of a jaw is limited by two micro switches that define "inner" and "outer" limits. When not in use, jaws are parked at the outer limit. Only one jaw at a time can be moved from it's parked position.

Starting from the outer limit, a jaw was moved inward in steps and lifetime of the beam was measured at each step.

Analysis of the data

A very convenient way to display the data is to calculate n from the formula given above for the quantum lifetime and plot it *vs* the scraper position. If the theory described above gives correct description of the beam distribution, the result would be a straight line pointing towards the origin. A typical set of data is shown in Fig. 16. The curve is certainly not a straight line, which shows that in a real machine the tails of the distribution deviate from a Gaussian due to processes like beam–gas bremsstrahlung or multiple Coulomb scattering on the residual gas, that contribute to the tail population and hence to the lifetime of the beam. Only when the scraper is driven well into the core of the beam the lifetime becomes dominated by the quantum fluctuations and the linear dependence is recovered. Unfortunately, the quantum lifetime regime is entered only when the lifetime becomes rather short, on the order of a minute. Such short lifetimes were difficult to measure with the available equipment. The measured emittance was heavily influenced by those points. In Fig. 17 data are reproduced from the run where lifetimes down to a

fraction of a minute were measured, providing better defined straight line.

The results of the measurements at 0.95 GeV were

$$\varepsilon_x = 1.1 \cdot 10^{-8}\, m\,rad \qquad \text{and} \qquad \varepsilon_y = 0.5 \cdot 10^{-8}\, m\,rad$$

or the equilibrium horizontal emittance with no coupling

$$\varepsilon_{x0} = \varepsilon_x + \varepsilon_y = 1.5 \cdot 10^{-8}\, m\,rad$$

§§*4.9.2 Synchrotron Light Monitor*

The synchrotron light monitor provides a direct measurement of the core of the beam distribution, as opposed to the previous method that studies the tails of the distribution to extract the core size.

The monitor uses light emitted by the beam in the bending magnet adjacent to the injection straight section. The location, shown in Fig. 18, is the only place in the damping ring free from the magnets that allows to look into a dipole magnet.

The light is reflected by a mirror inside the vacuum chamber, passes the quartz vacuum window and is imaged onto a TV camera by a single achromatic lens (focal length 450 mm) that is positioned just outside the vacuum window.

The mirror is made out of a piece of molibdenum and is polished flat to quarter of the typical optical wavelength. Its position inside the vacuum chamber is remotely controlled. It is water cooled. The light, which travels along the tangent to the trajectory of the beam inside the bending magnet, makes 1° angle with the axis of the straight section at the location of the mirror. The angle of the mirror surface is 44.5° so it sends the light normal to the axis of the straight section, as shown in Fig. 18.

The light is imaged onto a remotely controlled TV camera. The video signal is sent upstairs to the control room and is processed with a Colorado Video device

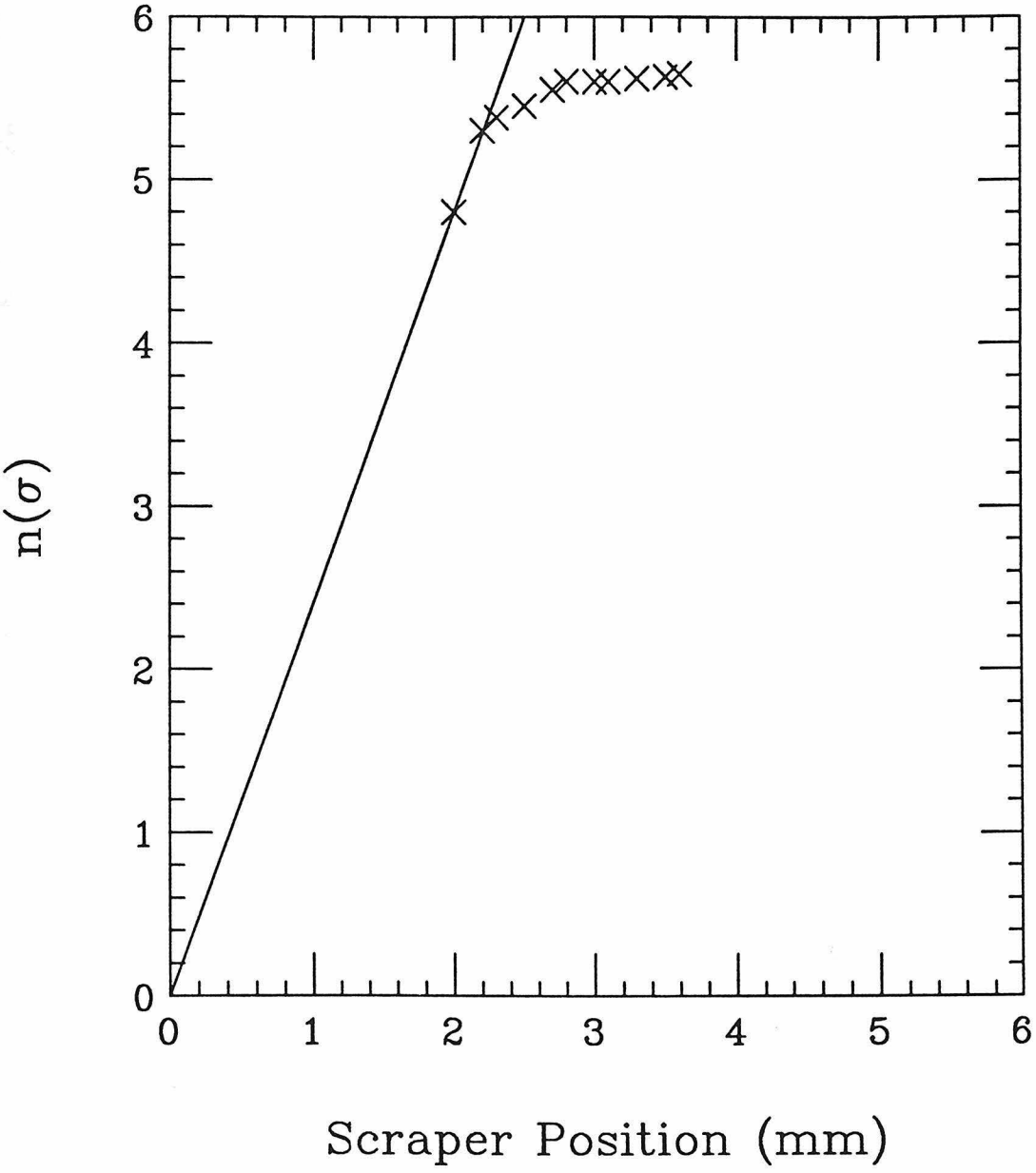

Figure 16. Calculated from lifetime measurements position of the scraper *vs* the real scraper position.

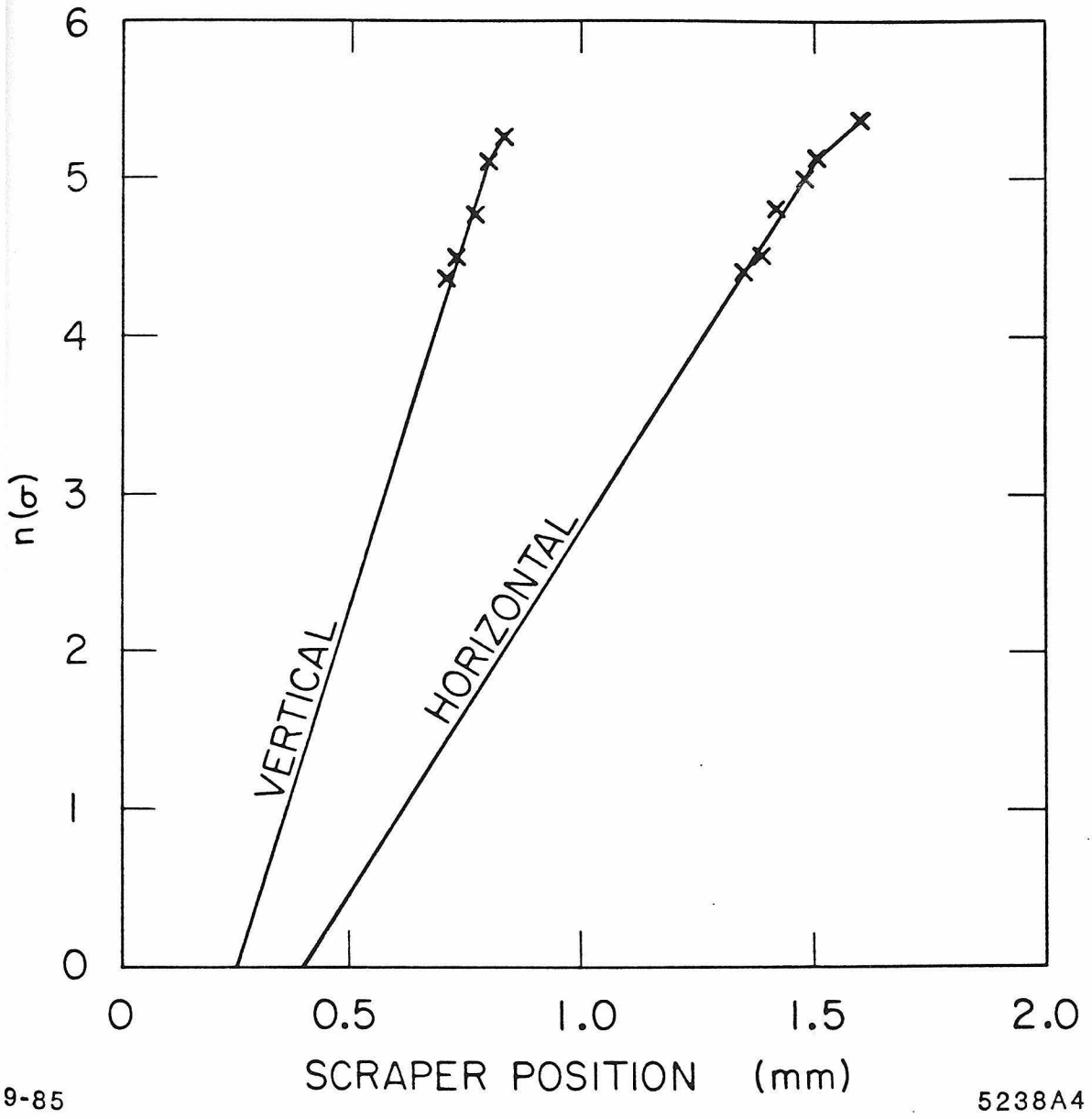

Figure 17. Very short lifetimes data.

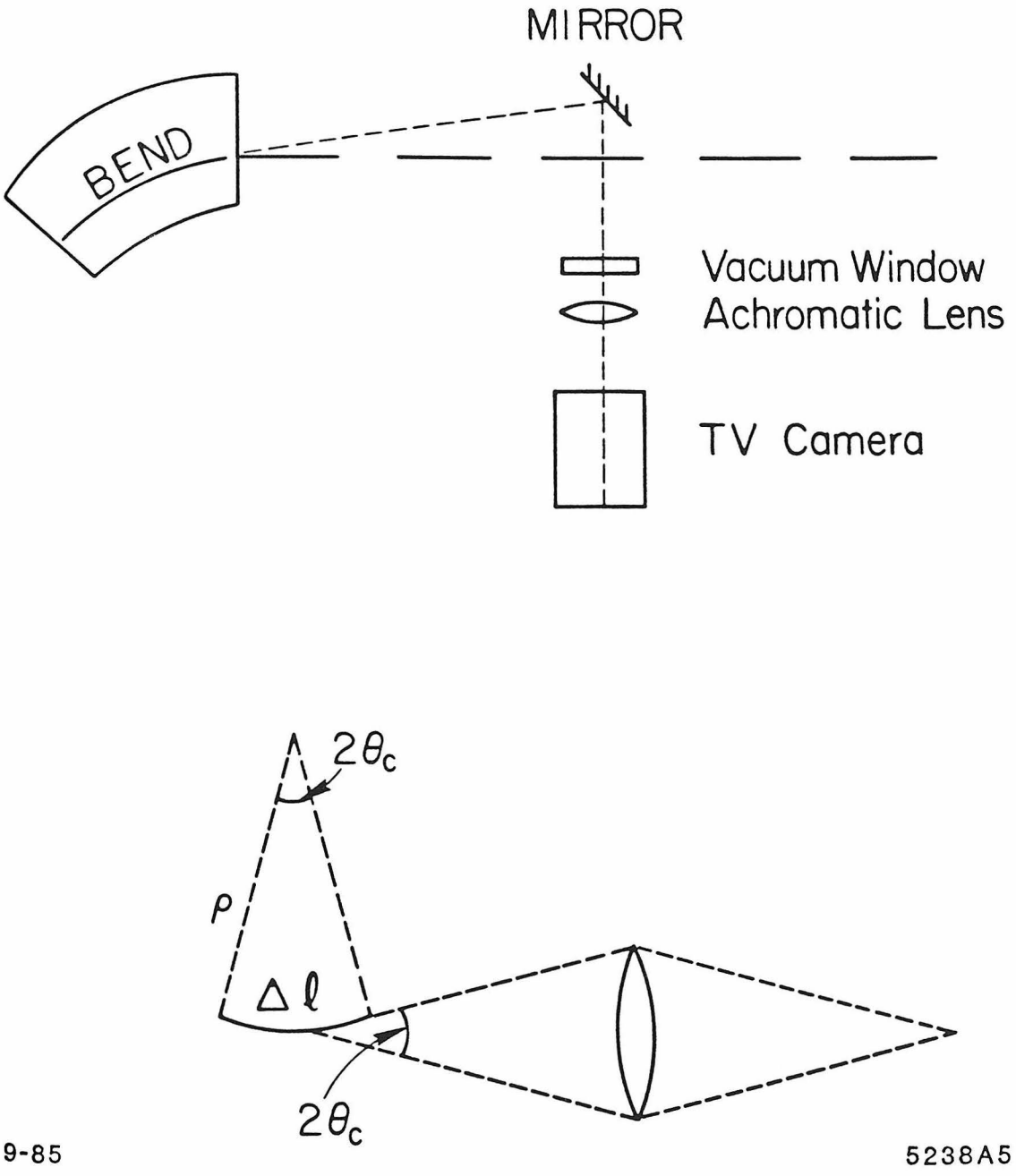

Figure 18. The general layout of the Synchrotron Light Monitor and surrounding ring components

(see section on quad and screen method).

Synchrotron light is strongly peaked in the forward direction and is mostly contained in a cone with a characteristic half opening angle

$$\theta \approx \frac{1}{\gamma} = 0.4\,\mathrm{mrad}$$

for the photons with energy close to the critical photon energy, which in the damping ring at $E = 1.21\,GeV$ is

$$u_c = 1.9\,KeV$$

For the light in the visible part of the spectrum the typical opening angle is much wider[28]

$$\theta_c = (\frac{3c}{\omega\rho})^{\frac{1}{3}} = (\frac{3\lambda}{2\pi\rho})^{\frac{1}{3}}$$

where $\rho = 2\,\mathrm{m}$ is the bending radius. If the angular acceptance of the monitor matches this angular divergence, as shown in Fig. 18, the monitor collects the light from a part of the trajectory of length

$$\Delta l = 2\rho\theta_c = (\frac{12}{\pi})^{\frac{1}{3}}\lambda^{\frac{1}{3}}\rho^{\frac{2}{3}}$$

For $\lambda = 600\,\mathrm{nm}$, $\theta_c = 5.2\,\mathrm{mrad}$ and $\Delta l = 2.1\,\mathrm{cm}$.

In the vertical plane the contributions to the resolution due to diffraction[29]

$$r_d \approx (\frac{\pi}{12})^{\frac{1}{3}}\lambda^{\frac{2}{3}}\rho^{\frac{1}{3}}$$

and the depth of field effect

$$r_f \approx \frac{\Delta l}{2}\theta_c = (\frac{3}{2\pi})^{\frac{2}{3}}\lambda^{\frac{2}{3}}\rho^{\frac{1}{3}}$$

are of the same order. In the horizontal plane, in addition, there is a contribution to the resolution due to the curvature of the orbit

$$r_\rho = \rho(1 - \frac{1}{2}\cos\theta_c) \approx \frac{1}{2}\rho\theta_c^2 = \frac{1}{2}r_f$$

The beam size at the source point of the light could have non–negligible contribution due to dispersion there

$$\sigma^2 = \varepsilon\beta + \eta^2\delta$$

where δ is the equilibrium energy spread of the beam. According to the design the dispersion at the light source is close to zero. We checked it by measuring the dispersion directly with the light monitor (see the section on dispersion measurements).

In determining the emittance from the measurements of the transverse beam sizes the β function values were taken from the model, which presented the biggest uncertainty in the measurements. The design values are

$$\beta_x = 0.7\,m \qquad \beta_y = 6.6\,m$$

For example, at $E = 0.95\,GeV$ we measured the transverse beam sizes

$$\sigma_x = 85\,\mu m \qquad \text{and} \qquad \sigma_y = 134\,\mu m$$

which correspond to the emittances of

$$\varepsilon_x = 1.0 \cdot 10^{-8}\,m\,rad \qquad \text{and} \qquad \varepsilon_y = 0.3 \cdot 10^{-8}\,m\,rad$$

or the equilibrium horizontal emittance with no coupling

$$\varepsilon_{x0} = \varepsilon_x + \varepsilon_y = 1.3 \cdot 10^{-8}\,m\,rad$$

The discussion of the comparisons with the expected values for the emittance is given in **Chapter 5** on the results.

§§4.9.3 *Extracted Beam*

An independent measurement of the Damping Ring beam emittance was made using the extracted beam from the Damping Ring. Measurements were made in the beginning of the Ring to Linac transport line as well as downstream in the linac itself. The method has been used at SLAC extensively[30].

Quad and Screen Method

A typical setup consists of an adjustable quadrupole lens and a profile monitor some distance downstream of it. Let us consider the horizontal emittance measurement, the vertical case being entirely analogous. For different strengths of the lens the width of the beam profile on the screen is measured on a profile monitor. The input beam is kept unaltered during the measurement. One then plots the square of the width as a function of the lens strength k. The resulting curve is a parabola. The three coefficients of the parabola are sufficient to determine the emittance of the input beam. To show that this is true we will use the σ matrix formalism summarized in **Appendix A.**

Let the input beam be represented by the σ^{in} matrix and the transfer matrix for the transport line between the lens and the screen be $\mathbf{R}_{tr}$.

$$\mathbf{R}_{tr} = \begin{pmatrix} r_{11} & r_{12} \\ r_{21} & r_{22} \end{pmatrix}$$

(We are assuming that the beam is "uncoupled" so that the two–by–two matrix formulation is valid. More on this point later.) The transfer matrix for the quad in the thin lens approximation is

$$\mathbf{Q} = \begin{pmatrix} 1 & 0 \\ k & 1 \end{pmatrix}$$

where k is the strength of the quad (measured in units of m^{-1}) is the inverse of the focal length. If k is positive, this matrix represents a defocusing lens. The total

transfer matrix for the measuring system is then

$$\mathbf{R} = \mathbf{R}_{tr}\mathbf{Q}$$

and the σ^S representing the beam at the screen is

$$\sigma^S = \mathbf{R}\sigma^{in}\mathbf{R}^T \tag{1}$$

where $\mathbf{R}^T$ is the transpose of $\mathbf{R}$. Multiplying the matrices we obtain

$$\sigma_{11}^S = (r_{11} + kr_{12})^2\sigma_{11}^{in} + 2r_{12}(r_{11} + kr_{12})\sigma_{12}^{in} + r_{12}^2\sigma_{22}^{in} \tag{2}$$

The measurement of the width of the beam profile on the screen determines the σ_{11}^S element of the beam matrix. It is indeed a quadratic function of k and fitting the data to a parabola one can extract the three elements that determine the symmetric beam matrix for the input beam. In particular, the emittance of the incoming beam is

$$\varepsilon_x = \sqrt{det\sigma^{in}} = \sqrt{\sigma_{11}^{in}\sigma_{22}^{in} - (\sigma_{12}^{in})^2} \tag{3}$$

Measuring setup in RTL

The optics used for the measurements is shown in Fig. 19. The four so-called matching quads, all individually controlled, are used to focus the beam spot on the downstream RTL profile monitor PRO4A.

The profile monitor consists of a remotely controlled fluorescent screen[31] that can be inserted into the beam and a TV camera viewing the screen through a vacuum window. The screen has dark $300 - \mu m$ diameter dots that are $1.5mm$ apart.

The TV camera has an RCA Ultricon^{TM} tube together with a lens that provides a magnification of $\times 2$ and has a remotely controlled iris.

The video signal is piped up into the control room where it is processed using a Colorado Video^{TM} device[32] that allows to select and measure the amplitude of

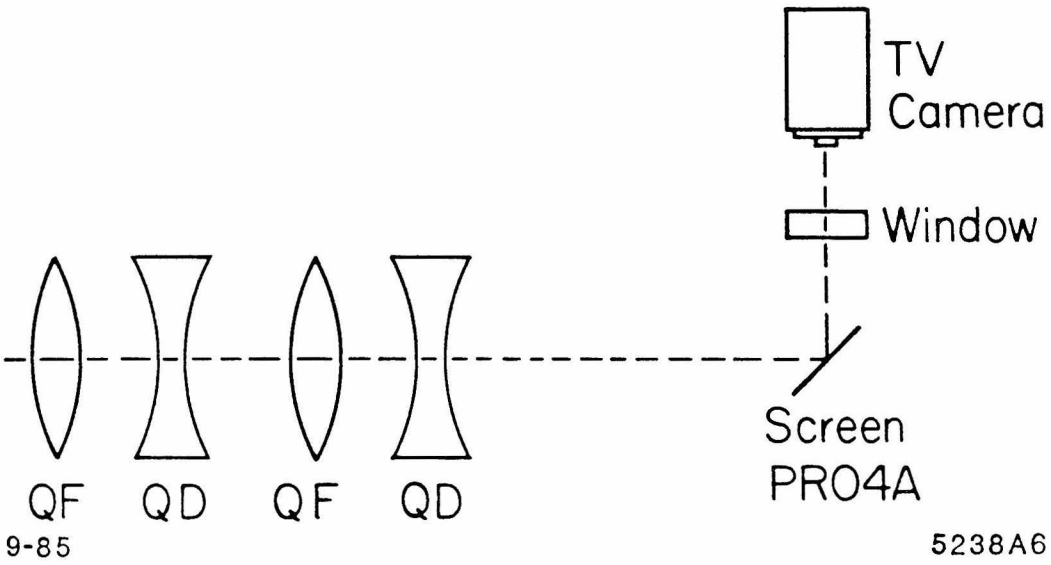

Figure 19. Optics setup in RTL.

a single horizontal scan line or a set of vertical samples. This section of the beam profile can then be viewed on a scope. Alternatively the section can be digitized, input into the computer and a gaussian can be fit to the profile.

The Measurement Procedure

For different settings of one of the quads the beam width and height were measured using the hardware described above and the results were fitted with a parabola. The parameters of the parabola thus determined were used to calculate the emittance of the beam. In Fig. 20 the results of a typical measurement are displayed. The errors on the individual points were calculated by measuring the profile for a given setting of the quad several times and adding in quadrature the known systematic errors due to the finite resolution of the system.

The Resolution and Errors

It is estimated[33] that the response of the measuring system to an infinitely thin bright line results in a measurement of the width of that line of approximately

$$\sigma_{res} \approx 80\mu m$$

The resolution error is added in quadrature to the beam size so it will result in the upwards shift of the parabola and from the Eqn. 2 it is clear that the σ_{22}^{in} term will be overestimated. From the Eqn. 3 then it follows that the emittance will be overestimated. From the same equation one can see that a good way to fight the error in emittance due to the resolution is to decrease the σ_{11}^{in} term for the incoming beam at the quad or, in other words, to make the beam there as small as possible.

The results

The results of the measurements of the emittance at 1.21 GeV are

$$\varepsilon_x = (2.2 \pm 0.2) \times 10^{-8}\, m\,rad \qquad \text{and} \qquad \varepsilon_y = (0.8 \pm 0.4) \times 10^{-9}\, m\,rad$$

and the errors reflect the averaging of the results of many measurements.

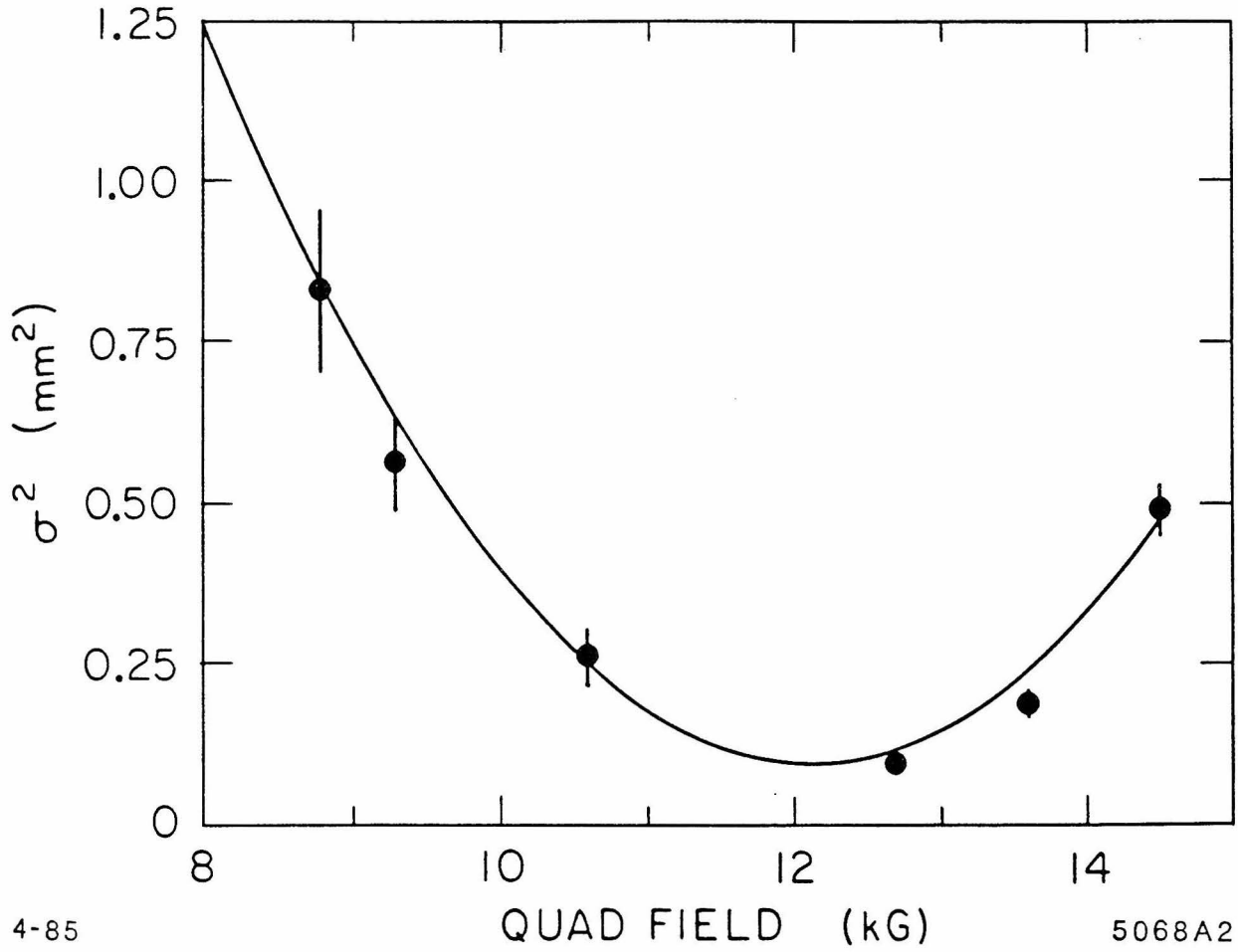

Figure 20. Fitted horizontal emittance data.

The Case of a Coupled Beam

The method described above will fail in some degree if the beam is "coupled" i.e., if the two–by–two off–diagonal submatrices of the sigma matrix are not zero. Then the measurements will overestimate the true invariant of motion—the four dimensional volume occupied by the beam in the transverse phase space. An uncoupled beam is represented by a block diagonal beam matrix

$$\sigma = \begin{pmatrix} \sigma_{11} & \sigma_{12} & 0 & 0 \\ \sigma_{12} & \sigma_{22} & 0 & 0 \\ 0 & 0 & \sigma_{33} & \sigma_{34} \\ 0 & 0 & \sigma_{34} & \sigma_{44} \end{pmatrix} = \begin{pmatrix} \mathbf{X} & \mathbf{0} \\ \mathbf{0} & \mathbf{Y} \end{pmatrix}$$

Four dimensional phase volume occupied by the beam at equilibrium, or four dimensional emittance, in this case, is just

$$\varepsilon_4 = \sqrt{det\sigma} = \sqrt{det\mathbf{X} det\mathbf{Y}} \tag{4}$$

and the experiment gives the right result.

If coupling is present, in general, the beam is represented by a positive-definite symmetric matrix

$$\sigma = \begin{pmatrix} \sigma_{11} & \sigma_{12} & \sigma_{13} & \sigma_{14} \\ \sigma_{12} & \sigma_{22} & \sigma_{23} & \sigma_{24} \\ \sigma_{13} & \sigma_{23} & \sigma_{33} & \sigma_{34} \\ \sigma_{14} & \sigma_{24} & \sigma_{34} & \sigma_{44} \end{pmatrix} = \begin{pmatrix} \mathbf{U} & \mathbf{C} \\ \mathbf{C}^T & \mathbf{V} \end{pmatrix}$$

If the transport line used for measurement does not contain any coupling elements (e. g. skewed quadrupoles), that is, if the transport matrix representing the beam line is of the form

$$\mathbf{R} = \begin{pmatrix} r_{11} & r_{12} & 0 & 0 \\ r_{21} & r_{22} & 0 & 0 \\ 0 & 0 & r_{33} & r_{34} \\ 0 & 0 & r_{43} & r_{44} \end{pmatrix} = \begin{pmatrix} \mathbf{R}_x & 0 \\ 0 & \mathbf{R}_y \end{pmatrix}$$

then from the transformation rules for the beam matrix,

$$\sigma_f = \mathbf{R}\sigma_i\mathbf{R}^T = \begin{pmatrix} \mathbf{R}_x\mathbf{U}\mathbf{R}_x^T & \mathbf{R}_x\mathbf{C}\mathbf{R}_y^T \\ \mathbf{R}_y\mathbf{C}^T\mathbf{R}_x^T & \mathbf{R}_y\mathbf{V}\mathbf{R}_y^T \end{pmatrix}$$

it is clear that the blocks **U** and **V** do not mix with the **C** blocks in an uncoupled channel. The determinants of the diagonal blocks are preserved since the determinants of $\mathbf{R}_x$ and $\mathbf{R}_y$ are equal to one. The method described in the previous section still determines only the **U** and **V** submatrices of the σ matrix.[34] The determinant of the full beam matrix is less than or equal to the product of the determinants of the diagonal blocks, and the four dimensional emittance will be overestimated in such a measurement

$$\varepsilon_4 \leq \varepsilon_x\varepsilon_y$$

The proof of this inequality is given in the **Appendix D.**

The beam extracted from the Damping Ring was coupled to some degree. Therefore these measurements could give only an upper limit on the emittance.

Estimates of the effect

If we take an uncoupled beam

$$\sigma_i = \begin{pmatrix} \sigma_{11} & \sigma_{12} & 0 & 0 \\ \sigma_{12} & \sigma_{22} & 0 & 0 \\ 0 & 0 & \sigma_{33} & \sigma_{34} \\ 0 & 0 & \sigma_{34} & \sigma_{44} \end{pmatrix} = \begin{pmatrix} \mathbf{H}_i & 0 \\ 0 & \mathbf{V}_i \end{pmatrix}$$

and take it through a thin lens skewed quad of strength k:

$$\mathbf{Q_{45}} = \begin{pmatrix} 1 & 0 & 0 & 0 \\ 0 & 1 & k & 0 \\ 0 & 0 & 1 & 0 \\ k & 0 & 0 & 1 \end{pmatrix}$$

the result will be

$$\sigma_f = \begin{pmatrix} \sigma_{11} & \sigma_{12} & 0 & k\sigma_{11} \\ \sigma_{12} & k^2\sigma_{33}+\sigma_{22} & k\sigma_{33} & k\sigma_{34}+k\sigma_{12} \\ 0 & k\sigma_{33} & \sigma_{33} & \sigma_{34} \\ k\sigma_{11} & k\sigma_{34}+k\sigma_{12} & \sigma_{34} & k^2\sigma_{11}+\sigma_{44} \end{pmatrix}$$

The determinant of the σ matrix did not change:

$$\epsilon_4^2 = det(\sigma_f) = det(\sigma_i) = det\mathbf{H}_i det\mathbf{V}_i$$

but the determinants of the diagonal submatrices now are

$$det\mathbf{H}_f = det\mathbf{H}_i + k^2\sigma_{11}\sigma_{33}$$

$$det\mathbf{V}_f = det\mathbf{V}_i + k^2\sigma_{11}\sigma_{33}$$

or in terms of emittance

$$\epsilon_{xf}^2 = \epsilon_{xi}^2 + k^2\beta_x\beta_y\epsilon_{xi}\epsilon_{yi}$$

$$\epsilon_{yf}^2 = \epsilon_{yi}^2 + k^2\beta_x\beta_y\epsilon_{xi}\epsilon_{yi}$$

where β_x and β_y are the values of the envelope functions at the location of the rotated quadrupole. And if the initial emittances are equal,

$$\epsilon_f^2 = \epsilon_i^2(1 + k^2\beta_x\beta_y)$$

The β function is rather high in parts of the extraction channel before the measuring apparatus. For example, at one of the quadrupoles $\beta_x = 20\,\mathrm{m}$ and $\beta_y = 60\,\mathrm{m}$. With the strength of that quadrupole $k = 4\,\mathrm{m}^{-1}$ and a half degree rotation around its axis, the resulting skewed quadrupole increases the measured emittance by 60%.

A new method that would permit the determination of all of the independent elements of the beam matrix has been proposed in Reference 34. It employs in addition to a normal quadrupole a rotated one.

§§4.9.4 *Summary*

We summarize here the results of the emittance measurements by all three methods, scaled to 1.21 GeV:

- Scrapers

$$\varepsilon_x = 1.8 \cdot 10^{-8}\, m\,rad \qquad \text{and} \qquad \varepsilon_y = 0.8 \cdot 10^{-8}\, m\,rad$$

$$\varepsilon_{x0} = \varepsilon_x + \varepsilon_y = 2.6 \cdot 10^{-8}\, m\,rad$$

- Synchrotron light monitor

$$\varepsilon_x = 1.6 \cdot 10^{-8}\, m\,rad \qquad \text{and} \qquad \varepsilon_y = 0.5 \cdot 10^{-8}\, m\,rad$$

$$\varepsilon_{x0} = \varepsilon_x + \varepsilon_y = 2.1 \cdot 10^{-8}\, m\,rad$$

- Quad and screen method

$$\varepsilon_x = (2.2 \pm 0.2) \cdot 10^{-8}\, m\,rad \qquad \text{and} \qquad \varepsilon_y = (0.8 \pm 0.4) \cdot 10^{-9}\, m\,rad$$

$$\varepsilon_{x0} = \varepsilon_x + \varepsilon_y = (3.0 \pm 0.5) \cdot 10^{-8}\, m\,rad$$

All three methods suffer from various uncertainties mentioned above and give the results that are somewhat higher than the design equilibrium emittance without coupling of

$$\varepsilon_{x0\,Design} = 1.8 \cdot 10^{-8}\, m\,rad$$

Some reasons that the emittance indeed might be higher than the design value are given in **Chapter 5.**

§4.10 Coupling Effects

The damping ring is designed to operate with the beam fully coupled. This is achieved by operating the ring on the so–called *difference resonance*, *i.e.* when the fractional parts of the horizontal and vertical tunes are equal. The design tunes are $\nu_x = 7.2$ and $\nu_y = 3.2$. On the difference resonance the horizontal betatron oscillations are linearly coupled to the vertical oscillations and the quantum fluctuations that drive the horizontal oscillations are now coupled into the vertical plane. Since the design damping times in both planes are the same, the horizontal equilibrium emittance in the absence of coupling, ε_{x0}, is now equally shared between the two planes[5]

$$\varepsilon_x = \frac{1}{2}\varepsilon_{x0} \qquad \text{and} \qquad \varepsilon_y = \frac{1}{2}\varepsilon_{x0}$$

gaining us a factor of two down in output emittance.

Even if the beam is not fully coupled, the following holds

$$\varepsilon_x + \varepsilon_y = \varepsilon_{x0}$$

We have measured the emittances of the stored beam in several optics configurations with different coupling, *i.e.* at different distances in the tune space from the difference resonance. In Fig. 21 we present the results of the measurements, which were done with the synchrotron light monitor.

Linear coupling is also caused by accidental skew quadrupole fields in the lattice. They can be due to the tilted normal quadrupoles or to the vertical orbit errors in the sextupoles. A finite amount of such skew quad component in the ring results in a finite minimum distance in the tune space between the two tunes and prevented us from reaching the difference resonance. The minimum distance we were able to achieve during the measurements of emittance was $\Delta\nu = 0.08$. Later on, the modeling group was able to pinpoint the source of some skew quad

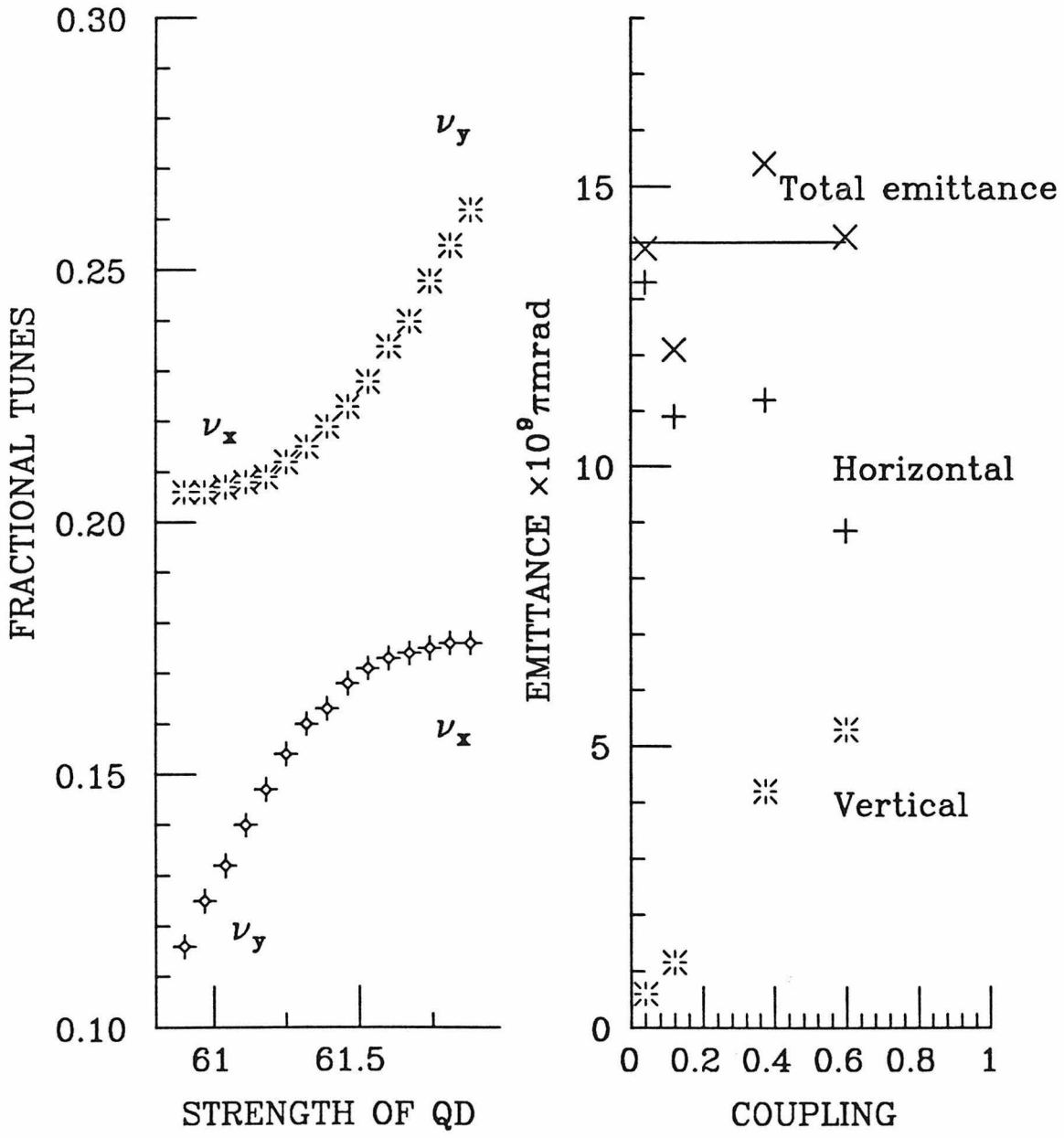

Figure 21. Horizontal and vertical emittance of the stored beam for different values of coupling, which were obtained by moving the operating point in tune space towards the difference resonance. Tunes *vs* quadrupole strength are shown as the working point passes through the coupling resonance.

component to a straight section family of quadrupoles QDI, which were slightly tilted. After realignment we were able to bring the tunes as close as $\Delta\nu = 0.03$. In the future it is planned to install variable rotated quadrupoles in the rings in order to compensate the residual skew quad component.

§4.11 Dynamic Aperture

The acceptance of the ring is defined as

$$\varepsilon_A = \frac{A_0^2}{\beta_0}$$

where A_0 is the aperture of the machine and β_0 is the value of the envelope function at that point. The aperture could be due to a piece of vacuum pipe, the physical aperture. Or it could be due to the non–linearities in the ring, in the sense that if particle's displacement from the ideal trajectory exceeds A_0 at that point, the particle would be lost from the ring.

For an ideal linear magnetic guide field consisting of only dipole and quadrupole fields, oscillations around the design orbit of arbitrarily large amplitudes are stable, and so the aperture is the physical aperture in the ring. We intentionally introduce non–linear elements, sextupoles, into the ring in order to correct the chromatic effects of the quadrupoles, the negative chromaticity. The sextupoles limit the range of stable particle amplitudes to a finite value. One tries to arrange the sextupole correction so that the dynamic aperture that they introduce lies outside the physical aperture. The dynamic aperture due to the sextupoles can be studied with such computer programs as PATRICIA[10] and MAD[9] by *tracking* the particles through the lattice that is modeled in the computer. Of course, there could be

other sources contributing to the reduction of the dynamic aperture, like accidental non–linearities, but the computer studies at least help to alleviate the problems due to the sextupoles.

The physical aperture in the damping ring is at the septum magnets in the straight sections. The distance from the design orbit to the septum is $A_{ph} = 6\,\mathrm{mm}$ and the design value for the envelope function there is $\beta = 4.4\,\mathrm{m}$. The resulting physical aperture is $\varepsilon_{A,physical} = 8.2 \times 10^{-6}\, m\,rad$, only a factor of two bigger than the design incoming positron emittance.

In Fig. 22 we show the results of such a computer study with the program PATRICIA. The initial conditions of 400 particles were evenly distributed within the boundaries of the plot and the particles were then tracked for 1000 turns through the design damping ring lattice. The particles that survived to the end are marked with points.

The dynamic aperture due to the sextupoles, according to this calculation, should be comparable to the physical aperture in the horizontal plane.

We have measured the horizontal aperture in the damping ring by the following method. A horizontal kicker magnet was used to excite the stored beam. The amplitude of the excitation was chosen such that the lifetime became short. Then the scraper was driven into the beam until the lifetime changed further. At that point the scraper position was matching some aperture in the machine, and since we knew the β function at the scraper, we could calculate the resulting horizontal acceptance

$$\varepsilon_A = (3.7 \pm 0.5) \times 10^{-6}\, m\,rad$$

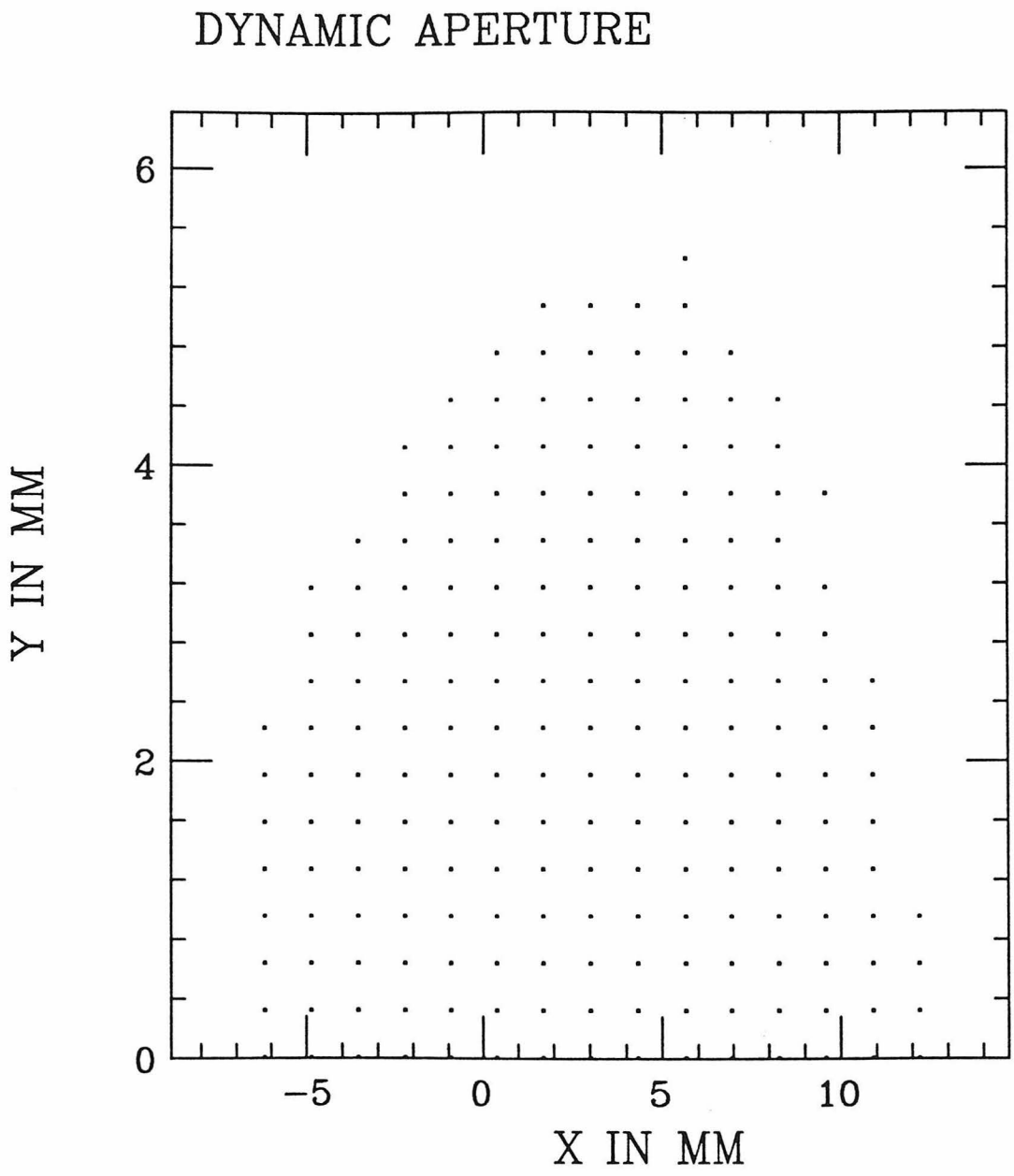

Figure 22. The results of tracking with program PATRICIA. Points indicate stable particles after 1000 turns.

§4.12 Impedance

The remaining sections of this chapter are concerned with intensity dependent effects in the damping ring. A bunch of charged particles in the ring interacts with the surrounding vacuum chamber. The induced wall image charges act back on the bunch resulting in various current dependent phenomena that lead to energy losses and instabilities. The changes in the wall geometry result in resonant cavities that can trap some of the energy that is carried in the electromagnetic field of the bunch. A concept of *impedance* of the vacuum chamber is usually introduced to characterize this interaction. We will describe it below, while treating the subject of this section, the intensity dependent energy losses, or so–called *parasitic mode loss.*

§§4.12.1 *Impedance*

Consider a bunch with the charge distribution $I(\tau)$ where τ denotes position within the bunch. A particle B at a position τ in the bunch sees a voltage due to a slice of charge A in front of it at a position τ'. If the amount of charge in slice A is $dq_A = I(\tau')d\tau'$, the voltage is

$$dV_B = dq_A\, G(\tau - \tau')$$

where $G(\tau - \tau')$ is the so–called wake potential, left by the slice A. Integrating over

all the slices in front of B, the total voltage seen by it is

$$V_B = \int G(\tau - \tau')I(\tau')d\tau'$$

The particle loses different amount of energy in different parts of the ring, *e.g.* the biggest losses occur in the RF cavities. Introducing $G(\tau - \tau')$ we smooth out the losses around the ring

$$G(\tau - \tau') = \oint E_w(\tau - \tau', s)ds$$

where E_w is the *wake field* left at a particular azimuth s.

The total power loss by the bunch is obtained by integrating over all the particles in the bunch

$$\mathcal{W} = \int_{-\infty}^{+\infty} V_B(\tau)I(\tau)d\tau$$

The *impedance* is defined as the Fourier transform of the wake potential

$$\mathbf{Z}(f) = \widetilde{G}(f)$$

and in this section we are concerned with the longitudinal impedance $\mathbf{Z}_{\|}$. Introducing the Fourier transform of the charge distribution $\widetilde{I}(f)$, we can write the power loss as

$$\mathcal{W} = \int_{-\infty}^{+\infty} \mathbf{Z}_{\|}(f)|\widetilde{I}^2(f)|df$$

The imaginary part of the impedance is an odd function of f and $|\widetilde{I}^2| = \widetilde{I}\widetilde{I}^*$ is an even function, thus the loss only depends on the real part of the longitudinal impedance.

For a bunch with a Gaussian distribution of charge, the parasitic mode loss is

$$\mathcal{W} = \int_{-\infty}^{+\infty} \mathbf{Z}_{\|R}(f)e^{-f^2/\sigma_f^2}df$$

The impedance consists of a series of delta function like peaks at the resonant frequencies of various cavities in the ring. These frequencies can be calculated with the existing computer programs for at least some known components, like RF cavities. But it is generally a very difficult problem to account for all the contributions to impedance from various components in the ring. A very useful approximate model of impedance is usually introduced for estimates and the interpretation of the measurements.[35] It is the impedance of a broad band resonator

$$\mathbf{Z}_{\parallel} = \frac{R_s}{1 - iQ_r(\frac{f_r}{f} - \frac{f}{f_r})}$$

where R_s is the so–called shunt impedance, Q_r is the quality factor, usually taken to be $Q_r = 1$, and f_r is the resonant frequency. It has been applied to several existing storage rings, giving good qualitative agreement with the computer predictions.[36]

Measurements

The parasitic mode loss results in a phase shift between the bunch and the RF cavity voltage, such that the bunch maintains the design energy at different intensities. We have measured this phase shift as a function of bunch current by comparing on a vector voltmeter the reference RF signal from the cavities to the 714 MHz component of the signal from a bunch intensity monitor. The setup was similar to the one used in the measurements of the radiation loss per turn. The intensity was varied by driving a scraper into the stored beam. In Fig. 23 we show the data from one such measurement.

The energy loss per turn can be parametrized as follows

$$U = U_0 + kQ$$

where U_0 is the radiation loss per turn, Q is the charge in the bunch and k is the so–called parasitic mode loss factor[37] that we extracted form the data. It can also be calculated from the broad band resonator model of impedance.[35] The measured and expected[38] values for the parasitic mode loss factor with the bunch length of

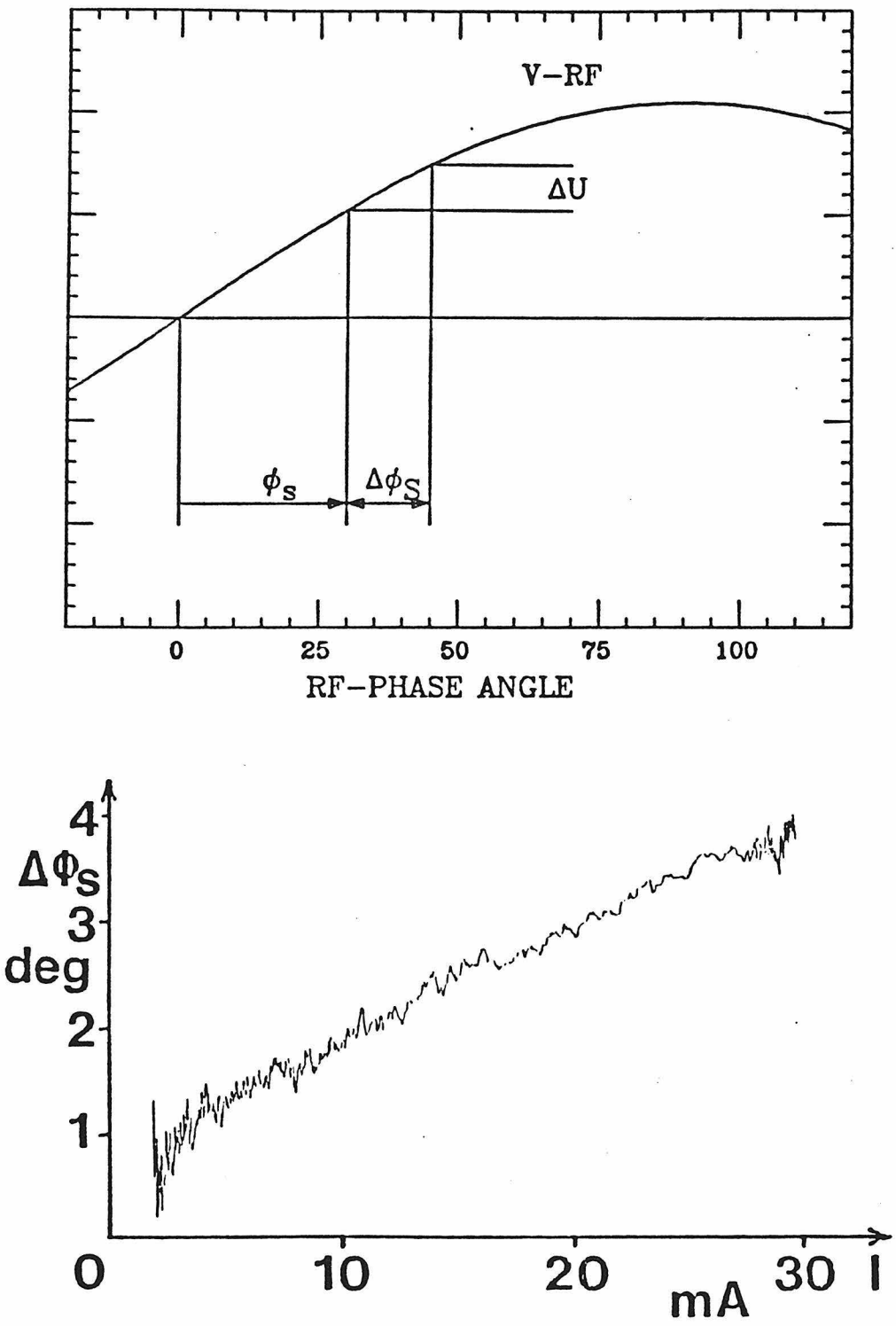

Figure 23. Measurement of the parasitic mode loss by observing the changes in the synchronous phase with bunch current.

$\sigma = 7\,\mathrm{mm}$ are

$$k_{meas} = (4.8 \pm 2.9)\,\frac{V}{pC} \qquad \text{and} \qquad k_{expect} = 3.2\,\frac{V}{pC}$$

The expected value was calculated taking into account only the theoretical impedance of the RF cavities and estimating the other impedance from experience. The agreement with the measurement is rather good. The measurement accuracy did not allow us to extract the broad band resonator model parameters from measurements of k at different bunch lengths.

§§4.12.2 *Synchrotron Frequency Shift*

The imaginary part of the longitudinal impedance leads to the so–called *potential well bunch lengthening.* It is usually predominantly inductive, and bunch induced voltage reduces the slope of the RF voltage, lengthening the bunch. It also lowers the frequency of the coherent quadrupole or "breathing" mode of longitudinal oscillations.[36] The coherent dipole mode is changed much less because the potential well moves with the bunch. The frequency shift is a function of impedance integrated over the bunch spectrum.[35]

We have measured the coherent dipole and quadrupole frequencies as a function of current. In Fig. 24 the measurements for two different bunch lengths are shown. The dipole mode of coherent energy oscillations was excited by phase modulating the RF voltage at the synchrotron frequency. The quadrupole mode was excited by amplitude modulation of the RF voltage at twice the synchrotron frequency. The frequencies were measured with the tune monitor.

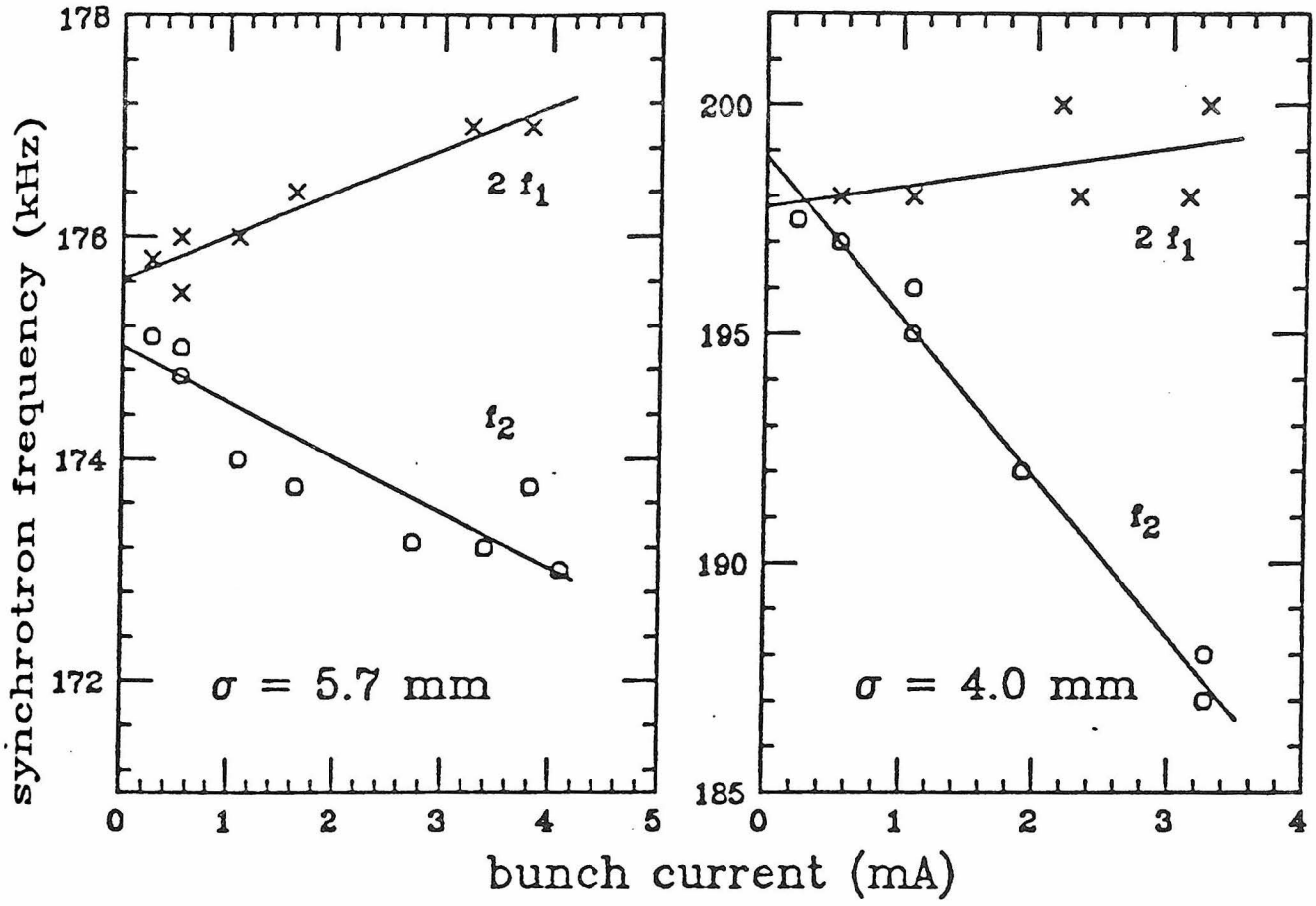

Figure 24. Intensity dependence of the coherent dipole and quadrupole synchrotron frequency.

The quadrupole mode shift at 1.21 GeV is

$$\Delta f_2 = -(0.34 \pm 0.03)\frac{MHz}{A}$$

and the dipole mode shift was small and positive.

§§4.12.3 *Longitudinal Impedance*

From the measurements of the parasitic mode loss and the coherent frequency shift the broad band model parameters were determined to be[27]

$$R_s = 2.8\,\mathrm{k}\Omega \qquad \text{and} \qquad f_r = 5\,\mathrm{GHz}$$

The resonant frequency is relatively high compared with other storage rings which is consistent with the fact that the transverse dimensions of the damping ring vacuum chamber are very small (7 mm radius in the RF cavities).

§§4.12.4 *Betatron Frequency Shift*

The bunch passing through the vacuum chamber off axis excites transverse electromagnetic fields that in turn act on the particles in the bunch. The transverse fields, integrated over one revolution, that result from the passage of a unit current

at a unit distance away from axis, are described by the transverse impedance $\mathbf{Z}_\perp$.[35] The imaginary part of the transverse impedance can lead to the betatron frequency shift.

Alternatively, we can describe the effect as follows. The head of the bunch leaves behind a wake field that acts on the tail, driving it resonantly, since both are oscillating with the betatron frequency. But since the particles in the bunch undergo energy oscillations, the head and the tail will interchange places after half of the synchrotron oscillation period. Analysis of the stability conditions of such a process[39] shows that there exists a threshold in bunch intensity, above which a so–called *strong head–tail instability* occurs. It is the instability that limits single bunch current in most of the existing storage rings.

Below the threshold the effect results in a betatron tune shift that grows linearly with intensity. When the intensity approaches the threshold the tune shift grows faster but if one extrapolates the linear tune shift, the threshold occurs when the betatron tune has shifted by half of the synchrotron tune ν_s.

We have observed the vertical tune shift with current of

$$\Delta\nu_y = -(1.2 \pm 0.3)\frac{KHz}{10^9 e^-}$$

Extrapolating this result to higher currents, and since the synchrotron tune in the damping ring is 120 KHz, the threshold for the strong head–tail instability is predicted at

$$I_{th} = (5.0 \pm 1.5) \times 10^{10} e^- \text{per} \quad \text{bunch}$$

The measurements were done at 0.95 GeV, and since the threshold scales linearly with energy,[39] the beam should be stable at the design intensity of 5×10^{10} particles per bunch. We have not seen the instability at the maximum stored current that we have achieved of 4×10^{10} electrons in one bunch.

Chapter 5. Results

§5.1 Linear Optics

A successful model of the damping ring linear optics has been developed.[40–42] It is able to predict and to correct the tunes of the machine, the β functions and the dispersion. Linear optics configurations, developed with the help of the model, enabled us to run the damping ring with the above mentioned parameters close to the design values. The model has also helped us to identify a source of substantial rotated quadrupole field component in the ring (see the section on coupling, **Chapter 4**).

§5.2 Damping Times and Emittance

The measurement of the sum of the damping rates that was done by measuring the radiation loss per turn, gave the result that was 11% lower than expected. The

measured and expected amount of radiation loss per turn at 1.21 GeV were

$$U_{0meas} = (84.0 \pm 0.4)\text{KeV} \qquad \text{and} \qquad U_{0design} = 93.1\,\text{KeV}$$

The discrepancy was traced to the fringe field effects in the damping ring dipole magnet. The dipole, described in **Chapter 3**, has been treated in the design model in the hard edge approximation (the field at the ends of the magnet rises from zero to the peak value discontinuously). In Fig. 25 we show the results of the magnetic field measurements in the dipole magnet. The integral of the square of the magnetic field along the magnet, taken from these data, was indeed 11% smaller than the hard edge approximation result. The radiation loss per turn is proportional to this integral (see **Chapter 2**)

$$U_0 = \frac{C_\gamma}{2\pi} E^4 I_2, \qquad I_2 = \oint \frac{ds}{\rho^2} \propto \frac{1}{E^2} \oint B^2\, ds$$

The change in U_0 of 11% in turn means that the sum of the damping rates

$$\frac{1}{\tau_x} + \frac{1}{\tau_y} + \frac{1}{\tau_\epsilon} = \frac{U_0}{2ET_0}(J_x + J_y + J_\epsilon) = \frac{2U_0}{ET_0} = 1180.2\,\text{sec}^{-1}$$

is also smaller by 11% . Since we have observed no vertical dispersion in the ring, the vertical damping partition number $J_y = 1$ and the vertical damping rate is equal to one quarter of the measured sum, or in terms of the damping time

$$\tau_{ymeas} = (3.40 \pm 0.05)\text{msec}$$

The horizontal and energy damping times are

$$\tau_x = \frac{1}{J_x}\frac{2ET_0}{U_0} \qquad \text{and} \qquad \tau_\epsilon = \frac{1}{J_\epsilon}\frac{2ET_0}{U_0}$$

and must also be longer by the same 11% . Moreover, in the design model the damping ring dipole magnet was treated as a rectangular magnet, for which[43]

$$J_x = 1 \qquad \text{and} \qquad J_\epsilon = 2$$

In reality, the magnet was built in such a way, that the calculated partition numbers become

$$J_x = 0.9 \qquad \text{and} \qquad J_\epsilon = 2.1$$

which further increases the horizontal damping time to

$$\tau_x = 3.8\,\text{msec}$$

The equilibrium emittance can be written as (see **Chapter 2**)

$$\varepsilon_{x0} = \frac{C_q E^2}{J_x} \frac{I_5}{I_2}$$

We have discussed how J_x and I_2 have been modified. For the same reasons that J_x changed, the fifth synchrotron radiation integral I_5 also changed. The calculated reduction is approximately 12%. In summary, what we believe to be actual emittance and the design value are

$$\gamma\varepsilon_{x0\,Act} = 4.8 \times 10^{-5}\, m\,rad, \qquad \gamma\varepsilon_{x0\,design} = 4.3 \times 10^{-5}\, m\,rad$$

The changes described above imply the extracted beam emittances for electrons (after 5.56 msec) and positrons (after 11.1 msec) of

$$\gamma\varepsilon^{-}_{out} = 3.6 \times 10^{-5}\, m\,rad$$
$$\gamma\varepsilon^{+}_{out} = 4.5 \times 10^{-5}\, m\,rad$$

where we have assumed full coupling, and the positron emittance is calculated under the assumption that the positron damping ring would be built as an exact replica of the present electron damping ring. These values exceed the SLC design emittance of

$$\gamma\varepsilon^{\pm}_{design} = 3 \times 10^{-5}\, m\,rad$$

The results of emittance measurements described in **Chapter 4** are consistent with the above conclusions but lacked sufficient accuracy to support them.

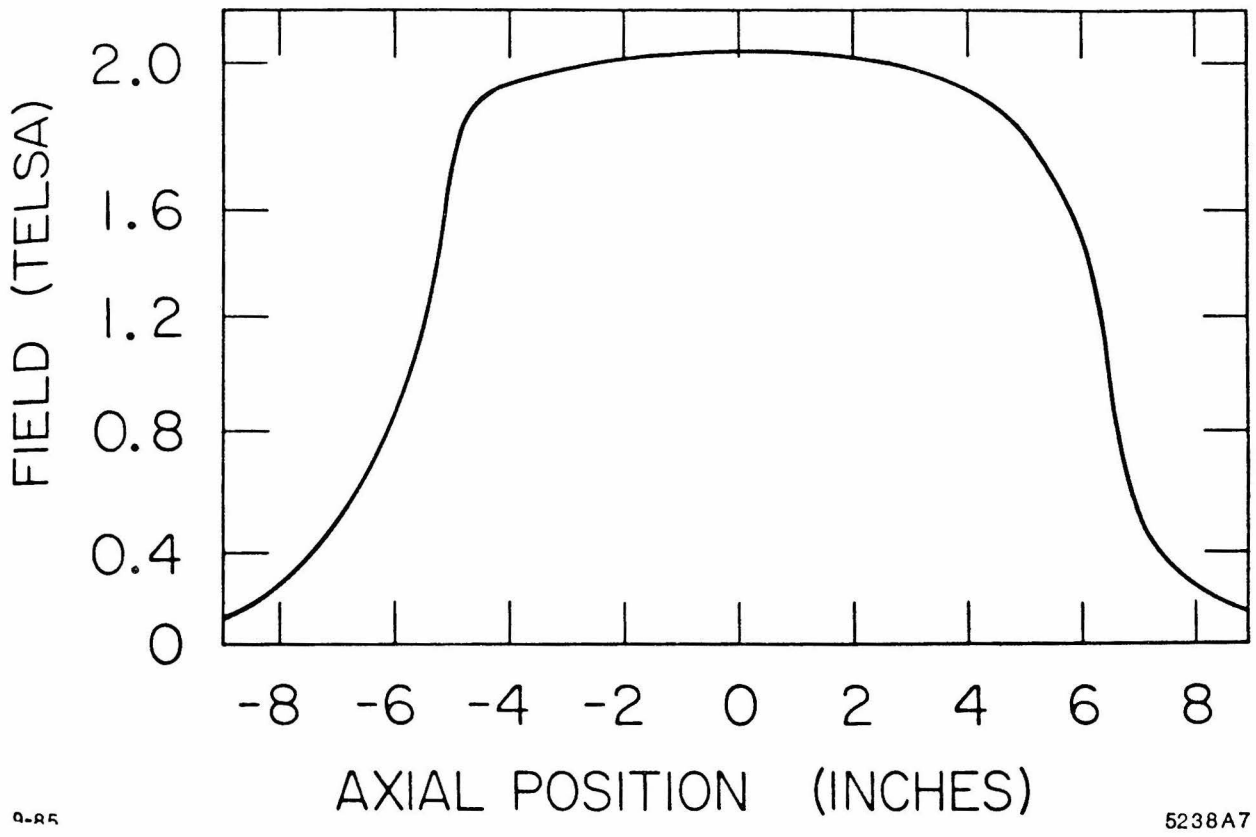

Figure 25. Magnetic field map of the damping ring dipole magnet. The soft edges are due to the saturation in the iron as well as to the specially shaped pole tips that provide the sextupole field component but lengthen the fringe fields.

§5.3 Chromaticity Correction

The bulk of the negative chromaticity is corrected in the present damping ring by the sextupoles that are built into the ends of the dipole magnets by shaping their pole pieces. This scheme turned out to be barely adequate. Although we were able to maintain slightly positive chromaticity for most of the running, it was achieved by operating all of the variable sextupoles in one polarity. Saturation in the pole tips as well as difficulty in positioning them correctly during the magnet construction were probably the reasons for the difficulties in the implementation of the correction scheme.

§5.4 Other Measurements

In all other aspects the damping ring has performed close to the design specifications.

The bunch length agreed with the predictions and we have not observed any bunch lengthening up to intensities of 1×10^{10} electrons per bunch.

The measurements on the intensity dependent phenomena also agreed with the predictions quite well and indicate no obstacles to achieving the design intensity in the ring of 5×10^{10} particles per bunch.

The maximum current in one bunch we have stored so far was 4×10^{10} electrons, with no signs of instabilities. We have also stored two bunches of electrons, 2×10^{10} particles each.

§5.5 Changes in the Design

We have proposed to change some aspects of the damping ring optics[44] in order to improve the output emittance and the chromaticity correction scheme. The main changes are

- to improve the field quality of the damping ring bending magnet by removing the specially shaped pole tip pieces that provide sextupole fields but lengthen the fringe field of the magnet. The calculations and measurements of the new dipoles show an improvement in the second synchrotron radiation integral I_2 by 3% , which will improve all of the damping times by the same amount.
- to make the dipole magnet as a rectangular magnet, so that the horizontal damping partition number will become $J_x = 1$. This will reduce the horizontal damping time and the equilibrium emittance by 10% .
- to increase the horizontal betatron phase advance per cell from 114° ($\nu_x = 7.2$) to 135° ($\nu_x = 8.2$), which will give a reduction in the equilibrium emittance of 25% (see **Appendix B**).
- to install Samarium Cobalt permanent sextupole magnets[45] instead of the removed pole tips, as well as to double the number of variable sextupoles. This should improve the chromaticity correction scheme.

The resulting characteristics of the new design optics are compared in Table 2 with the original design and with the actual values in the present damping ring.

The higher design tune of $\nu_x = 8.2$ leads to larger negative chromaticity and thus to stronger sextupoles that are to correct it. The sextupole configuration has been optimized with the help of the computer tracking program PATRICIA[10] and the resulting dynamic aperture is shown in Fig. 26 (see the section on dynamic aperture, **Chapter 4**, for comparisons with the original design).

Table 2. The general parameters of the damping ring optics that were changed in the new design are compared to the original design and actual numbers.

		Units	Design (CN 139)	Actual (e^- D.R.)	Proposed (e^+ D.R.)
Second synchrotron integral	I_2	m^{-1}	3.084	2.731	2.804
Fourth synchrotron integral	I_4	m^{-1}	0.0	0.261	0.0
Fifth synchrotron integral	I_5	m^{-1}	0.0264	0.0232	0.0177
Horizontal damping partition number	J_x		1	0.904	1
Horizontal damping time	τ_x	msec	3.06	3.82	3.36
Vertical damping time	τ_y	msec	3.06	3.45	3.36
Horizontal tune	ν_x		7.20	7.20	8.20
Equilibrium emittance (no coupling)	$\gamma\varepsilon_{x0}$	μrad m	43.1	48.3	32.2
Equilibrium emittance (full coupling)	$\gamma\varepsilon$	μrad m	21.6	23.0	16.1
180 pps (120 pps) extracted electron normalized emittance	$\gamma\varepsilon_{e-}$	μrad m	28.9 (22.8)	35.9 (25.8)	26.5 (17.6)
180 pps (120 pps) extracted positron normalized emittance	$\gamma\varepsilon_{e+}$	μrad m	28.6 (21.7)	44.9 (24.0)	29.5 (16.6)

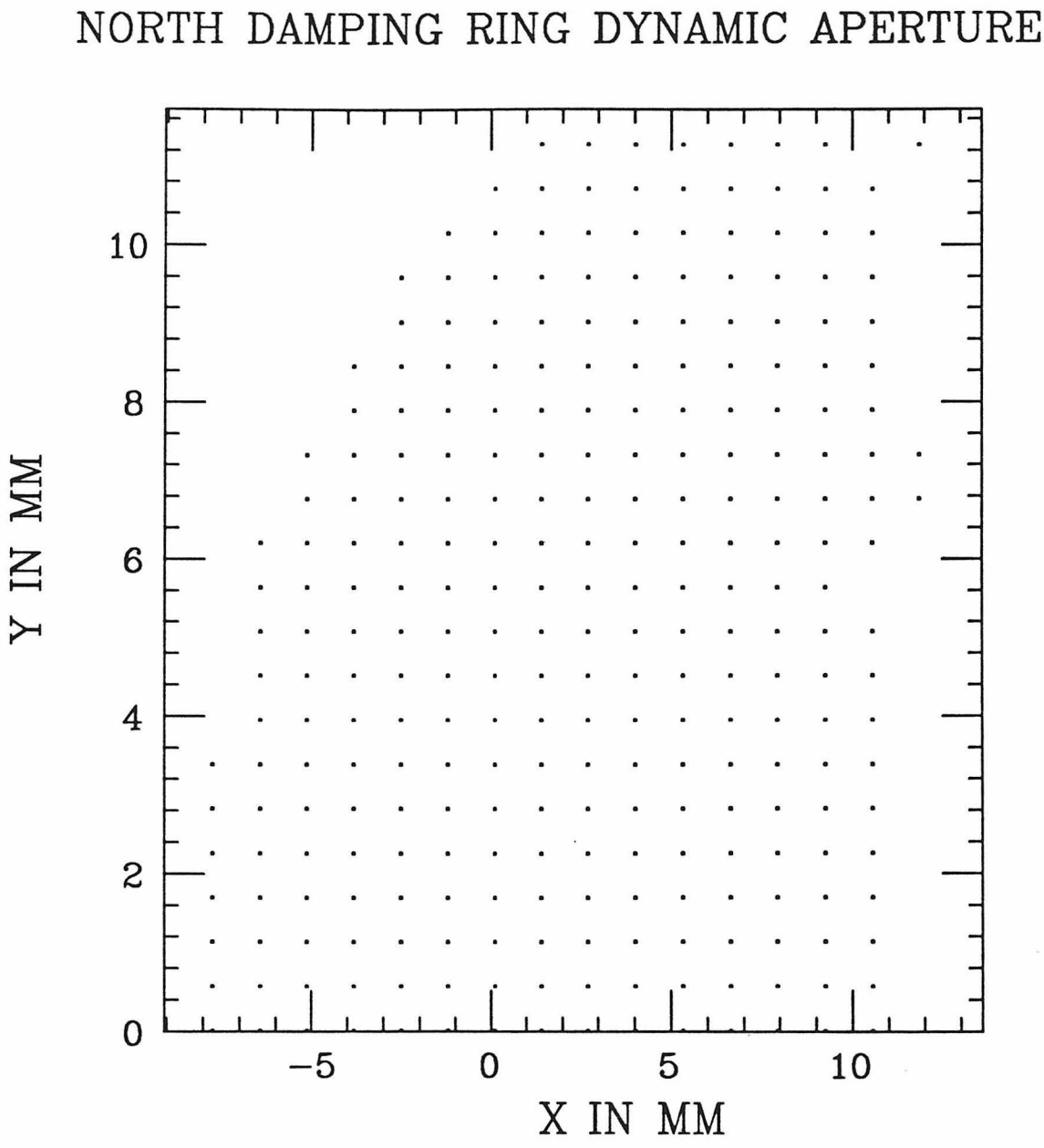

Figure 26. The result of the computer tracking studies of the new design sextupole correction scheme. The resulting dynamic aperture is comparable to the physical aperture.

Appendix A. Beam Parametrization

Two approaches to the beam parametrization have been prevalent in the literature on the accelerator physics. Those are the σ–matrix formalism[46–48] and the Courant–Snyder parameters[6]. In this appendix a brief sketch of how they are related to each other is given. For simplicity, the case of one degree of freedom is considered throughout.

Single Particle Motion

The transverse betatron motion of a particle is that of a harmonic oscillator, which amplitude and phase are modulated. The motion is described by the Hill's equation

$$x'' + k(s)x = 0 \tag{5}$$

where the dependence of k on s provides for the amplitude and phase modulation of the motion. In a circular accelerator k is a periodic function of s, the period being the circumference of the machine. The solution, then, is also periodic in s and is written as

$$x(s) = a\sqrt{\beta(s)}\cos[\phi(s) - \vartheta] \tag{6}$$

where β is also called the envelope function, is periodic in s and is connected to the $\phi(s)$ in the following way

$$\phi(s) = \int_0^s \frac{d\bar{s}}{\beta(\bar{s})} \tag{7}$$

Beam Envelope

Consider now a beam of particles with a certain normalized density distribution in phase space $\varrho(x,p;s)$

$$\int \varrho(x,p;s)\,dx\,dp = 1$$

The beam is described by the moments of this distribution defined in the usual way. For example

$$\overline{x} = \int x\varrho(x,p;s)\,dx\,dp$$

$$\overline{p^2} = \int p^2\varrho(x,p;s)\,dx\,dp \quad etc.$$

It can be shown[49] that the first moments satisfy the same Hill's equation

$$\overline{x}'' + k(s)\overline{x} = 0$$

and that there exists an invariant of motion involving second moments

$$\varepsilon^2 = \overline{x^2}\,\overline{p^2} - (\overline{xp})^2$$

where we have assumed $\overline{x} = \overline{p} = 0$. The correlation matrix for the distribution is the beam matrix

$$\sigma = \begin{pmatrix} \overline{x^2} & \overline{xp} \\ \overline{xp} & \overline{p^2} \end{pmatrix} = \varepsilon^2 \begin{pmatrix} \beta & -\alpha \\ -\alpha & \gamma \end{pmatrix}$$

and the Courant–Snyder parameters are used to parametrize the beam matrix in the way shown above. Since $det\sigma = \varepsilon^2$

$$\beta\gamma - \alpha^2 = 1$$

The β function in Equation 6 is the same as above for the case of a circular machine.

§A.1 σ - Matrix Formalism

This formalism was originally developed for the beam optics program TRANSPORT. It has been mainly used for the design and operation of beam transport lines.

Beam is represented by an ellipse in (x, x') phase-space

$$\mathbf{X}^T \sigma^{-1} \mathbf{X} = 1$$

where $\mathbf{X}$ - coordinate vector, and σ is a symmetric, positive-definite matrix. The area of the ellipse is

$$A = \pi \sqrt{\det \sigma}$$

If $\mathbf{R}$ is a transfer matrix between two points in a transport line, so that

$$\mathbf{X}_2 = \mathbf{R}\mathbf{X}_1$$

the σ matrix transforms as

$$\sigma_2 = \mathbf{R}\sigma_1\mathbf{R}^T$$

The formalism can be used in a higher dimensional phase space in a straightforward way.

Appendix B. FODO Cell Lattice

The equilibrium transverse emittance in the ring is a strong function of the average value of $\mathcal{H}$ in the bending magnets. We will derive here an analytic expression for $\langle \mathcal{H} \rangle_{\text{mag}}$ in a uniform field dipole magnet, the kind used in the majority of the storage rings. We will then use this expression first to derive the formula for the emittance of the simple FODO cell lattice and second to find an optimized set of parameters to obtain the lowest possible emittance in a ring using such magnets.

The expression we are set out to calculate is

$$\langle \mathcal{H} \rangle_{\text{mag}} = \frac{1}{L} \int_{-L/2}^{L/2} \mathcal{H}(s)\, ds$$

where we are integrating over the length L of the magnet and

$$\mathcal{H}(s) = \gamma(s)\eta^2(s) + 2\alpha(s)\eta(s)\eta'(s) + \beta(s)\eta'^2(s)$$

The dispersion parameters transform within the magnet as[6]

$$\begin{pmatrix} \eta(s) \\ \eta'(s) \\ 1 \end{pmatrix} = \begin{pmatrix} C & \rho S & \rho(1-C) \\ -\frac{S}{\rho} & C & S \\ 0 & 0 & 1 \end{pmatrix} \begin{pmatrix} \eta_0 \\ \eta'_0 \\ 1 \end{pmatrix}$$

where ρ is the bending radius,

$$C \equiv \cos\frac{s}{\rho}, \qquad S \equiv \sin\frac{s}{\rho}$$

and η_0, η_0' are the initial values, taken in the middle of the magnet.

Similarly, the Courant–Snyder parameters evolve within the magnet as

$$\begin{pmatrix} \beta(s) \\ \alpha(s) \\ \gamma(s) \end{pmatrix} = \begin{pmatrix} C^2 & -2\rho CS & \rho^2 S^2 \\ \frac{1}{\rho}CS & C^2 - S^2 & \frac{1}{\rho}CS \\ \frac{1}{\rho^2}S^2 & \frac{2}{\rho}CS & C^2 \end{pmatrix} \begin{pmatrix} \beta_0 \\ \alpha_0 \\ \gamma_0 \end{pmatrix}$$

where the initial values β_0, α_0 and γ_0 are also taken in the middle of the magnet.

The initial value for the $\mathcal{H}$ in the middle of the magnet is

$$\mathcal{H}_0 = \gamma_0\eta_0^2 + 2\alpha_0\eta_0\eta_0' + \beta_0\eta_0'^2$$

and a distance s away within the magnet

$$\begin{aligned} \mathcal{H}(s) = \mathcal{H}_0 & \\ & + \gamma_0[-2C\rho^2 + 2C\rho\eta_0 - \rho^2S^2 + 2\rho^2 - 2\rho\eta_0] \\ & + \alpha_0[2C\rho\eta_0' + 2CS\rho - 2S\rho + 2S\eta_0 - 2\rho\eta_0'] \\ & + \beta_0[S^2 + 2S\eta_0'] \end{aligned}$$

Taking the integral of the above expression we then obtain the average value of $\mathcal{H}$ as a function of the initial values of the Courant–Snyder and dispersion parameters in the middle of the magnet:

$$\begin{aligned} \langle\mathcal{H}\rangle_{\text{mag}} = \frac{1}{L}\int_{-L/2}^{L/2} \mathcal{H}(s)\,ds &= \gamma_0\eta_0^2 + 2\alpha_0\eta_0\eta_0' + \beta_0\eta_0'^2 \\ & + \gamma_0[-\frac{4}{L}\sin(\frac{L}{2\rho})\rho^3 + \frac{4}{L}\sin(\frac{L}{2\rho})\rho^2\eta_0 + \frac{\rho^3}{2L}\sin(\frac{L}{\rho}) + \frac{3}{2}\rho^2 - 2\rho\eta_0] \\ & + \alpha_0[\frac{4\rho^2}{L}\sin(\frac{L}{2\rho})\eta_0' - 2\rho\eta_0'] \\ & + \beta_0[-\frac{\rho}{2L}\sin(\frac{L}{\rho}) + \eta_0'^2 + \frac{1}{2}] \end{aligned}$$

This result is valid for any uniform field bending magnet in the hard edge approximation, *i.e.* the field at the ends of the magnet is a step function. Similar

expression is given in Ref. 7 where the initial values of the optical parameters are taken at one end of the magnet. We found the choice of the middle of the magnet as the initial point more convenient for the minimization procedure that follows below.

The edges of the magnet sometimes produce horizontal focusing, as in the case of a rectangular magnet (the magnet boundary is not normal to the ideal orbit). In our case the treatment of the edge effects is delayed until the initial optics parameters at the middle of the magnet are evaluated for a particular lattice.

If the bending angle per magnet $\theta = \frac{L}{\rho}$ is small, the result can be approximated as follows

$$\langle \mathcal{H} \rangle_{\text{mag}} = \gamma_0 \eta_0^2 + 2\alpha_0 \eta_0 \eta_0' + \beta_0 \eta_0'^2 + \gamma_0 [\frac{1}{320}\frac{L^4}{\rho^2} - \frac{1}{12}\frac{L^2}{\rho}\eta_0] - \alpha_0 [\frac{1}{12}\frac{L^2}{\rho}\eta_0'] + \beta_0 [\frac{1}{12}\frac{L^2}{\rho^2}]$$

§B.1 Emittance of the FODO Cell Lattice

The FODO cell lattice consists of alternating focusing and defocusing quadrupoles with bending magnets in between. A single cell contains one focusing and one defocusing quadrupole and two bending magnets and is shown in Fig. 27.

We will consider the FODO cell in the following approximation. The quadrupoles are treated as thin lenses of equal strength and the bending magnets of length L occupy all of the space between the quadrupoles. Thus the total length of the cell is $2L$.

We will consider the case of rectangular bending magnets. The focusing due an edge of the magnet is modeled as a thin lens defocusing quadrupole[7] with strength

$$k_E = \frac{1}{\rho}\tan\frac{\theta}{2} \qquad \theta = \frac{L}{\rho}$$

where θ is the bending angle per magnet. The transfer matrix in the horizontal

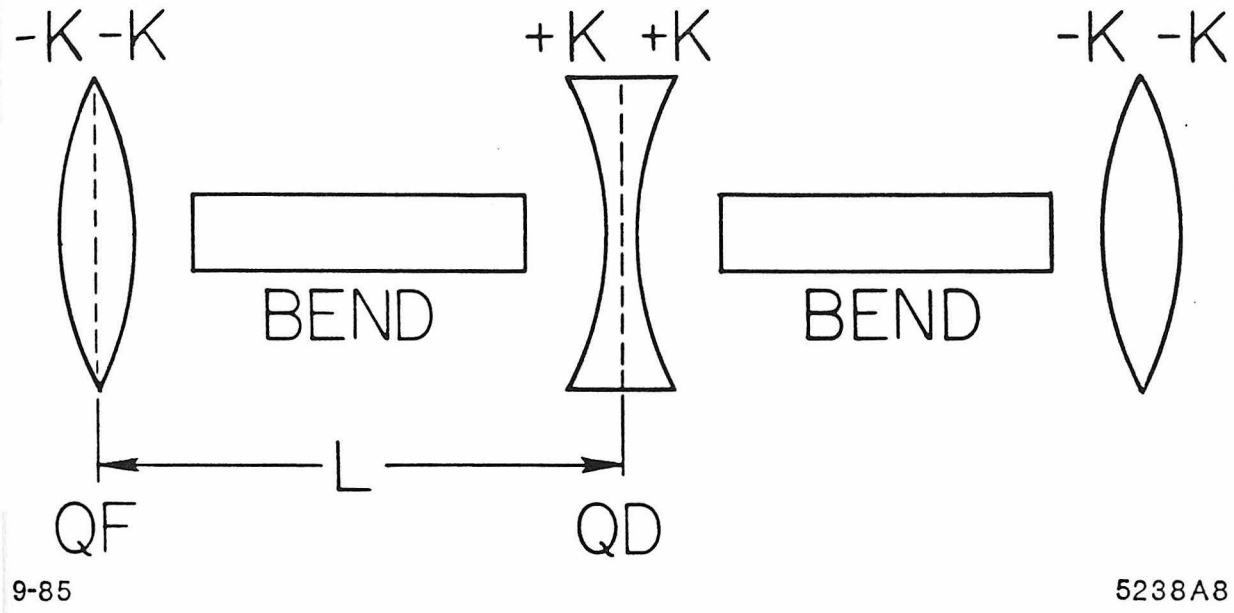

Figure 27. FODO cell optics elements

plane for half of the bending magnet can be written as

$$\mathbf{R}_{\frac{1}{2}B} = \begin{pmatrix} 1 & 0 \\ \frac{1}{\rho}\tan\frac{\theta}{2} & 1 \end{pmatrix} \begin{pmatrix} \cos\frac{\theta}{2} & \rho\sin\frac{\theta}{2} \\ -\frac{1}{\rho}\cos\frac{\theta}{2} & \cos\frac{\theta}{2} \end{pmatrix} = \begin{pmatrix} \cos\frac{\theta}{2} & \rho\sin\frac{\theta}{2} \\ 0 & 1/\cos\frac{\theta}{2} \end{pmatrix}$$

and the transfer matrix for the whole magnet is

$$\mathbf{R}_B = \begin{pmatrix} 1 & \rho\sin\theta \\ 0 & 1 \end{pmatrix}$$

We observe that in the rectangular bending magnet the horizontal focusing due to the edges is cancelled by the weak focusing due to the main body of the magnet. In the small bending angle per magnet approximation the rectangular bend can be treated as a drift as far as Courant–Snyder parameters are concerned.

In what follows we will use small bending angle per magnet approximation, since as it will become clear shortly, we will be interested in that regime. The horizontal transfer matrix for half of the FODO cell, consisting of half of the focusing quadrupole, bend and half of the defocusing quadrupole is

$$\begin{aligned} \mathbf{R}_{\frac{1}{2}cell} &= \begin{pmatrix} 1 & 0 & 0 \\ -k & 1 & 0 \\ 0 & 0 & 1 \end{pmatrix} \begin{pmatrix} 1 & L & \frac{L^2}{2\rho} \\ 0 & 1 & \frac{L}{\rho} \\ 0 & 0 & 1 \end{pmatrix} \begin{pmatrix} 1 & 0 & 0 \\ k & 1 & 0 \\ 0 & 0 & 1 \end{pmatrix} \\ &= \begin{pmatrix} 1+kL & L & L^2/2\rho \\ -k^2L & 1-kL & \frac{L}{2\rho}(2-kL) \\ 0 & 0 & 1 \end{pmatrix} \end{aligned}$$

where k is the strength of half of the quadrupole and we are using the three dimensional matrices that specify the transformation of the dispersion parameters. Their two–by–two upper left corner is the usual horizontal transfer matrix.

The full cell transfer matrix is

$$\mathbf{R} = \begin{pmatrix} 1-2k^2L^2 & 2L(1+kL) & \frac{L^2}{\rho}(2+kL) \\ -2k^2L(1-kL) & 1-2k^2L^2 & \frac{L}{\rho}(2-kL-k^2L^2) \\ 0 & 0 & 1 \end{pmatrix}$$

All of the main characteristics of the FODO cell can be parametrized in terms of betatron phase advance per cell.[17] In particular, since the trace of the full horizontal transfer matrix specifies the phase advance per cell[6]

$$2\cos 2\mu = \mathbf{R}_{11} + \mathbf{R}_{22} = 2 - 4k^2L^2 \quad \Longrightarrow \quad \sin\mu = kL$$

where we have introduced the phase advance per half cell μ. The stability condition for the betatron oscillations is

$$0 \leq kL \leq 1$$

in the thin lens, equal strength quadrupoles FODO cell lattice.

Solving for the Courant–Snyder parameters in the middle of a bending magnet, we obtain

$$\beta_0 = \frac{L(2-\sin^2\mu)}{\sin 2\mu}, \qquad \alpha_0 = \frac{1}{\cos\mu}, \qquad \gamma_0 = \frac{2}{L}\tan\mu$$

and the values of the dispersion parameters there are

$$\eta_0 = \frac{L^2}{8\rho}\frac{8-\sin^2\mu}{\sin^2\mu}, \qquad \eta_0' = -\frac{L}{\rho\sin\mu}$$

Using the above initial conditions in the expression for the average value of $\mathcal{H}$ derived in the previous section, we obtain the following result for the FODO cell

$$\langle\mathcal{H}\rangle_{\rm mag} = \frac{2L^3}{\rho^2\sin^2\mu\sin 2\mu}[1 - \frac{3}{4}\sin^2\mu + \frac{1}{60}\sin^4\mu]$$

which coincides exactly with the result obtained in Ref. 14.

The transverse equilibrium emittance in the FODO cell lattice can be written then as

$$\varepsilon_x = \frac{C_q E^2\langle\mathcal{H}\rangle_{\rm mag}}{J_x\rho} = \frac{2C_qE^2}{J_x}\theta^3 F_{FODO}(\mu)$$

where $\theta = L/\rho$ is the bending angle per magnet and we have introduced an emittance form–factor for the FODO cell lattice F_{FODO} which is a function of the betatron phase advance per half–cell only.

$$F_{FODO}(\mu) = \frac{1}{\sin^2\mu\sin 2\mu}[1 - \frac{3}{4}\sin^2\mu + \frac{1}{60}\sin^4\mu]$$

A plot of this form–factor is given in Fig. 28.

We should note that with larger phase advance come stronger quadrupoles. And with stronger focusing the chromatic effects of the optics get worse. The usual parameter used to characteries the strength of the chromatic aberrations is called chromaticity. It relates the change in tune or normalized phase advance with change in energy of the particle:

$$\xi = -\frac{\Delta\nu}{\delta}$$

where δ is the relative energy deviation and

$$\nu = \frac{1}{2\pi}\int \frac{ds}{\beta(s)}$$

The chromaticity in a FODO cell lattice can be expressed as a function of the phase advance[17]

$$\xi = -\frac{\sin\mu}{2\pi\sqrt{1-\sin^2\mu}}$$

and we see that as the phase advance per half–cell approaches 90°, the chromaticity starts to grow very fast. The negative chromaticity has to be corrected with sextupole magnets in order to avoid head–tail instability. Strong sextupole magnets limit stable betatron oscillation amplitudes, introducing small *dynamic aperture.*

Thus we try to choose the horizontal phase advance as far away from 90° as is consistent with our desire to get small emittance. In the vertical plane in an ideal flat machine there is no dispersion, no quantum fluctuations. We do not need strong focusing and in the damping ring the vertical phase advance was chosen to be much smaller then horizontal, typically 22.5° degrees per half–cell.

This in turn means that the defocusing quadrupoles are weaker then focusing ones. What happens to our simple model of the FODO cell and to the emittance in this situation is the subject of the next section.

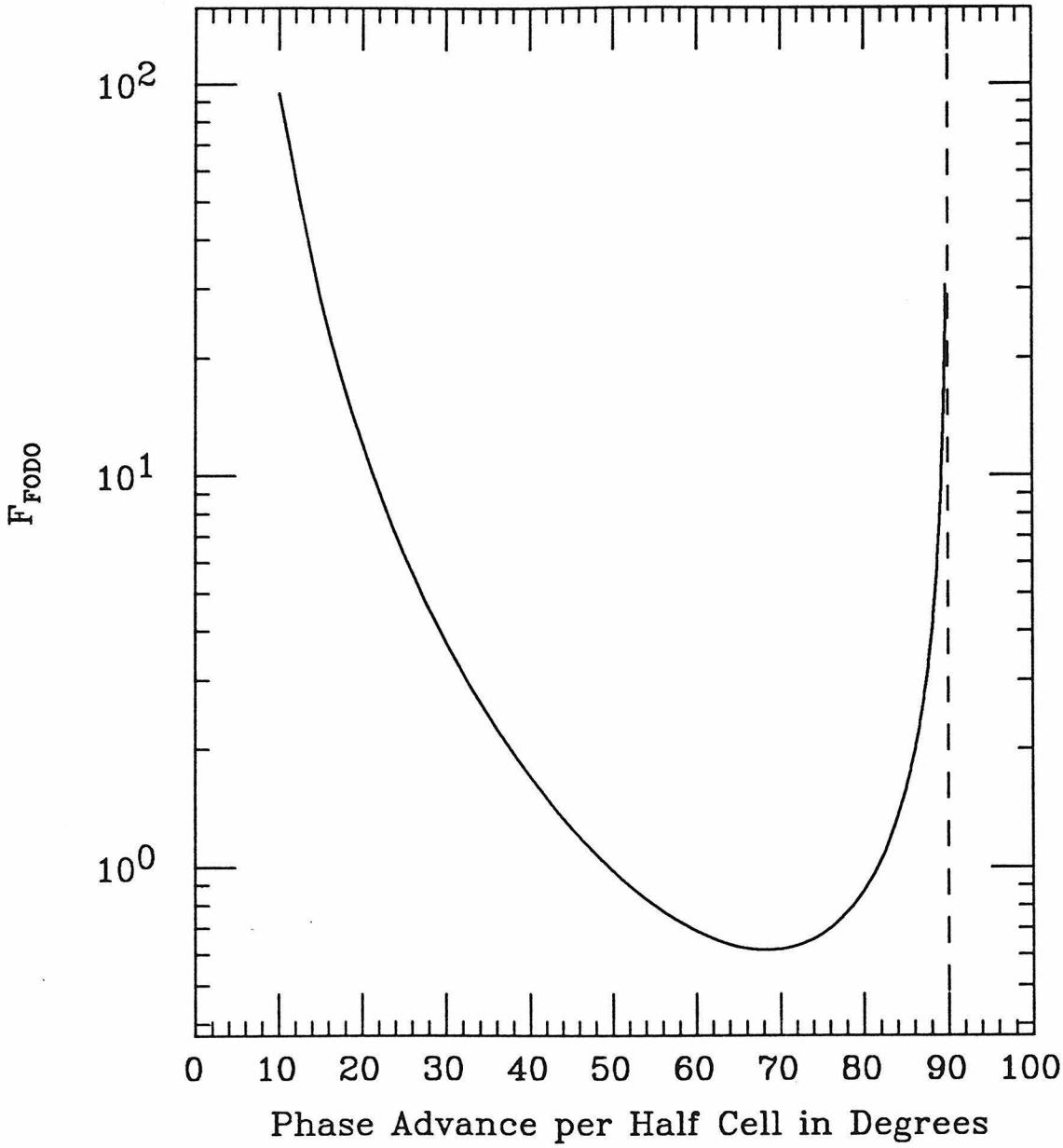

Figure 28. The emittance of the FODO cell lattice as a function of the phase advance per half cell.

§§*B.1.1 Different Phase Advances in the Two Planes*

The transfer matrix for the half–cell is now

$$\mathbf{R}_{\frac{1}{2}cell} = \begin{pmatrix} 1 & 0 & 0 \\ -k_f & 1 & 0 \\ 0 & 0 & 1 \end{pmatrix} \begin{pmatrix} 1 & L & \frac{L^2}{2\rho} \\ 0 & 1 & \frac{L}{\rho} \\ 0 & 0 & 1 \end{pmatrix} \begin{pmatrix} 1 & 0 & 0 \\ k_d & 1 & 0 \\ 0 & 0 & 1 \end{pmatrix}$$
$$= \begin{pmatrix} 1 + k_d L & L & \frac{L^2}{2\rho} \\ -k_f k_d L - k_f - k_d & 1 - k_f L & \frac{L}{2\rho}(2 - k_f L) \\ 0 & 0 & 1 \end{pmatrix}$$

where k_f and k_d are the strengths of halves of the focusing and defocusing quadrupoles respectively. The full cell transfer matrix is

$$\mathbf{R} = \begin{pmatrix} 1 - 2X + 2Y - 2XY & 2L(1+Y) & \frac{L^2}{\rho}(2+Y) \\ \frac{2}{L}(1-X)(Y - X - XY) & 1 - 2X + 2Y - 2XY & \frac{L}{\rho}(2 - 2X + Y - XY) \\ 0 & 0 & 1 \end{pmatrix}$$

where we have introduced normalized strengths

$$X \equiv k_f L \qquad \text{and} \qquad Y \equiv k_d L$$

The stability criterion for the horizontal betatron oscillations is ($\cos 2\mu_x = 1 - 2X + 2Y - 2XY$)

$$-1 \leq 1 - 2X + 2Y - 2XY \leq 1$$

and changing the signs of X and Y for vertical oscillations

$$-1 \leq 1 + 2X - 2Y - 2XY \leq 1$$

and the stability or "necktie" region[6] is shown in Fig. 29.

The transverse emittance in the case of different phase advances in the two planes becomes

$$\varepsilon_x = \frac{2C_q E^2}{J_x}\theta^3 F_{FODO}(\mu_x, X-Y)$$

where the new form factor now depends not only on the horizontal phase advance per half–cell, but also on the difference between the normalized strengths $(X-Y)$

$$F_{FODO}(\mu_x, X-Y) = \frac{1}{\sin^2\mu_x \sin 2\mu_x}[1 - \frac{3}{4}\sin^2\mu_x + \frac{1}{60}\sin^4\mu_x + (-\frac{1}{4} + \frac{7}{60}\sin^2\mu_x)(X-Y)]$$

The effect actually lowers the emittance, but not by a large amount. In the damping ring it lowers the emittance by 11% with typical phase advances in the two planes

$$\mu_x = 57^\circ \qquad \text{and} \qquad \mu_y = 22.5^\circ$$

§§*B.1.2 Filling Factor*

Another approximation that we have made in the calculations of emittance was the fact that the bending magnets occupy all of the space between the thin lens quadrupoles. In reality space has to be left for diagnostics equipment, sextupoles and the quadrupoles usually are of finite length. The bending magnets occupy then only a fraction of the cell length that we will call F_m

$$L_{bend} = F_m L$$

and typically only half of the cell length is occupied by dipoles.

Modelling the space between the thin lens quadrupoles and the bends by the drifts of length

$$l = \frac{L - L_{bend}}{2} = \frac{1 - F_m}{2}L$$

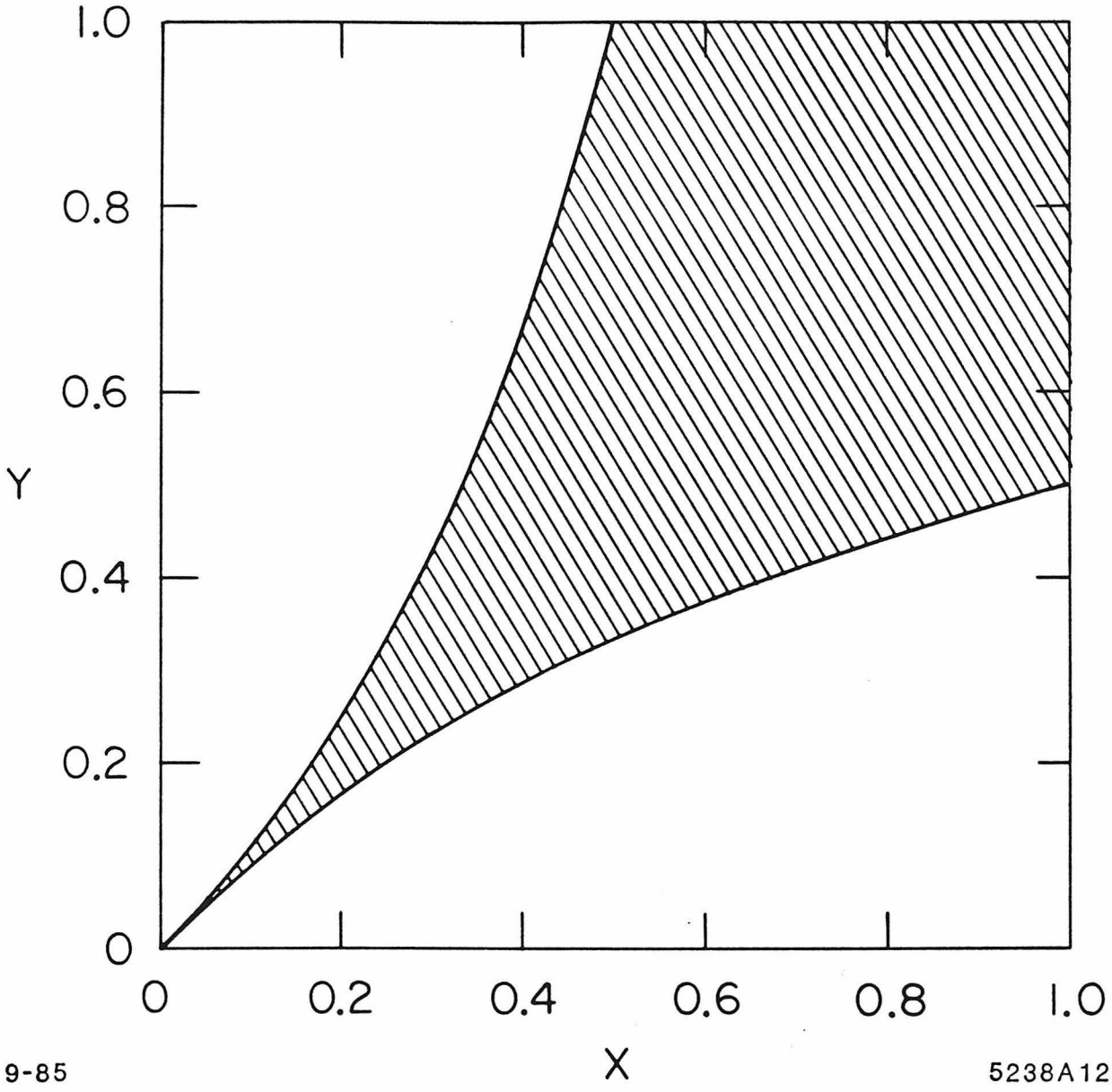

Figure 29. The shaded area is the stability region for the FODO cell lattice. The coordinates are the normalized quadrupole strengths X and Y.

and reverting back to the equal strength quadrupoles, we find that the effect on emittance is as follows

$$\varepsilon_x = \frac{2C_q E^2}{J_x}\theta^3 F_{FODO}(\mu, F_m)$$

where the new form factor is

$$F_{FODO}(\mu, F_m) = \frac{1}{\sin^2\mu \sin 2\mu}\frac{1}{F_m}[1 - \frac{3}{4}\sin^2\mu + \frac{1}{60}\sin^4\mu - \frac{1-F_m}{6}\sin^2\mu + \frac{4-5F_m+F_m^2}{60}\sin^4\mu]$$

The emittance is increased by roughly $1/F_m$ factor, *i.e.* typically by a factor of 2, although the terms that depend on F_m in the brackets change this by a few percent. In the limit of F_m becoming small, the terms inside the brackets stop changing the form factor, but the overall factor $1/F_m$ still remains. In Fig. 30 we show how the terms dependent on F_m inside the brackets influence the shape of the emittance form factor.

§§*B.1.3 Second Region in the Stability Diagram*

The emittance form factor for the FODO cell lattice diverges as the phase advance per half–cell approaches 90°. What happens when the phase advance per half–cell is greater then 90°? To be sure, in a thin lens FODO cell that we have considered so far, the betatron oscillations are unstable above 90° (see the conditions on stability in the above subsections). But if we modify the lattice, a second region of stability appears[27] and the phase advance per half–cell of greater then 90° becomes possible. We will illustrate this situation on a particular example

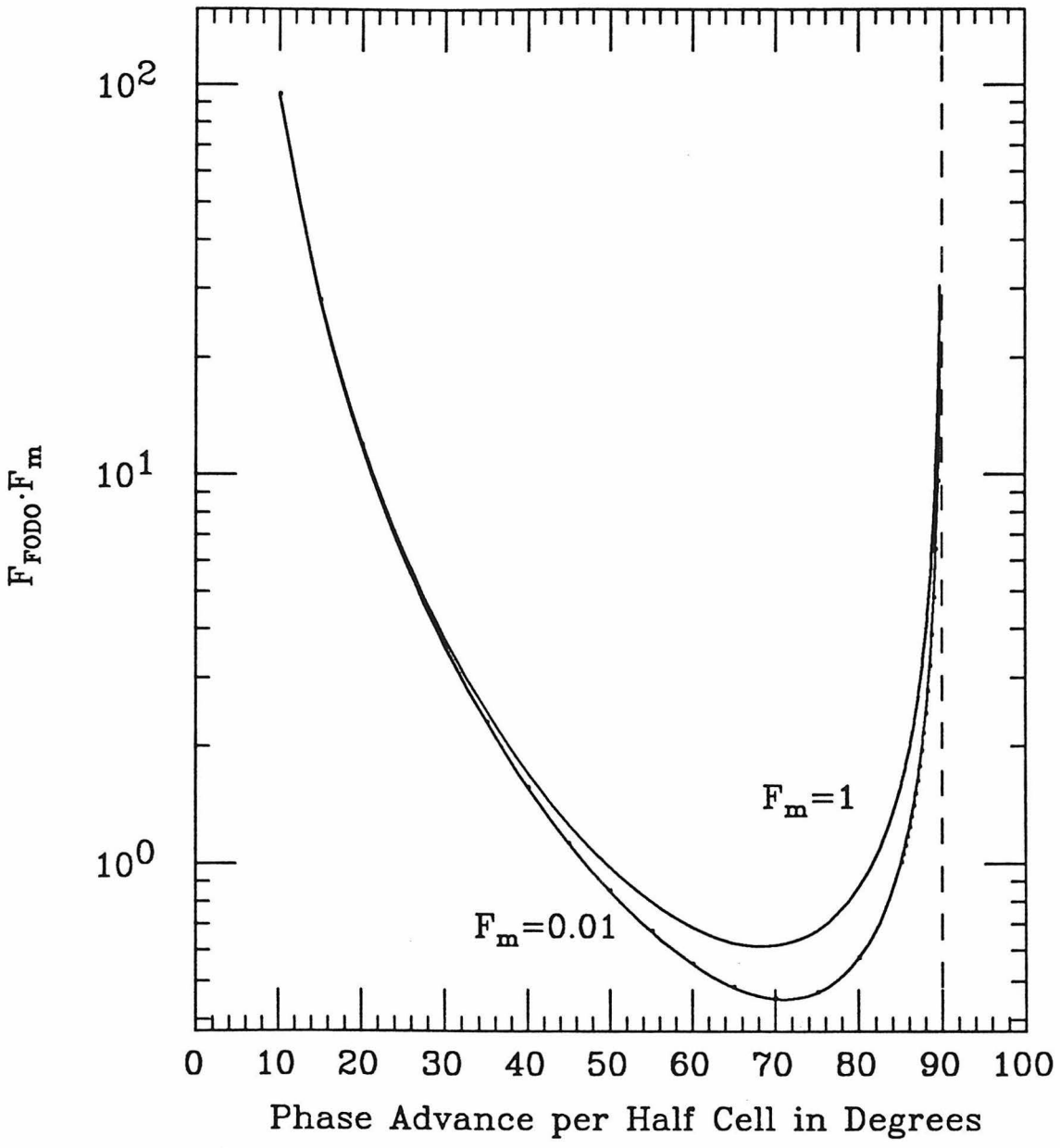

Figure 30. Plotted is the emittance form factor multiplied by the filling factor F_m. The two curves are the two limiting cases of $F_m = 1.0$ and $F_m = 0.01$.

of a cell that is very close to the SPEAR cell[50] and is very close to the FODO cell. The focusing quadrupole is split into two halves and they are separated by a distance L equal to the half–cell length of our FODO lattice. The optics elements of this FOFOD cell are shown in Fig. 31.

Computing the traces of the transfer matrices for this cell we can write down the stability conditions for the betatron oscillations in both planes:

$$-1 \leq 1 + 3Y - 3X - 4XY + X^2 + X^2Y \leq 1 \qquad \text{in} \quad \text{x}$$

$$-1 \leq 1 - 3Y + 3X - 4XY + X^2 - X^2Y \leq 1 \qquad \text{in} \quad \text{y}$$

where we are again using the normalized quadrupole strengths

$$X \equiv k_f L \qquad \text{and} \qquad Y \equiv k_d L$$

The stability regions for this cell are shown in Fig. 32 and in order to operate the lattice in the second stable region the strength of the focusing quadrupoles has to be several times higher than in the simple FODO cell lattice.

A simple illustration of the second stable region[50] is given in Fig. 31 where two possible stable trajectories are drawn. The one belonging to the second stable region crosses the axis between the focusing quadrupoles.

The emittance form factor for FOFOD cell has been calculated using the program COMFORT for a particular case of vertical phase advance per half–cell of 45°. The results are presented in Fig. 33. We see that by going to the second region in the stability diagram we do not gain very much. The minimum value of the emittance is reduced by a factor of two, as compared with the emittance in the first stability region. A more efficient way of reducing the emittance is presented in **Appendix C.**

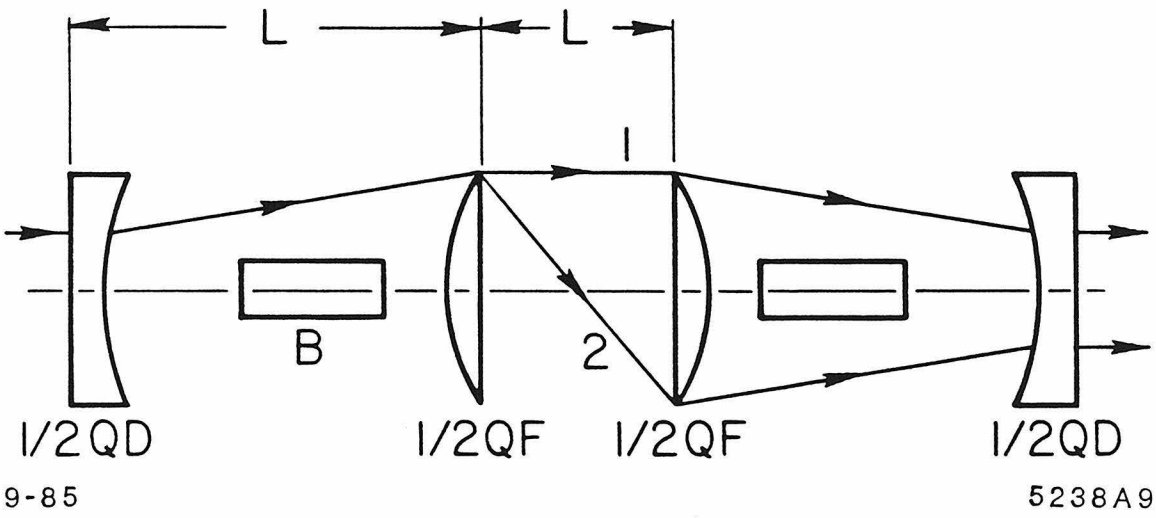

Figure 31. Arrangement of the optical elements in the FOFOD cell example

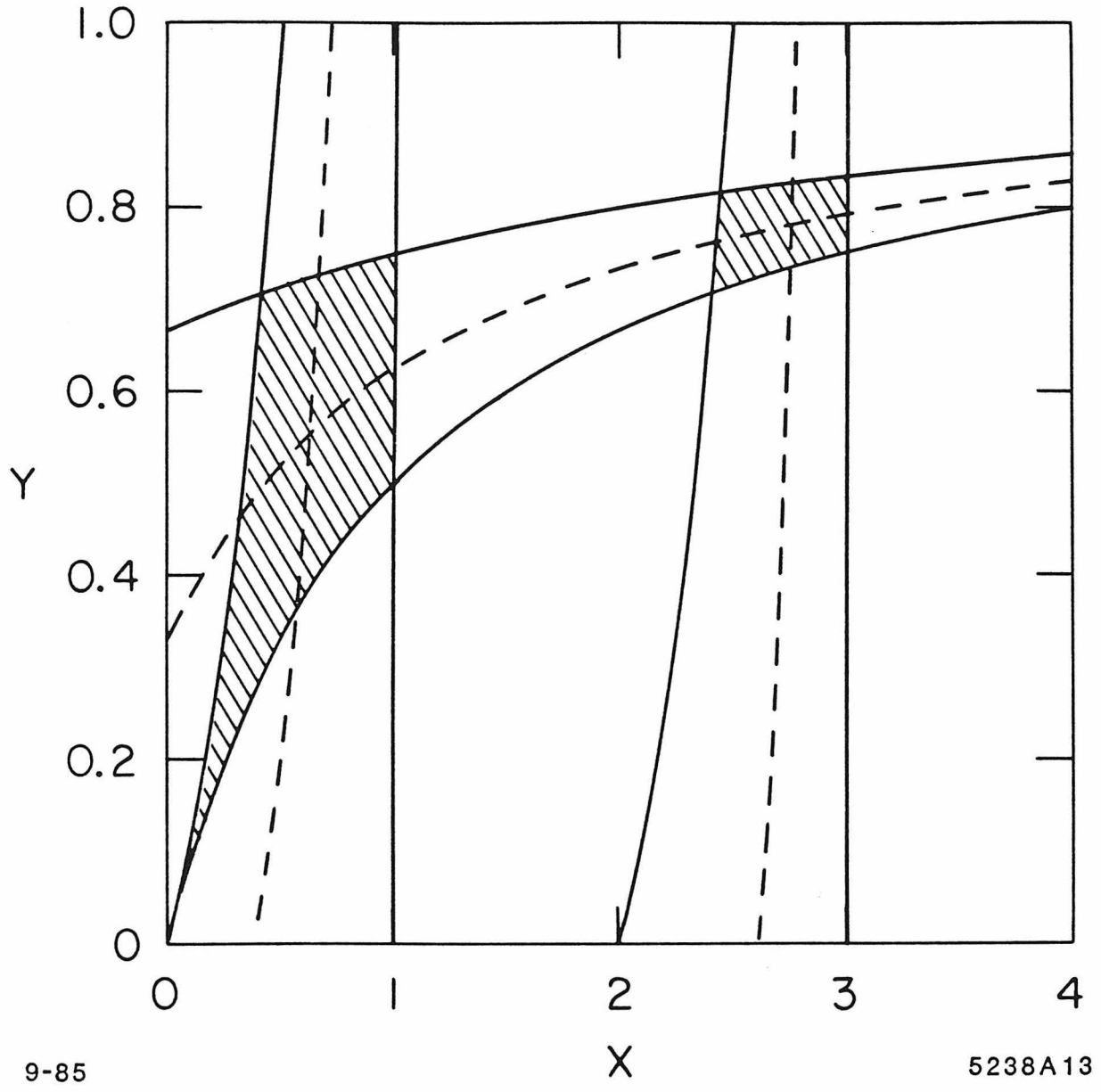

Figure 32. The two stable regions of the FOFOD cell are shown. The dashed lines correspond to 90° or 180° phase advance per half–cell

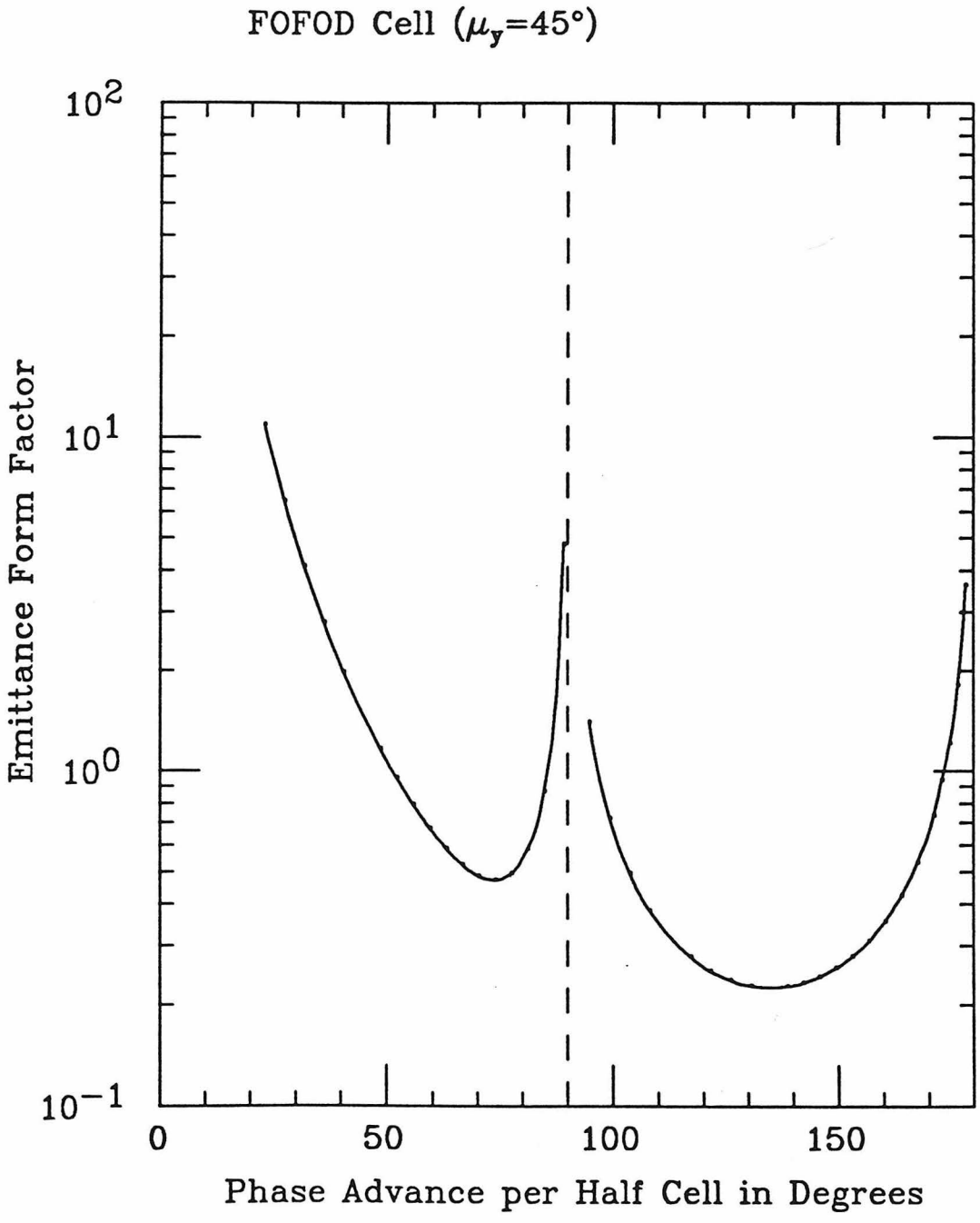

Figure 33. The emittance of FOFOD cell lattice as a function of the horizontal phase advance. Vertical phase advance was kept at 45° per half–cell.

Appendix C. Minimization

In this appendix we are going to investigate how small an emittance can be achieved in a storage ring that uses rectangular uniform field dipole magnets. The emittance can be written as

$$\varepsilon_x = \frac{C_q E^2 \langle \mathcal{H} \rangle_{\text{mag}}}{J_x \rho} \qquad C_q = 1.468 \cdot 10^{-6} \frac{\text{m}}{\text{GeV}^2}$$

where the average value of $\mathcal{H}$ in the dipole magnets as a function of the initial optics parameters in the middle of the magnet is

$$\begin{aligned}\langle \mathcal{H} \rangle_{\text{mag}} = {} & \gamma_0 \eta_0^2 + 2\alpha_0 \eta_0 \eta_0' + \beta_0 \eta_0'^2 \\ & + \gamma_0 [\frac{1}{320} \frac{L^4}{\rho^2} - \frac{1}{12} \frac{L^2}{\rho} \eta_0] - \alpha_0 [\frac{1}{12} \frac{L^2}{\rho} \eta_0'] + \beta_0 [\frac{1}{12} \frac{L^2}{\rho^2}]\end{aligned}$$

in the small bending angle per magnet $\theta = \frac{L}{\rho}$ approximation.

It is convenient to introduce normalized initial optical parameters as follows: the Courant–Snyder parameters

$$\beta_0 = \frac{\bar{\beta}_0 L}{2}$$

$$\alpha_0 = \bar{\alpha}_0$$

$$\gamma_0 = \frac{2\bar{\gamma}_0}{L}$$

and the dispersion parameters

$$\eta_0 = \bar{\eta}_0 \frac{L^2}{8\rho}$$

$$\eta_0' = \bar{\eta}_0' \frac{L}{2\rho}$$

The average $\mathcal{H}$ becomes

$$\langle \mathcal{H} \rangle_{\text{mag}} = \frac{L^3}{32\rho^2}[\bar{\gamma}_0(\bar{\eta}_0^2 - \frac{2}{3}\bar{\eta}_0 + \frac{1}{5}) + \bar{\alpha}_0(4\bar{\eta}_0\bar{\eta}_0' - \frac{4}{3}\bar{\eta}_0') + \bar{\beta}_0(4\bar{\eta}_0'^2 + \frac{4}{3})$$

The expression for the emittance can be rewritten then as follows

$$\varepsilon_x = \frac{C_q E^2 \langle \mathcal{H} \rangle_{\text{mag}}}{J_x \rho} = \frac{2C_q E^2}{J_x}\theta^3 F_{min}$$

where the emittance form factor F_{min} is

$$F_{min} = \frac{1}{64}[\bar{\gamma}_0 A(\bar{\eta}_0) + \bar{\alpha}_0 B(\bar{\eta}_0, \bar{\eta}_0') + \bar{\beta}_0 C(\bar{\eta}_0')]$$

and we have introduced the coefficients that depend only on the initial dispersion parameters

$$A(\bar{\eta}_0) = \bar{\eta}_0^2 - \frac{2}{3}\bar{\eta}_0 + \frac{1}{5}$$
$$B(\bar{\eta}_0, \bar{\eta}_0') = 4\bar{\eta}_0\bar{\eta}_0' - \frac{4}{3}\bar{\eta}_0'$$
$$C(\bar{\eta}_0') = 4\bar{\eta}_0'^2 + \frac{4}{3}$$

The minimization procedure

For arbitrary initial dispersion parameters the initial values of the Courant–Snyder parameters that achieve the minimum value of F_{min} are

$$\bar{\beta}_0^* = \frac{2A}{\sqrt{4AC - B^2}}$$
$$\bar{\alpha}_0^* = \frac{-B}{\sqrt{4AC - B^2}}$$
$$\bar{\gamma}_0^* = \frac{2C}{\sqrt{4AC - B^2}}$$

and the minimum value is

$$F_{min} = \frac{1}{64}\sqrt{4AC - B^2}$$

To find the optimum values for the $\bar{\eta}_0$ and $\bar{\eta}_0'$ that minimize the F_{min} we first write down the following partial derivatives

$$\frac{\partial(4AC - B^2)}{\partial\bar{\eta}_0} = \frac{32}{3}(\bar{\eta}_0 - \frac{1}{3})$$
$$\frac{\partial(4AC - B^2)}{\partial\bar{\eta}_0'} = \frac{128}{45}\bar{\eta}_0'$$

and the optimum values are

$$\bar{\eta}_0'^* = 0, \qquad \bar{\eta}_0^* = \frac{1}{3}$$

Under these conditions the coefficients A,B and C are

$$A = \frac{4}{45}, \qquad B = 0, \qquad C = \frac{4}{3}$$

Absolute minimum

Reverting to the usual notation for the initial optical parameters, we can write down the conditions for the absolute minimum as follows

$$\eta_0'^* = 0$$
$$\eta_0^* = \frac{L^2}{24\rho}$$
$$\alpha_0^* = 0$$
$$\beta_0^* = \frac{L}{2\sqrt{15}}$$
$$\gamma_0^* = \frac{\sqrt{15}}{2}L$$
$$F_{min}^* = \frac{1}{24\sqrt{15}}$$

The minimum value of the form factor under these conditions is a factor of 58 smaller then the minimum value of the emittance form factor for the FODO cell lattice.

The lowest transverse equilibrium emittance that can be achievedd in a ring that uses uniform field dipole magnets with bending angle per magnet θ and operated at an energy E is

$$\varepsilon_x = \frac{1}{12\sqrt{15}} \frac{C_q E^2}{J_x} \theta^3 = 3.158 \times 10^{-8} \frac{E^2}{J_x} \theta^3$$

Similar optimization procedures have been carried out by several authors[51–53] and the minimum conditions agree with their results.

The emittance is a steep function of the bending angle per magnet θ. However there is a lower bound on the possible transverse emittance[5] due to the fact that the synchrotron radiation is emitted into a cone with the half opening angle of $1/\gamma$. So far we have assumed that the emission of a photon was along the tangent to the trajectory. If we write again the change in the betatron displacement and slope due to a single emission of a photon of energy u making an angle θ_γ with the trajectory

$$\delta x_\beta = -\eta \frac{u}{E}, \qquad \delta x'_\beta = -\eta' \frac{u}{E} - \theta_\gamma \frac{u}{E}$$

the change in the betatron amplitude becomes

$$\begin{aligned} \delta a^2 &= \gamma(\delta x_\beta)^2 + 2\alpha(\delta x_\beta)(\delta x'_\beta) + \beta(\delta x'_\beta)^2 \\ &= \left(\frac{u}{E_0}\right)^2 \left[(\gamma\eta^2 + 2\alpha\eta\eta' + \beta\eta'^2) + 2(\alpha\eta + \beta\eta')\theta_\gamma + \beta\theta_\gamma^2\right] \\ &= \left(\frac{u}{E_0}\right)^2 \left[\mathcal{H} + \mathcal{H}'\right] \end{aligned}$$

where

$$\mathcal{H}' = 2(\alpha\eta + \beta\eta')\theta_\gamma + \beta\theta_\gamma^2$$

Since θ_γ can be positive or negative, the term linear in it will give no net contribution to the emittance and thus the estimate of the lower limit for the horizontal emittance is

$$\varepsilon_{x,min} = C_q \frac{E^2}{\gamma^2} \frac{\beta_n}{\rho}$$

where we took a typical value for $\theta_\gamma = \frac{1}{\gamma}$ and β_n is the average β function in the bending magnet. Under the conditions for the minimum emittance the average value

$$\beta_n = \beta_0^* + \frac{1}{\beta_0^*}\frac{L^2}{12} \approx 0.78L$$

so that the corresponding emittance is

$$\varepsilon_{x,min} = 0.78\, C_q \frac{E^2}{\gamma^2}\theta$$

We can now solve for the value of θ that would give the emittance under the minimum conditions equal to $\varepsilon_{x,min}$. Assuming that $J_x = 1$ (rectangular bends), the lower limit on the bending angle per magnet is

$$\theta_{min} = \frac{6}{\gamma} \quad \text{rad}$$

and the lower bound on emittance becomes

$$\gamma\varepsilon_{min} = 1.78 \times 10^{-12}\, m\, rad$$

Appendix D. Proof of an Inequality

Definition

A matrix $\mathbf{S}$ is called positive-definite, if for any non-zero coordinate vector $\mathbf{X}$

$$\mathbf{X}^T\mathbf{S}\mathbf{X} > 0$$

LEMMA

Any symmetric positive-definite matrix $\mathbf{S}$ can be written in the following way

$$\mathbf{S} = \mathbf{P}^T\mathbf{P}$$

where $\mathbf{P}$ is a non-singular matrix ($det\mathbf{P} \neq 0$).

PROOF

It is well known that a symmetric, positive-definite matrix has positive real eigenvalues and can be diagonalized with an orthogonal matrix, that is

$$\mathbf{S} = \mathbf{M}^T\mathbf{D}\mathbf{M} = \mathbf{M}^T \begin{pmatrix} \lambda_1 & 0 & \dots & 0 \\ 0 & \lambda_2 & \dots & 0 \\ \vdots & \vdots & \ddots & \vdots \\ 0 & 0 & \dots & \lambda_n \end{pmatrix} \mathbf{M}; \quad \mathbf{M}^T = \mathbf{M}^{-1}$$

Then it is sufficient to take

$$\mathbf{P} = \begin{pmatrix} \sqrt{\lambda_1} & 0 & \dots & 0 \\ 0 & \sqrt{\lambda_2} & \dots & 0 \\ \vdots & \vdots & \ddots & \vdots \\ 0 & 0 & \dots & \sqrt{\lambda_n} \end{pmatrix} \mathbf{M}$$

to satisfy the lemma.

LEMMA

The following inequality is true for any positive-definite, symmetric matrix

$$det\mathbf{S} \leq \left[\frac{Tr\mathbf{S}}{n}\right]^n$$

where $\mathbf{S}$ is n by n matrix.

PROOF

The eigenvalues of $\mathbf{S}$ are real and positive, so they must satisfy the Cauchy inequality[54] which states that their arithmetic mean is greater or equal then their geometric mean

$$\frac{\lambda_1 + \lambda_2 + \ldots + \lambda_n}{n} \geq \sqrt[n]{\lambda_1 \lambda_2 \ldots \lambda_n}$$

Raising both sides to the nth power, we get

$$\lambda_1 \lambda_2 \ldots \lambda_n \leq \left[\frac{\lambda_1 + \lambda_2 + \ldots + \lambda_n}{n}\right]^n$$

But this is just the inequality we are trying to prove written for the $\mathbf{D}$ matrix of eigenvalues of $\mathbf{S}$ since

$$det\mathbf{D} = \lambda_1 \lambda_2 \ldots \lambda_n$$

$$Tr\mathbf{D} = \lambda_1 + \lambda_2 + \ldots + \lambda_n$$

And to show that the inequality of the lemma is true for $\mathbf{S}$ as well, it is sufficient to notice that

$$det\mathbf{S} = det(\mathbf{M}^T\mathbf{D}\mathbf{M}) = det(\mathbf{M}^{-1}\mathbf{D}\mathbf{M}) = det\mathbf{D}$$

since $\mathbf{M}^T = \mathbf{M}^{-1}$ and

$$Tr\mathbf{S} = Tr(\mathbf{M}^T\mathbf{D}\mathbf{M}) = Tr(\mathbf{M}^{-1}\mathbf{D}\mathbf{M}) = Tr\mathbf{D}$$

because of the cyclic property of the trace.

MAIN PROOF

We now consider the case of two coupled transverse degrees of freedom. For the corresponding σ matrix, written in the 2×2 blocks form

$$\sigma = \begin{pmatrix} \mathbf{H} & \mathbf{C} \\ \mathbf{C}^T & \mathbf{V} \end{pmatrix}$$

blocks $\mathbf{H}, \mathbf{V}$ are symmetric, positive-definite, so according to the first lemma we can write them as

$$\mathbf{H} = \mathbf{P}^T\mathbf{P} \qquad det\mathbf{H} = (det\mathbf{P})^2$$

$$\mathbf{V} = \mathbf{Q}^T\mathbf{Q} \qquad det\mathbf{V} = (det\mathbf{Q})^2$$

and we can write the beam matrix as

$$\sigma = \begin{pmatrix} \mathbf{P}^T & 0 \\ 0 & \mathbf{Q}^T \end{pmatrix} \begin{pmatrix} \mathbf{I} & \mathbf{X} \\ \mathbf{X}^T & \mathbf{I} \end{pmatrix} \begin{pmatrix} \mathbf{P} & 0 \\ 0 & \mathbf{Q} \end{pmatrix}$$

where $\mathbf{I}$ is a 2×2 unit matrix and $\mathbf{X}$ can be determined from $\mathbf{C} = \mathbf{P}^T\mathbf{X}\mathbf{Q}$.

Taking the determinant of both sides,

$$det(\sigma) = det\mathbf{H}det\mathbf{V}det\overline{\mathbf{D}}$$

and applying the inequality from the second lemma since the $Tr\overline{\mathbf{D}} = 4$ and $n = 4$,

$$det\overline{\mathbf{D}} \leq 1$$

we obtain

$$det(\sigma) \leq det\mathbf{H}det\mathbf{V}$$

Q.E.D.

REFERENCES

1. *LEP Design Report*
   CERN–LEP/84–01, June 1984
2. Burton Richter, (SLAC), Nucl. Inst. and Meth. **136**, 47, 1976
   Very high energy electron–positron colliding beams for the study of the weak interactions
3. Burton Richter, SLAC–PUB–3669, May 1985
   Very High Energy Colliders
   Invited paper presented at the 1985 Particle Accelerator Conference, Vancouver, Canada.
4. Burt Richter, (SLAC), Proc. XIth Int. Conf. on High Energy Acc., Geneva, 1980
   The SLAC Linear Collider.
5. Matthew Sands, (UC Santa Cruz), SLAC-121, UC-28, November 1970.
   The Physics of Electron Storage Rings, An Introduction
6. E. D. Courant and H. S. Snyder, Annals of Physics, **3**, 1 (1958)
   Theory of the Alternating–Gradient Synchrotron
7. R. H. Helm, M. J. Lee, P. L. Morton and M. Sands, IEEE Nucl. Sci. **NS–20**, no. 3, 900 (1973)
   Evaluation of Synchrotron Radiation Integrals
8. M. D Woodley, M. J. Lee, J. Jäger and A. S. King, SLAC–PUB–3068
   Control of machine functions or transport systems
9. F. Ch. Iselin, CERN–LEP–TH/85-15, 1985
   The MAD program (Methodical Accelerator Design): Reference manual
10. Helmut Wiedemann, PEP Note 220, 1976
    Chromaticity correction in large storage rings
11. Helmut Wiedemann, SSRL–ACD–Note 22 or ESRP–IRM–72/84
    Users Guide to PATRICIA
12. Helmut Wiedemann, (SLAC), Internal Note AATF/79/8

Some remarks on the parameters of a damping ring for the linac collider project.

13. Helmut Wiedemann, (SLAC), Proc. XIth Int. Conf. on High Energy Acc., Geneva, 1980
    Scaling of damping rings for colliding linac beam systems.
14. R. H. Helm and H. Wiedemann, (SLAC), PEP Note 303, 1979
    Emittance in a FODO cell lattice
15. F. Bulos and A. Odian, SLAC–PUB–3453, 1984
    Design of a matched fast kicker system
16. M. A. Allen, H. D. Schwarz and P. B. Wilson, SLAC–PUB–3084, 1983
    Damping ring RF system for SLC
17. Helmut Wiedemann, PEP Note 39, PEP Summer Study, 1973
    Scaling of FODO cell parameters
18. J.–L. Pellegrin, (SLAC), Proc. Proc. XIth Int. Conf. on High Energy Acc., Geneva, 1980
    A review of accelerator instrumentation
19. G. E. Fischer and J.–L. Pellegrin, (SLAC), Collider Note 80, 1981
    Some beam position monitor considerations for the damping ring complex
20. Marc Ross, Private communication
21. G. E. Fischer, (SLAC), Collider Note 98, 1981
    Some more orbit correction considerations for the damping ring
22. G. E. Fischer and S. Kheifets, (SLAC), Collider Note 122, 1981
    Damping ring beam position correcting scheme
23. E. Close, M. Cornacchia, A. S. King, M. J. Lee, (SLAC), PEP Note 271, 1978
    A proposed orbit and vertical dispersion correction system for PEP
24. J. C. Sheppard, J. E. Clendenin, M. B. James, R. H. Miller and M. C. Ross, SLAC–PUB–3584, 1985
    Real time bunch length measurements in the SLC linac

25. J. T. Seeman, M. C. Ross, J. C. Sheppard and R. F. Stiening, SLAC–PUB–3673, 1985
Observations of accelerated high current low emittance beams in the SLC linac

26. K. Robinson, Physical Review **111**, 373 (1958)
Radiation Effects in Circular Electron Accelerators

27. Albert Hofmann, Private communication

28. J. D. Jackson, *Classical Electrodynamics*, Second edition, Wiley, New York, 1975

29. A. Hofmann and F. Méot, (CERN), NIM **203**, (1982) 483
Optical resolution of beam cross–section measurements by means of synchrotron radiation

30. J. C. Sheppard et al., (SLAC), SLAC-PUB-3080, March 1983.
Emittance Calculations for the Stanford Linear Collider Injector

31. John Seeman, (SLAC), Private communication

32. Colorado Video Corporation, Technical Information

33. Marc Ross, (SLAC), Collider Note 280

34. John Rees and Lenny Rivkin, (SLAC and Caltech), SLAC-PUB-3305, March 1984.
On measuring emittances and sigma matrices

35. A. Hofmann and J. R. Maidment, LEP Note 168, 1979
Current dependent phenomena in LEP

36. Albert Hofmann, (CERN), Proc. XIth Int. Conf. on High Energy Acc., Geneva, 1980
Diagnostics and cures for beam instabilities

37. P. Wilson, J. Styles and K. Bane, IEEE Trans. on Nucl. Sci. **NS 22–3**, 1838, (1975)

38. Perry Wilson, (SLAC), Collider Note 35, 1981
Parasitic mode losses in the damping ring

39. A. W. Chao, AIP Conf. Proc. No. 105, 1983

Coherent instabilities of a relativistic bunched beam

40. M. J. Lee, J. C. Sheppard, M. Sullenberger and M. D. Woodley, SLAC–PUB–3217, 1983
Models and simulations
41. J. Jäger, M. J. Lee, M. D. Woodley and J. P. Delahaye, SLAC–PUB–3408, 1984
Modeling of the SLC electron damping ring
42. I. Almog, J. Jäger, M. Lee and M. Woodley, SLAC–PUB–3608, 1985
On line model driven control of the SLC electron damping ring
43. M. Sands, Private communication
44. J. P. Delahaye and L. Rivkin, SLAC–PUB–3649, 1985
SLC positron damping ring optics design
45. J. E. Spencer, SLAC–PUB–3647, 1985
Some uses of REPMM's in storage rings and colliders
46. Karl L. Brown, (SLAC), SLAC-Report-75, June 1982.
A First- and Second–Order Matrix Theory for the Design of Beam Transport Systems and Charged Particle Spectrometers
47. Brown K. L., Carey D. C., Iselin Ch. and Rothacker F., (SLAC), SLAC-Report-91, 1974.
TRANSPORT, a Computer Program for Designing Charged Particle Beam Transport Systems
48. K. L. Brown and R. V. Servranckx, SLAC–PUB–3381, 1984
First and second order charged particle optics
49. Weissberg, H., (Caltech), Lecture Notes (1983), Unpublished
Introduction to the Accelerator Physics
50. Phil Morton, Private communication
51. M. Sommer, LAL/RT/83–15, 1983
Optimization of the emittance of the electrons (positrons) storage rings
52. L. C. Teng, (ANL–FNAL), LS–17, 1985

Minimum emittance lattice for synchrotron radiation storage rings

53. Helmut Wiedemann, Private communication

54. G. Pólya, G. Szegö, *Problems and Theorems in Analysis*,Volume 1, Springer-Verlag, 1972